RESEARCH

UDOT CONNECTING COMMUNITIES

Utah Department of Transportation–Research Division
4501 South 2700 West, Box 148410 - Salt Lake City, Utah 84114-8410

**Report No. UT-03.20**

# ESTIMATION OF PRECONSOLIDATION STRESS AND COMPRESSION RATIO FROM FIELD AND LABORATORY MEASUREMENTS FROM THE I-15 RECONSTRUCTION PROJECT, SALT LAKE CITY, UTAH

**Prepared For:**
Utah Department of Transportation
Research Division
Salt Lake City, Utah

**Submitted By:**
Dept. of Civil and Environmental Engineering
University of Utah

**Authored By:**
Steven F. Bartlett, Ph.D., P.E.
Patrick Alcorn

**May 2004**

Inside Cover

# DISCLAIMER

The authors alone are responsible for the preparation and accuracy of the information, data, analysis, discussion, recommendations, and conclusions presented herein. The contents do not necessarily reflect the views, opinions, endorsements, or policies of the Utah Department of Transportation (UDOT) or the US Department of Transportation (USDOT). The Utah Department of Transportation makes no representation or warranty of any kind, and assumes no liability therefore.

Page Left Blank Intentionally

# UDOT RESEARCH & DEVELOPMENT REPORT ABSTRACT

| | | |
|---|---|---|
| **1. Report No.** UT-03.20 | **2. Government Accession No.** | **3. Recipient's Catalog No.** |
| **4. Title and Subtitle**<br><br>Estimation of Preconsolidation Stress and Compression Ratio from Field and Laboratory Measurements from the I-15 Reconstruction Project, Salt Lake City, Utah | **5. Report Date** May 2004<br><br>**6. Performing Organization Code** | |
| **7. Author(s)**<br><br>Steven F. Bartlett, Ph.D., P.E., Assistant Professor<br>Patrick Alcorn, Graduate Student | **9. Performing Organization Report No.** | |
| **9. Performing Organization Name and Address**<br><br>Department of Civil and Environmental Engineering<br>University of Utah<br>122 South Central Campus Drive, Suite 104<br>Salt Lake City, Utah 84112-0561 | **10. Work Unit No.**<br><br>**11. Contract No.**<br><br>02-9021 | |
| **12. Sponsoring Agency Name and Address**<br><br>Research Division<br>Utah Department of Transportation<br>4501 South 2700 West (PO Box 148410)<br>Salt Lake City, UT 84119 (84114-8410) | **13. Type of Report and Period Covered**<br><br>Technical Report, 2004<br><br>**14. Sponsoring Agency Code**<br><br>PIC No. TB98-029 | |
| **15. Supplementary Notes**<br><br>N/A | | |

**16. Abstract**

This report discusses past research regarding estimation of consolidation properties and develops methods for these properties for clayey soils in the Salt Lake Valley, Utah using the cone penetrometer test (CPT). The primary focus is developing methods for estimating the preconsolidation pressure and the compression ratio from data obtained from the I-15 Reconstruction Project. The relations developed herein were done so using field instrumentation, laboratory data and cone penetrometer soundings.

| | | | |
|---|---|---|---|
| **17. Key Words**<br><br>preconsolidation stress, compressibility, soft clays, settlement, numerical modeling, cone penetrometer | | **18. Distribution Statement**<br><br>Available: UDOT Research Division<br>PO Box 148410<br>Salt Lake City, UT 84114-8410<br>http://www.udot.utah.gov/index.php/m=c/tid=195 | |
| **19. Security Classification (of this report)**<br>Unclassified | **20. Security Classification (of this page)**<br>Unclassified | **21. No. of Pages**<br><br>88 | **22. Price** |

Page Left Blank Intentionally

## TABLE OF CONTENTS

**1 Introduction ..... 1-1**
1.1 Background Information ..... 1-1
1.2 Summary of the Surficial Geology of the Salt Lake Valley ..... 1-1
1.2.1 Physiography ..... 1-1
1.2.2 Surficial Geology and Sediments Important to Engineering Evaluations ..... 1-2
1.3 General Discussion of Methods to Determine Soil Properties ..... 1-2
1.3.1 Laboratory Tests ..... 1-5
1.3.2 In-Situ Tests ..... 1-5
1.3.3 Back-Analysis from Instrumentation ..... 1-6
1.3.4 Technical Approach ..... 1-7

**2 Historical Development of the CPT Test ..... 2-1**
2.1 Introduction ..... 2-1
2.2 Summary of CPT Development ..... 2-1
2.2.1 1932 ..... 2-1
2.2.2 1935 ..... 2-1
2.2.3 1948 ..... 2-1
2.2.4 1953 ..... 2-1
2.2.5 1965 ..... 2-2
2.2.6 1974 ..... 2-2
2.2.7 Present ..... 2-2
2.2.8 The Role of the CPT ..... 2-3

**3 Analytical Methods ..... 3-1**
3.1 Discussion of Available Data and Data Collection ..... 3-1
3.1.1 Downhole Magnetic Extensometer ..... 3-3
3.1.2 Standard Penetration Test ..... 3-5
3.1.3 Cone Penetrometer (CPT) ..... 3-6
3.1.4 Sampling ..... 3-8
3.1.5 Laboratory Testing ..... 3-8
3.2 Screening and Interpretation of Laboratory Data ..... 3-9
3.2.1 Selection of Laboratory Data ..... 3-9
3.2.2 Interpretation of Laboratory Consolidation Curves ..... 3-11
3.2.3 Calculation of Preconsolidation Stress from Laboratory Data ..... 3-12
3.2.4 Calculation of Field Consolidation Curve from Laboratory Data ..... 3-12
3.3 Interpretation of Consolidation Properties from Magnet Extensometer Data ..... 3-15
3.3.1 Development of Subsurface Profile ..... 3-17
3.3.2 Available Magnetic Extensometer Data ..... 3-18
3.3.3 Calculation of Beginning of Primary Consolidation Settlement ..... 3-18
3.3.4 Calculation of End of Primary Consolidation Settlement ..... 3-20
3.3.5 Calculation of Vertical Strain from Magnet Extensometer Data ..... 3-21
3.3.6 Calculation of Compression Ratio for Primary Consolidation ..... 3-23
3.4 Calculation of Preconsolidation Stress Using Numerical Modeling ..... 3-23

**4 Development of Regression Model ..... 4-1**
4.1 Introduction to Multiple Linear Regression ..... 4-1
4.2 Pairing of CPT Data with Estimates of Consolidation Properties ..... 4-4
4.3 Development of Regression Models for Preconsolidation Stress ..... 4-13
4.4 Development of Regression Models for Compression Ratio ..... 4-20

**5 Conclusions and Summary ..... 5-1**
5.1 Significance of Research Findings ..... 5-1
5.2 Recommended Empirical Model ..... 5-1
5.3 Implementation of the Empirical Model ..... 5-2
5.4 Future Research and Improvements ..... 5-3

**6 References ..... 6-1**

## List of Figures

Figure 1-1 Geological Map of Northern Salt Lake Valley. ..... 1-3

Figure 1-2 Geological Map of Southern Salt Lake Valley. ..... 1-4

Figure 2-1 Dutch Cone Penetrometer Tip. ..... 2-5

Figure 2-2 Electrical Friction Cone with Cut-Away Friction Sleeve. ..... 2-6

Figure 2-3 Typical Electric Cone (Bowles, 1996). ..... 2-7

Figure 2-4 Electric Cone Definitions (Bowles, 1996). ..... 2-8

Figure 2-5 Piezocone Penetrometer Tip. ..... 2-9

Figure 3-1 Example of Typical CPT Log from the I-15 Reconstruction Project. ..... 3-2

Figure 3-2 Installation of Magnet Extensometer. ..... 3-4

Figure 3-3 CPT Log with Piezocone Measurements Showing Delayed Pore Pressure Response. ..... 3-7

Figure 3-4 Erroneously Low Pore Pressure Measurements in CPT Sounding from the I-15 Reconstruction Project (after Ladd and DeGroot, 2003). ..... 3-8

Figure 3-5 Casagrande's Method for Determining Preconsolidation Stress (Holtz and Kovacs, 1981). ..... 3-13

Figure 3-6 Illustration of Schmertmann Procedures to Obtain the Field Virgin Compression Curve for OC Soil (Holtz and Kovacs, 1981). ..... 3-14

Figure 3-7 Illustrations of Schmertmann (1955) and Casagrande (1936) Techniques to Find the Preconsolidation Stress and the Field Consolidation Curve. ..... 3-16

Figure 3-8 Example of Fill Height Versus Elapsed Time Data from the I-15 Reconstruction Project, Salt Lake City, Utah. ..... 3-19

Figure 3-9 Example of Settlement Versus Elapsed Time from Magnetic Extensometer for the I-15 Reconstruction Project, Salt Lake City, Utah. ..... 3-19

Figure 3-10 Illustration of Asaoka Procedure to Calculate the EOP Consolidation. ..... 3-20

Figure 3-11 Example Layout of Soil Profile and Embankment with Surcharge Using SIGMA/W. ..... 3-26

Figure 3-12 Example Stress Distribution Output from SIGMA/W. ..... 3-27

Figure 4-1 Examples of Standard Residual Plots. (a) Satisfactory residual plot gives overall impression of horizontal box centered on zero line. (b) A plot showing nonconstant variance. (c) A plot showing a linear trend suggesting that the residuals are not independent and that another variable is needed in the model. (d) A plot illustrating the need for a transformation or a higher order term to alleviate curvature in the residuals. ..... 4-3

Figure 4-2 Preconsolidation Pressures in the 600 South Area that Consists of Laboratory Data, Magnet Extensometer High, Average, and Low Range of Data. ..... 4-5

Figure 4-3 Preconsolidation Pressures in the 2400 South Area that Consist of Laboratory Data, Magnet Extensometer High, Average, and Low Range of Data. ..... 4-6

Figure 4-4 Compression Ratios in the 600 South Area that Consists of Laboratory Data, Magnet Extensometer High, Average, and Low Range of Data..... 4-7

Figure 4-5 Compression Ratios in the 2400 South Street Area that Consists of Laboratory Data, Magnet Extensometer High, Average, and Low Range of Data ..... 4-8

Figure 4-6 Plot of Woodward Clyde Correlation Equation with Data from this Report. ..... ..... 4-14

Figure 4-7 Plot of Mayne and Chen Correlation with Salt Lake Valley. ..... 4-14

Figure 4-8 Plot of Corrected Tip Stress Divided by Total Stress and Preconsolidation Stress ..... 4-15

Figure 4-9 Plot of Variables Used in Equation 4-24..... 4-18

Figure 4-10 Plot of Woodward Clyde Correlation Equation with this data. ..... 4-20

Figure 4-11 Plot of tip stress divided by total stress and compression ratio..... 4-21

## List of Tables

Table 3-1 Sample Quality Designations ..... 3-10

Table 3-2 Average Unit Weights for Soil Layers in the 600 South Design Area..... 3-17

Table 3-3 Average Unit Weights for Soil Layers in the 2400 South Design Area..... 3-17

Table 3-4 Example Calculations from Magnetic Extensometer M34-2-1..... 3-22

Table 3-5 Properties Used for SIGMA/W Analysis ..... 3-24

Table 3-6 Example Calculations from SIGMA/W Modeling in Tabular Form..... 3-28

Table 4-1 Magnetic Extensometers and CPT Soundings Used in Regression Analysis. ..... ..... 4-10

Table 4-2 Magnets, Their Locations, and the Calculated Preconsolidation Stresses and Compression Ratios. ..... 4-11

Table 4-3 Linear regression output using log of corrected tip stress as X1 and average sleeve stress as X2; Y = log of preconsolidation stress. ..... 4-16

Table 4-4 Linear Regression Output for Equation 4-24. ..... 4-18

Table 4-5 Linear Regression Output for Equation 4-26. ..... 4-19

Table 4-6 Linear Regression Output for Equation 4-27. ..... 4-19

Table 4-7 Linear Regression Output for Compression Ratio ..... 4-22

Page Left Blank Intentionally

# 1 Introduction

## 1.1 Background Information

This report discusses past research regarding estimation of consolidation properties and develops methods for these properties for clayey soils in the Salt Lake Valley, Utah using the cone penetrometer test (CPT). The primary focus is developing methods for estimating the preconsolidation pressure and the compression ratio from data obtained from the I-15 Reconstruction Project. The relations developed herein were done so using field instrumentation, laboratory data and cone penetrometer soundings.

Interstate I-15 is a major freeway that runs through southern California, Nevada, Utah, eastern Idaho, Montana and ends at the Canadian border. The seventeen-mile section that passes through the central part of Salt Lake Valley was originally built in the mid 1960's. However, with time the interstate aged and overreached its capacity, thus the I-15 Reconstruction Project was started in 1998 to relieve heavy traffic volumes and to replace and expand the deteriorating road and bridge system. This project was an approximate $1.5 billion design-build project that added two lanes in each directions and replaced all bridges in the seventeen-mile (27-km) alignment. A total of 144 bridges were constructed as part of this project.

Most of the bridges along the I-15 alignment are overpass type structures. Typical embankment construction at the bridge approaches required placement of granular fill to heights of 10 to 15 meters (33 to 50) above original ground. These same embankments are typically 100 to 150 m (330 to 500 ft) wide, which constitutes a significant new construction load to the foundation soils. Underlying these embankments is about 5 meters (16 ft) of recent alluvium, which in turn is underlain by about 20 meters (66 ft) of soft, compressible lake deposits from prehistoric Lake Bonneville. In the vicinity of the downtown area, these lacustrine soils are clay (CL, CH), clayey silt (MH) and silt (ML) with inter-bedded, thin, fine, sand layers (SM, SP-SM).

The compressibility and shear strength of the Lake Bonneville deposits were important considerations during the design and reconstruction of I-15. Regarding settlement performance, the major concerns were: (1) the large amount of primary settlement, (2) the relatively long duration of primary settlement and (3) the rate and amount of secondary settlement. Because of strict project time constraints and scheduling issues, prefabricated vertical drains were used in the clay layers to accelerate the rate of primary consolidation. The embankments were also surcharged to minimize the amount of secondary consolidation and reduce its rate with time. The surcharge amounts were typically 30 to 40 percent of the embankment height in areas with soft clayey deposits.

## 1.2 Summary of the Surficial Geology of the Salt Lake Valley

### 1.2.1 Physiography

The Salt Lake Valley is the eastern-most basin of the Basin and Range physiographical province that extends from the Wasatch Range in north central Utah westward to the

Sierra Nevada Range in western Nevada. The Salt Lake Valley is a typical valley of the Basin and Range province, which is characterized by north-trending faulted block mountains and intervening deep, sediment-filled basins. The mountains of the Basin and Range are generally bounded on both sides by moderately to steeply dipping normal faults. The intervening basins are filled with up to several hundred meters of lacustrine, alluvial and fluvial deposits derived from the adjacent mountain ranges. The Oquirrh and Wasatch Mountains form the western and eastern boundaries of Salt Lake Valley, respectively (Figures 1-1 and 1-2).

### 1.2.2 Surficial Geology and Sediments Important to Engineering Evaluations

The surficial and shallow geology of the Salt Lake Valley is dominated by Holocene sediments deposited after the regression of Lake Bonneville in shallow lakes, flood plain and river and stream channels that occupy much of the valley (Lund, 1990) (Figures 1-1 and 1-2). In general, the northern I-15 alignment crosses Holocene lacustrine, marsh and alluvial sediments deposited after the last major regression of Lake Bonneville. These recent deposits include clay, silt, sand, peat, and minor gravel. The southern section of the I-15 Reconstruction Project is underlain by Holocene stream alluvium deposited within the Jordan River and its flood plain. The stream alluvium consists of sand, silt, and minor clay and gravel. The deposits of stream alluvium, which reach maximum thickness of about 5 to 10 meters (16 to 33 ft), are underlain by clay, silt, and minor fine sand and gravel deposited by Lake Bonneville.

The total thickness of Lake Bonneville deposits near the northern section of the I-15 Reconstruction Project is not clearly defined, but is usually greater than 10 meters (33 ft). Much of the Salt Lake valley was occupied by Lake Bonneville during the late Pleistocene time (between about 30,000 years ago and 10,000 years ago) (Personius and Scott, 1992). The lake regressed about 10,000 years ago and has since remained close to the present level of the Great Salt Lake.

Underlying the Lake Bonneville deposits is a considerable thickness of alluvial and lacustrine sediments that were deposited between 30,000 and 800,000 years ago (Lund, 1990). Estimates of the total thickness of Pleistocene and Holocene deposits in the Salt Lake Valley range from approximately 600 meters (2,000 ft) to as much as 1,200 meters (4,000 ft) (Adan and Rollins, 1993; Kleinfelder, 1996).

## 1.3 General Discussion of Methods to Determine Soil Properties

There are three general ways to determine engineering properties of foundation soils: (1) laboratory testing; (2) in-situ testing; and (3) back analysis of soil properties using geotechnical instrumentation and field monitoring of geotechnical systems and/or full-scale prototypes. The selection and application of each approach is linked to the local geology, the type of construction and the method of analysis that one intends to adopt for a specific design. There are numerous advantages and disadvantages to each approach. The following paragraphs provide a brief summary as presented by Jamiolkowski et al. (1985).

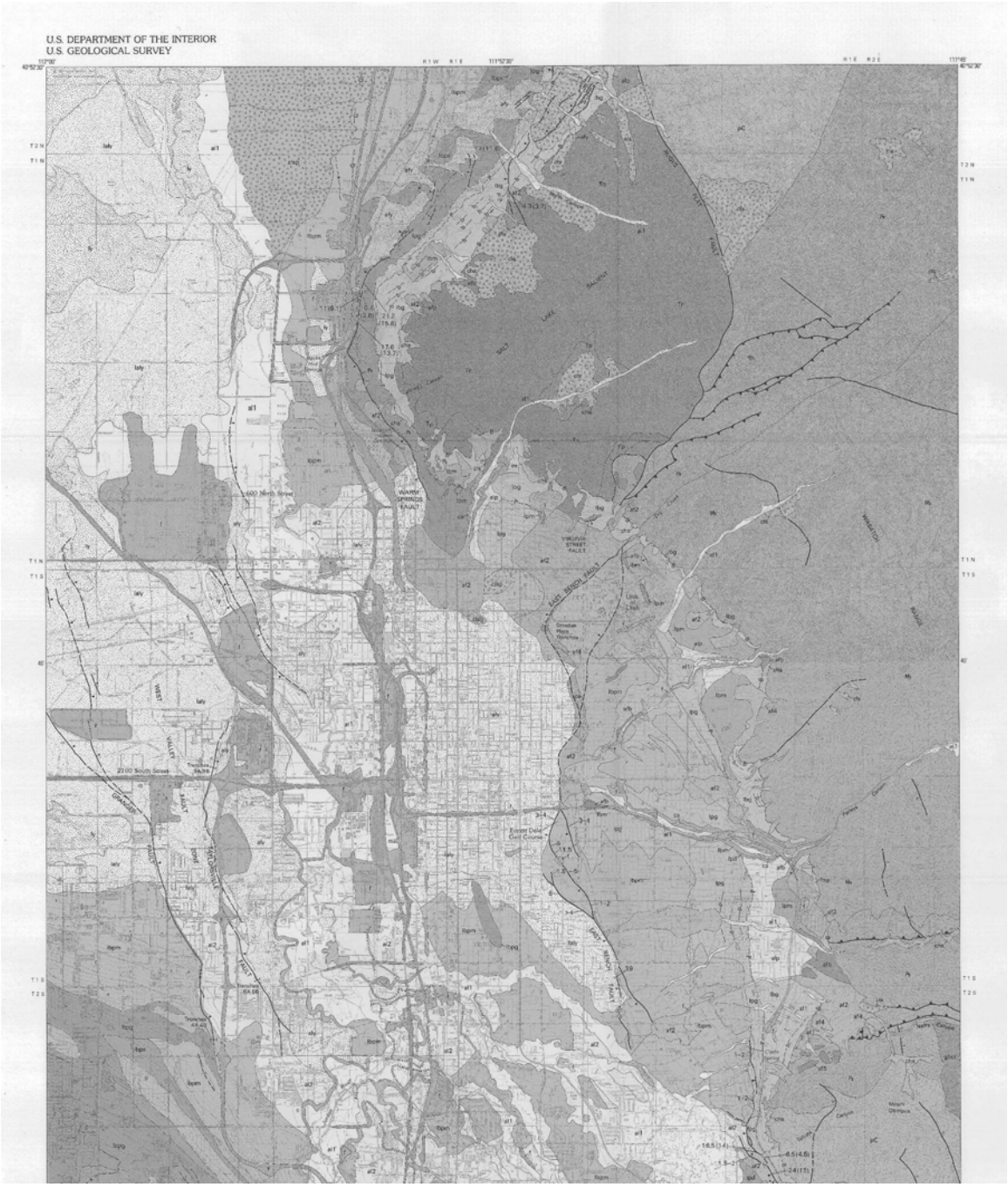


**Figure 1-1 Geological Map of Northern Salt Lake Valley.**

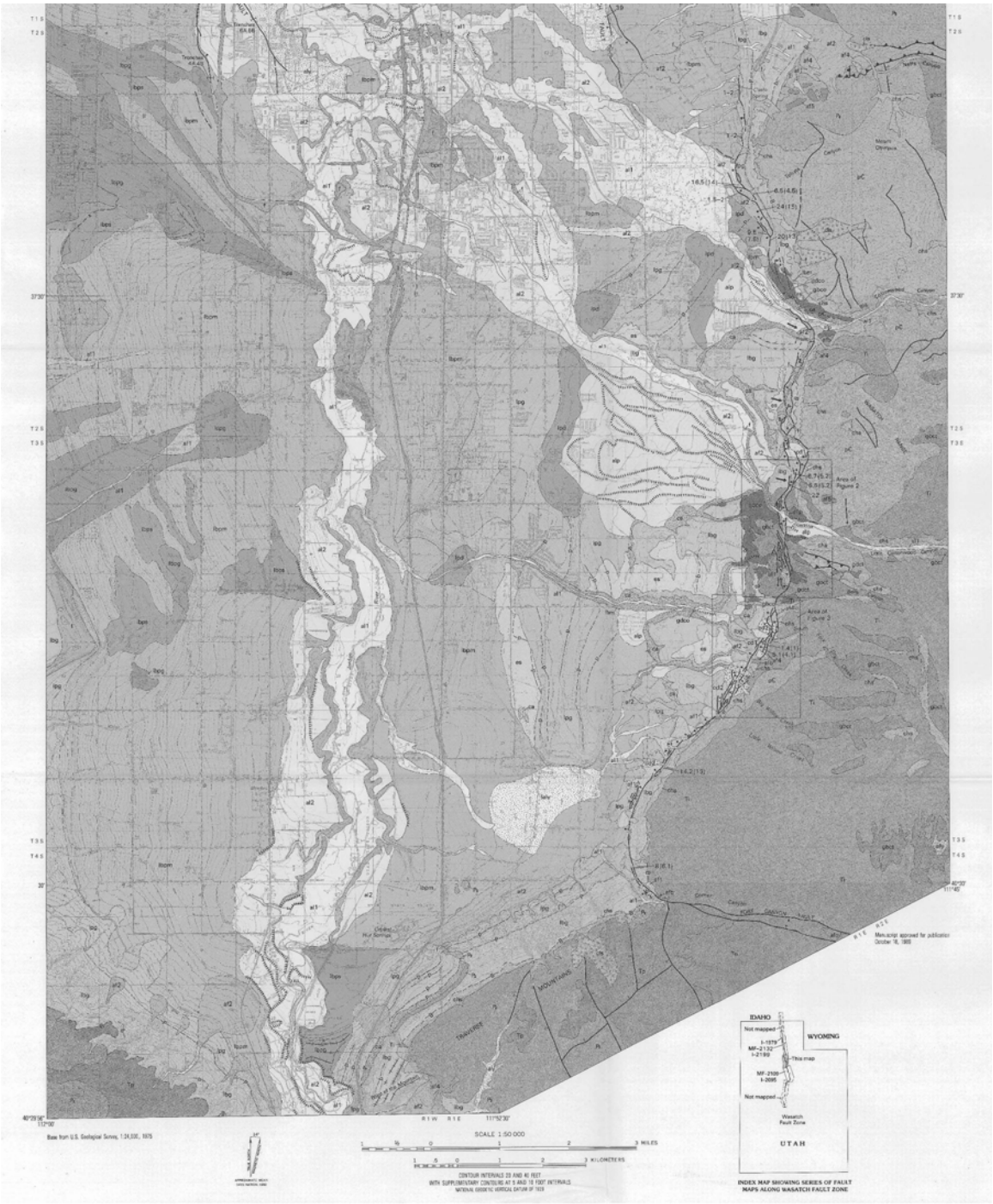


**Figure 1-2 Geological Map of Southern Salt Lake Valley.**

### 1.3.1 Laboratory Tests

There are several *advantages* offered by laboratory tests. In summary these are:

- Well-controlled loading conditions.
- Well-defined boundary conditions.
- Strictly controlled drainage conditions.
- Pre-selected and well-defined stress paths can be followed during the tests.
- Soil nature and physical features are positively identified.

The *disadvantages* of laboratory tests are:

- Effects of sample disturbance are often difficult to measure and are poorly understood for cohesive soils.
- Undisturbed sampling of cohesionless soils is essentially impossible using methods employed in typical geotechnical practice.
- Problems associated with the small volume of laboratory specimens (Rowe, 1972) that often do no incorporate macrofabric and inhomogeneities of natural soil deposits.
- The discontinuous nature of information obtained from laboratory tests may lead to erroneous modeling of the behavior of a large soil mass.
- Boundary conditions in the laboratory may differ from those found in the field.
- The factors associated with the formation of shear planes and shear stress concentrations are poorly understood.
- Higher costs generally associated with determining engineering properties of foundation soils using laboratory.

### 1.3.2 In-Situ Tests

The *advantages* of in-situ testing are:

- A larger volume of soil is tested therefore in-situ tests should in principle reflect more accurately the influence of the macrofabric on the measured soil characteristics.
- Several devices currently in use (e.g., CPT, dilatometer, pressuremeter) produce a continuous record of the soil profile that allows the soil macrofabric

and layer boundaries to be determined. They also allow relatively efficient determination of the distribution of soil layers spatially.

- The distribution of soil layers can be determined relatively precisely both spatially and with depth.
- In-situ tests can be carried out in soil deposits in which undisturbed sampling is still impossible or unreliable.
- The soils are tested in their natural environment that may not be preserved in laboratory tests.
- In general terms, determining engineering properties of foundation soils by means of in-situ techniques is more economical and less time consuming than investigations based on laboratory tests.

The *disadvantages* of in-situ testing are:

- Boundary conditions in terms of stresses and/or strains are generally poorly defined, and a rational interpretation of in-situ tests is often difficult.
- Drainage conditions during the tests are generally unknown and make it uncertain if the derived soil characteristics reflect undrained, drained or partially drained behavior.
- The degree of disturbance caused by advancing the device in the ground and its influence on the test results is generally large but of unknown magnitude.
- Modes of deformation and failure imposed on the surrounding soil are generally different from those of civil engineering structures; furthermore, they are frequently not well established.
- The strain fields are non-uniform and strain rates are probably always higher than those applied in laboratory tests or those that are anticipated in the foundation under a structure.
- The nature of the tested soil is not directly identified by in-situ tests.
- The limitations of in-situ tests lead to a situation in which almost all present interpretation techniques are empirical.

### 1.3.3 Back-Analysis from Instrumentation

In some cases, it is possible to use back analysis to determine the pertinent soil properties for design. Often for cases where back analysis is used, the geometry and deformation behavior of the soil deposit have been measured. This information, in conjunction with numerical modeling or analyses, is used to estimate the soil properties that produced the measured behavior. Because of the classic works by Terzaghi (1950), Skempton and Brown (1961), Skempton and La Rochelle (1965), Peck (1969), Bjerrum (1972), and

Lambe (1973), many accept this procedure as the one that leads to the most reliable assessment of geotechnical design properties.

The *advantages* of back-analysis are:

- The real soil behavior is known and does not have to be estimated.
- It can be used to verify a specific constitutive soil model and its related computation procedure.
- It can assess relevant soil parameters that affect the soil behavior.

The *disadvantages* of back-analysis are:

- Reliable soil parameters may not be guaranteed by a back-analysis of field records alone.
- The soil model and the related computational procedures are either unknown or require many simplifying assumptions.
- The drainage conditions and boundaries are usually unknown and may require simplifying assumptions.
- The initial state variables of the considered problem, including soil stratigraphy, ground water conditions, initial stress state, and stress history of the soil deposit are generally unknown and may require many simplifying assumptions.
- Auxiliary soil characteristics often needed in back-analysis often outnumber the number of parameters that the analysis itself can yield.
- The sensitivity of back-analyzed soil characteristics is not always evaluated with respect to a given set of assumptions.
- There can be substantial differences between soil parameters derived from a back-analysis of field data and those obtained from the analysis of average foundation conditions.

### 1.3.4 Technical Approach

We believe that detailed geotechnical investigations are vital to successful project design. However, such investigations are often costly and there is increasing expectations placed on the practicing geotechnical engineer to economize the investigation and design phases. Subsurface investigations that rely solely on relatively expensive drilling, undisturbed sampling and laboratory testing can deplete limited projects funds rather rapidly. Thus, we believe that it would benefit UDOT if more geotechnical design properties could be obtained from in-situ measurements.

This report contains laboratory, in-situ and back analyses of consolidation properties associated with the clayey sediments that underlie the Salt Lake Valley. The luxury of

being able to use multiple data sources to develop the predictive correlations presented herein was made possible because of the large amount of laboratory, in-situ and field performance measurements obtained from the I-15 Reconstruction Project. This large and important project provided us with an excellent opportunity to develop statistical correlations for improving the efficiency of future geotechnical investigations performed by UDOT and its consultants.

This report focuses on two essential parameters used in settlement calculations: (1) the preconsolidation stress and (2) the compression ratio. Because considerable project funds were expended to define these parameters for the I-15 Reconstruction Project, we believe that it is important that this body of information be synthesized and incorporated in future geotechnical design. We have selected to use the CPT as the in-situ investigative tool of choice due to the large amount of CPT testing that was done for this project. The following section outlines the historical development of the CPT as a subsurface investigative tool. The subsequent sections discuss our screening of the laboratory and field performance data and the correlation of these data with the CPT.

# 2 Historical Development of the CPT Test

## 2.1 Introduction

During the cone penetrometer test (CPT), a cone penetrometer is positioned on the end of a series of rods and is pushed into the ground at a constant rate while continuous measurements are made. The cone penetrometer consists of the cone, friction sleeve and other sensors and measuring systems, as well as the connections to the push rods. CPT systems commonly record the tip resistance and sleeve friction or the tip resistance, sleeve friction and pore water pressure. When pore water pressure measurements are made, the cone is called a piezocone and given the symbol CPTU.

## 2.2 Summary of CPT Development

Probing with rods through weak ground to locate a firmer stratum has been practiced since about 1917. It was in the Netherlands in about 1932 that the CPT was introduced in a form recognizable today. The method has earlier been referred to as the static penetration test, quasi-static penetration test and Dutch sounding test. Current CPT systems can be divided into three main groups: (1) mechanical cone penetrometers, (2) electric cone penetrometers and (3) piezocone penetrometers.

### 2.2.1 1932

The first Dutch penetrometer tests were made in 1932. A gas pipe of 19 mm (0.75 in) inner diameter was used; inside this a 15-mm (0.6 in) steel rod could move freely up and down. A cone tip was attached to the steel rod. Both the outer pipe and the inner rod with the 10 $cm^2$ (1.6 $in^2$) cone with a $60^o$ apex angle were pushed into the ground..

### 2.2.2 1935

Delft Soil Mechanics Laboratory in the Netherlands designed the first manually operated ten-ton cone penetration rig in 1935. The cone was first pushed with a 150 mm (6.0 in) (maximum stroke) and then the outer pipe was pushed until it reached the cone tip. Then the casing and the inner rods were pushed together, until the next level was reached and the tip resistance could be measured again.

### 2.2.3 1948

In 1948, the original Dutch cone test was improved by changing the geometry to prevent soil from entering the gap between the casing and the inner rods. This model is still being used in current practice (Figure 2-1).

### 2.2.4 1953

In 1953, the Dutch cone test was significantly improved by adding a friction sleeve behind the cone. Using this new device, the local friction could be measured in addition to the cone resistance. Typically, measurements were made every 0.2 m (0.7 ft).

### 2.2.5 1965

Figure 2-2 shows the front view of a typical current electrical friction cone with cut-away friction sleeve. Fugro developed an electric cone in 1965 (Figures 2-3 and 2-4). The shape and dimensions of this cone formed the basis for the International Reference Test Procedure (IRTP, 1977, 1989, 1999, 2001).

The main improvements of the electric cone penetrometer are: (1) the elimination of wrong readings due to friction between inner rods and the outer tubes, (2) a continuous testing with a continuous rate of penetration without the need for alternative movements of different parts of the penetrometer, influencing the cone resistance, (3) a continuous reading of the cone resistance and easy recording of the results.

### 2.2.6 1974

Measurement of the pore water pressure and of its dissipation was first made in Sweden in the early 1970s. No measurement of cone resistance or skin friction was possible. In 1973, the Norwegian Geotechnical Institute introduced a pore-pressure probe of the same shape as the reference tip, but again only pore-pressure measurement could be made, and it was necessary to carry out a separate CPT in order to combine the measurements of pore pressure and cone resistance. Alternatively, the pore-pressure results were correlated with adjacent borehole data.

In a separate development in 1969, a piezometer element was incorporated into a 50-kN (11.2 kip) capacity cone penetrometer. This device was without a friction sleeve and was developed for the purpose of measuring the excess pore pressures in sand layers below the Dutch polders. The porous element was placed in the shaft of the tip, immediately above the base of the cone. Subsequent developments involved the combination of pore pressure measurement with measurement of both cone resistance and skin friction.

### 2.2.7 Present

In the CPT and CPTU, a cone on the end of a series of rods is pushed into the ground at a constant rate, and continuous or intermittent measurements are made of resistance to penetration of the cone. If required, measurements are also made of either the combined resistance to penetration of the cone and outer surface of the rods or the resistance of a surface sleeve.

Today there are mechanical and electrical CPT systems in use. Mechanical cones are not as accurate as the electrical cones and should not be used. Both electrical and mechanical types consist of a cone on the end of a series of rods, which are pushed into the ground at a constant rate. Measurements from these two types of cones can be made continuously or intermittently along with the surface sleeve friction. Both the European and American Standards specify that the cone have an apex angle of 60 degrees and the base area cone tip be 10 $cm^2$ (1.6 $in^2$) with a friction sleeve surface area of 150 $cm^2$ (23.3 $in^2$) (ASTM, 1986).

The piezocone (CPTU) has replaced the pore-pressure probe used in the past, and various designs of the piezocone incorporate a porous filter element at the cone point, on the face of the cone, or on the shaft between the cone and the sleeve. The piezocone can be used for profiling and assessment of engineering properties, and may be utilized in various engineering applications such as: (1) assistance in the interpretation of cone resistance and skin friction in terms of shear strength and deformation characteristics; (2) assessment of in-situ permeability and consolidation characteristics; (3) assistance in the assessment of stress history and OCR of cohesive soils; (4) measurement of static porewater pressures and (5) profiling subsurface stratigraphy. The CPTU sounding is particularly useful in mixed soil deposits where it is often difficult to know whether the data indicate drained or undrained conditions using only the CPT.

Also, the electronic piezocone (CPTU) is used to provide hydrogeological profiling for environmental and geotechnical projects. The CPTU provides a rapid, reliable and economical means of determining stratigraphy, relative density, strength and hydrogeological information without generating waste cuttings. The CPTU test is performed in accordance with ASTM standards (D3441). CPTU measurements of cone bearing ($Q_c$), sleeve friction ($f_s$) and dynamic pore water pressure (u) are recorded at 5-cm (2.0 in) intervals during penetration to provide a nearly continuous hydrogeological log. At selected depth intervals, pore water pressure can be monitored over time to determine relative hydraulic conductivity and hydrostatic head. CPT data reduction and interpretation is performed in real time, facilitating the on-site decision making process. Figure 2.5 is an example of a CPTU probe.

### 2.2.8 The Role of the CPT

In current practice, the CPT has three major applications (Meigh, 1987):

1. To determine the soil profile and identify the soils present.
2. To interpolate ground conditions between control boreholes.
3. To evaluate the engineering properties of soils for bearing capacity, settlement and other engineering assessments.

In the third role for certain applications, the evaluation is essentially preliminary in nature, to be supplemented by borings and by other tests (e.g., in-situ or laboratory tests). In this respect, the CPT provides information to aid in deciding on the nature and extent of additional testing. It also helps to determine the positions and depths at which in-situ tests or soil sampling should be undertaken. Where the subsurface geology is fairly uniform and the soil has already been characterized by other laboratory and field measurements, the CPT test has been used as the sole investigation tool for some projects.

The CPT has several advantages over drilling and sampling techniques (Meigh, 1987):

- It provides continuous, or virtually continuous, record of ground conditions. It also avoids the disturbance of the ground associated with boring and sampling, particularly that which occurs with the Standard Penetration Test (SPT).
- It makes measurements of the soil in its in-place, undisturbed state.
- Furthermore, the disturbance resulting from the advancement of the cone is consistent between one test and another.
- There is less variation due to resulting from operator error and handling.
- It is generally less expensive.

In some circumstances one might be tempted to use the CPT solely, however it is usually better to accompany the CPT soundings by additional tests or borings for one or more of the following reasons:

- To assist where there is difficulty in interpretation of the CPT results.
- To further investigate layers with relatively low cone resistance.
- To explore below the maximum depth attainable by CPT.
- To aid in projects that involve excavation, where samples may be required for laboratory testing and where the knowledge of groundwater levels and permeability is required.
- To sample very dense or gravelly soils, where CPT soundings cannot be performed.

The CPTU for the I-15 Reconstruction Project was performed by ConeTec Inc. of Salt Lake City. Only the electrical cone was used in the I-15 studies. The ASTM standard for this test is ASTM D 3441. The CPT testing consisted of CPTU, CPTU with pore pressure dissipation testing and a limited number of SCPT (seismic cone penetrometer).

Generally, CPTU and SCPT soundings were completed to a maximum depth of about 35 to 40 m (115 to 130 ft) on the I-15 Reconstruction Project. Below this depth, the soil is either too dense or too stiff for the reaction capacity of the CPT rig. Woodward-Clyde Consultants provided us with a partial set of the CPT data that covers the area from 600 North to 3300 South Streets. A database containing these soundings has been added to the ArcView GIS database. Hard copy plots of the CPT data are found in Dames and Moore (1996a, b, c) and Kleinfelder (1996a, b, c, d). These files and plots included tip stress, sleeve friction, and pore pressure measurements.

The next section discusses the other types of data obtained from the project and how these data were integrated for our assessment.

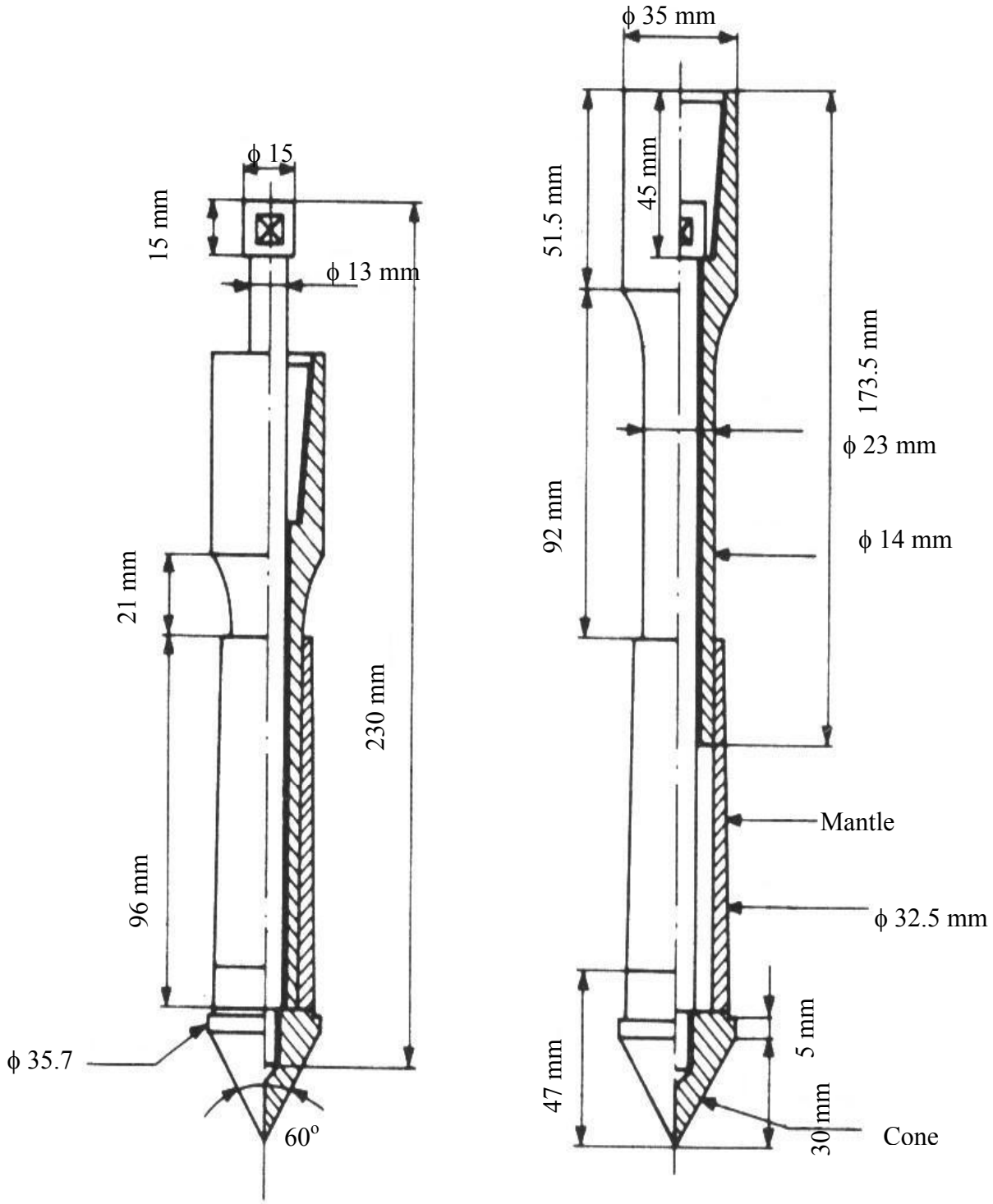


**Figure 2-1 Dutch Cone Penetrometer Tip.**

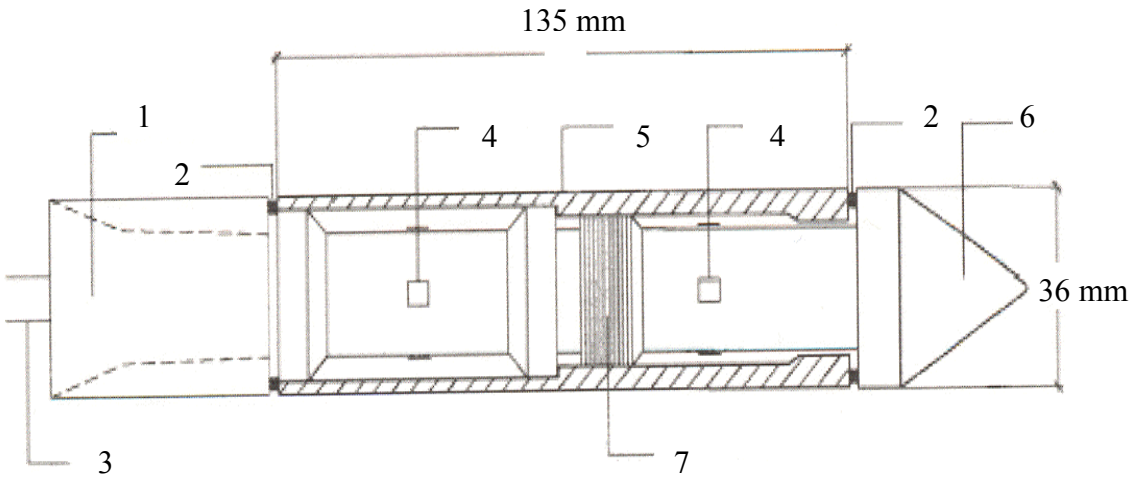


| | | | |
|---|---|---|---|
| 1 | Connection with Rods | 2 | Dirt Seal |
| 3 | Cable | 4 | Strain Gauges |
| 5 | Friction Sleeve | 6 | Conical Point |
| 7 | Screwed Connection with Friction Sleeve | | |

**Figure 2-2 Electrical Friction Cone with Cut-Away Friction Sleeve.**

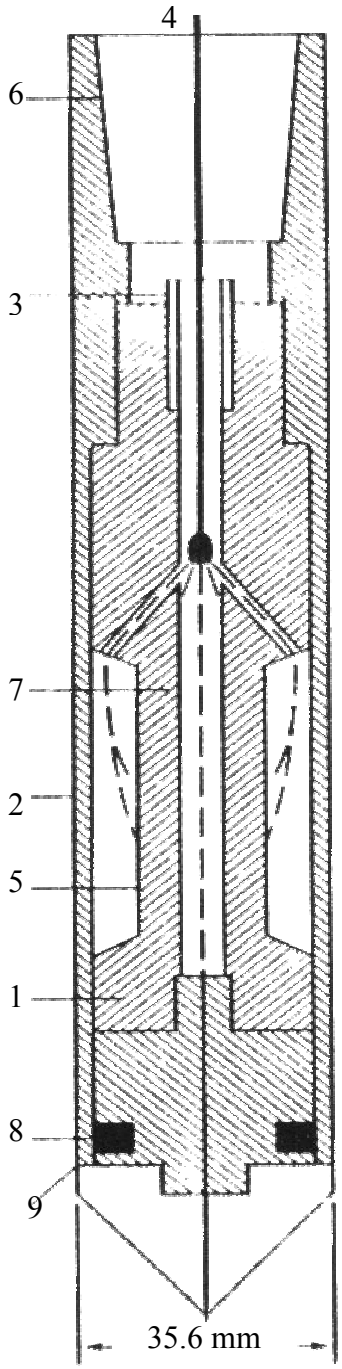


1. Load cell
2. Friction sleeve
3. Waterproof bushing
4. Cable
5. Strain gages
6. Connection with rods
7. Inclinometer
8. O-ring water seal
9. Soil seal

**Figure 2-3 Typical Electric Cone (Bowles, 1996).**

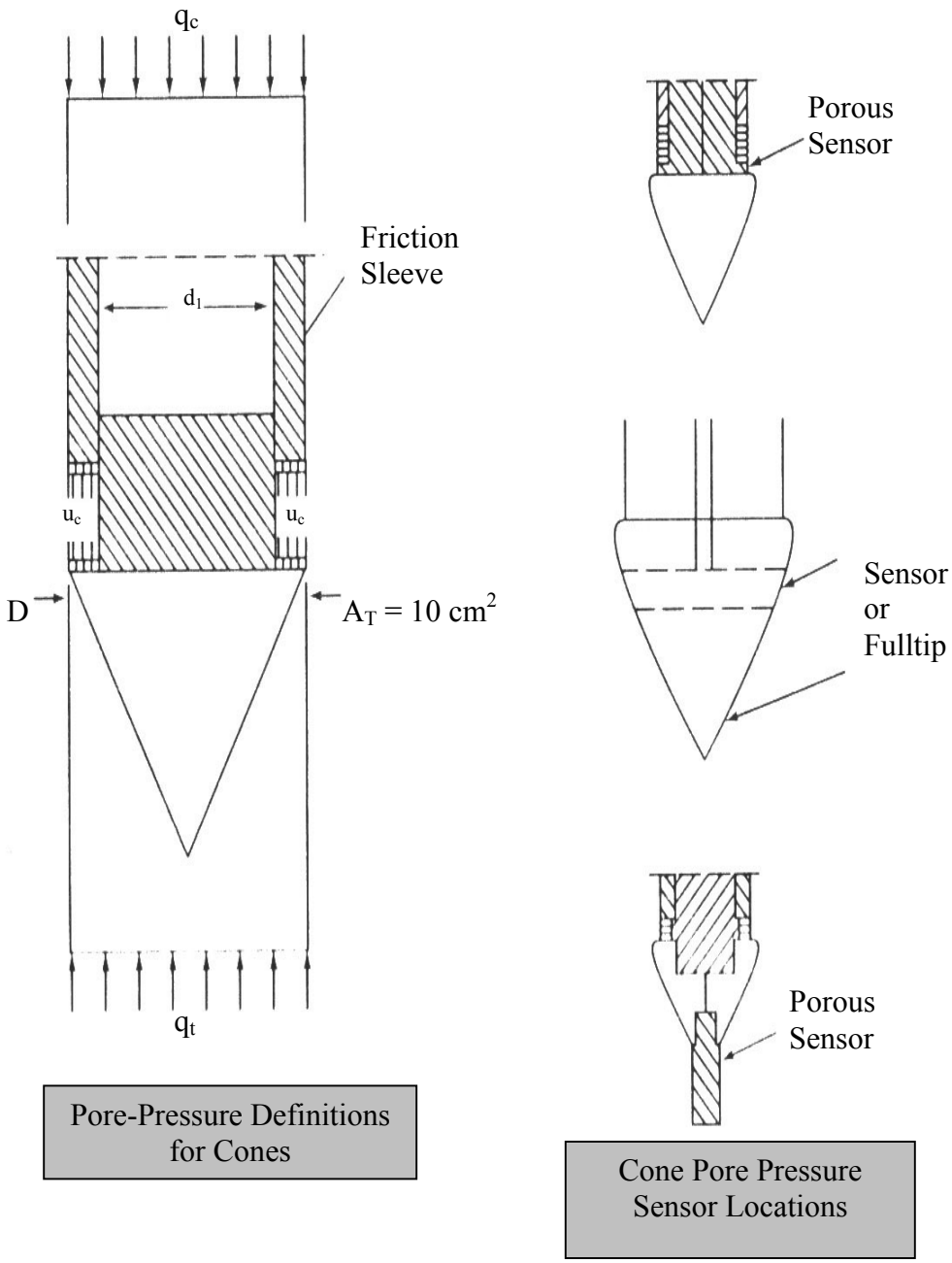


**Figure 2-4 Electric Cone Definitions (Bowles, 1996).**

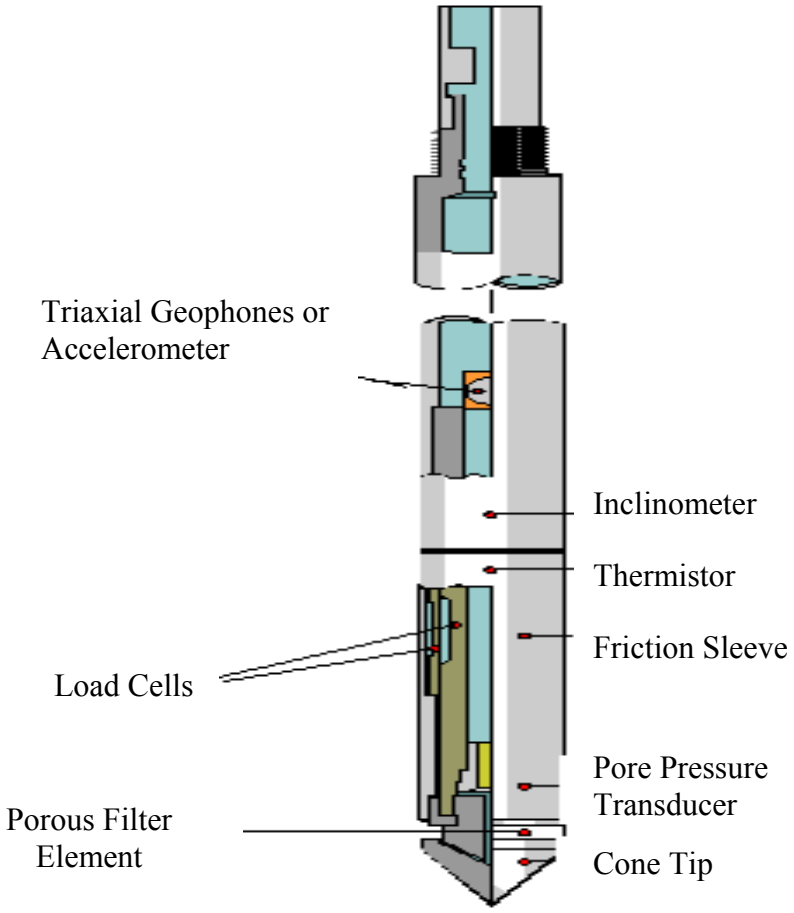


**Figure 2-5 Piezocone Penetrometer Tip.**

Page Left Blank Intentionally

# 3 Analytical Methods

## 3.1 Discussion of Available Data and Data Collection

There was a large amount of geotechnical data gathered from the I-15 Reconstruction Project. The primary sources of data that were incorporated into the design included: (1) borehole logs with SPT and undisturbed (i.e., Shelby tube) samples, (2) CPT soundings, and (3) laboratory consolidation and shear strength tests. These data were collected by various geotechnical firms prior to the bidding and award of the I-15 Reconstruction contract. The corresponding geotechnical reports were supplied to UDOT and the potential design-build teams on compact disk (Dames and Moore, 1996a, b, c; Kleinfelder, 1996a, b, c, d). These disks were supplied to us for this research.

During reconstruction, the design-build contractor also collected additional field monitoring data. The design-build team installed and monitored settlement plates, magnetic extensometers, vertical inclinometers, open and closed-end piezometers and optical surveying of fill heights and settlement monuments. The project team used these data to validate key design assumptions and to assess embankment stability and the time rate of settlement at various locations (Bartlett et al., 2001). Also, during the second phase of the project the construction monitoring data were used to modify the foundation treatment layout and embankment design, as required.

The I-15 Reconstruction Project geotechnical and construction monitoring data cover the part of the interstate that starts in north Salt Lake City (approximately 600 North Street) and extends to as far south as Draper City (approximately 10600 South Street). This is about 17 miles (27 km) of I-15 alignment that runs through the heart of Salt Lake City and its southern suburbs. Much of the monitoring program focused on large embankments in the 2400 South area (i.e., the Spaghetti Bowl Interchange) and the downtown area between 2100 South and North Temple Streets. From a geotechnical perspective, these areas were more problematic because of the presence of soft Lake Bonneville clay layers (Figure 3.1). For example, the clay in a representative CPT sounding from this area begins at the ground surface and extends to a depth of about 15 m (50 ft) . Below this depth are interbedded layers of gravel, sand, silt and clay that were deposited by Pleistocene streams and lakes predating Lake Bonneville.

For design purposes, the design-build contractor grouped the geotechnical data in the northern part of the I-15 alignment into four geographical areas: 600 South, 1300 South, 2400 South, and 3300 South. This research focuses on reducing and interpreting the field, laboratory and construction monitoring data in these areas. Field and laboratory data that were reduced and interpreted include borehole and CPT logs and laboratory oedometer tests. Construction monitoring data that were interpreted and used include settlement plate, magnetic extensometers and fill height versus elapsed time surveys.

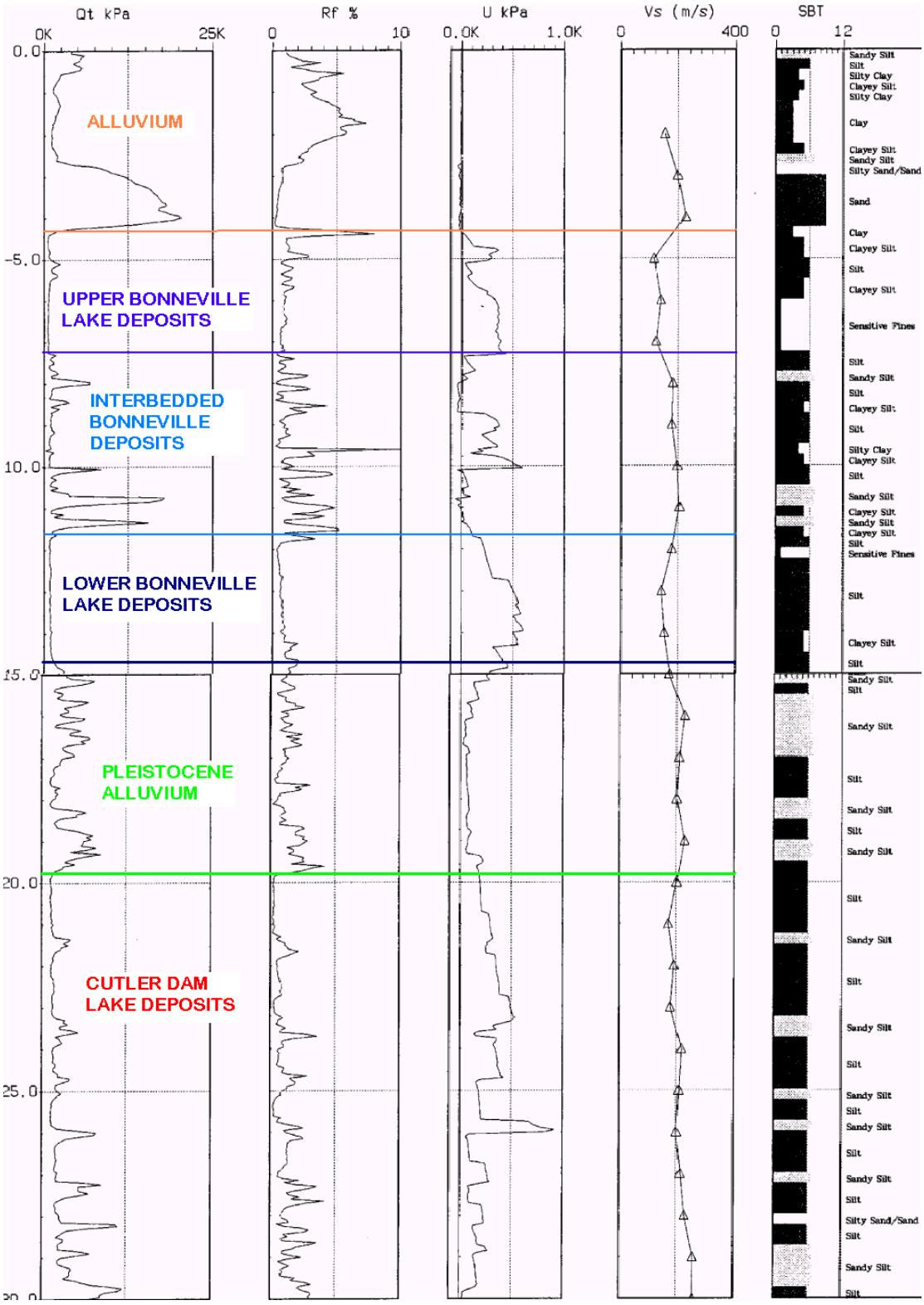


**Figure 3-1 Example of Typical CPT Log from the I-15 Reconstruction Project.**

Unfortunately, there was no contract deliverable requiring the design-build contractor to supply UDOT with the construction monitoring data. Thus, a secondary objective of this research was to compile these data into an ArcView™ GIS database for subsequent evaluation and public use. This has been done and the electronic files were supplied to UDOT Research in an ArcView GIS database. The original data obtained from the design-build team were obtained from unpublished spreadsheets compiled by Terracon Consultants Western Inc. and Woodward-Clyde Consultants (now URS Corporation). Subsequently the spreadsheets were reviewed for duplicates and errors. The reviewed database and compiled data were also included in the ArcView GIS database.

### 3.1.1 Downhole Magnetic Extensometer

The magnetic extensometer can be used to monitor settlement and heave in foundation and embankment soils influenced by excavations, foundations, dams, and other applied loads. It can also be installed behind retaining structures (e.g., sheet piles and slurry walls) and above underground openings (e.g., tunnels and shafts). The advantages of the magnetic extensometer are: (1) it can monitor large settlements, (2) it works with inclinometer casing and can supplement inclinometer data, (3) it is relatively easy to operate, and it indicates incremental settlements and strain. The limitations of the magnetic extensometer are: (1) it requires a skilled operator, (2) it is not easily automated and is labor intensive, (3) it is difficult to install more than 15 or 20 magnets in a single borehole and (4) it can only be installed vertically. The I-15 Reconstruction Project used downhole extensometers (Figure 3.2). Data from the downhole extensometer indicate the depths at which settlement has occurred, the total amount of settlement and the time rate of settlement. Also, because multiple magnets are deployed at various intervals in the borehole (Figure 3.2), the amount of strain in individual soil layers can be determined. To accomplish this, the layer(s) of interest are bracketed (top and bottom) by a set of magnets. The ability to estimate strain in individual layers is the major advantages of this system. This feature will be used to calculate layer compressibility and estimate the preconsolidation stress of bracketed layers, as described later in this report.

A magnetic extensometer generally consists of several magnets and an access pipe that is placed and grouted into a borehole (Figure 3.2). Before installation into the borehole, the cylindrical-shaped magnets are pre-positioned with their “spider” arms in a retracted position along the length of a 25.4 mm (1.0 in) PVC access pipe. The position of each magnet corresponds to the desired installation depth within the borehole. The assembly is then lowered into the borehole and the magnet arms are released causing a springing outward and a coupling of the magnets arms into position in the borehole wall (Figure 3.2). The magnet assembly and PVC access pipe are also stabilized in their desired position by adding a weak grout (bentonitic mud plus a minor amount of Portland Concrete Cement) to the annulus between the borehole sidewall and the outside of the PVC access pipe. Also, telescoping couplers can be used in the PVC casing to allow for compression of the casing as settlement progresses. This is often necessary to prevent “snaking” or “kinking” of the PVC pipe, if the amount of settlement or compression is large. Such couplers were used on the I-15 Reconstruction Project.

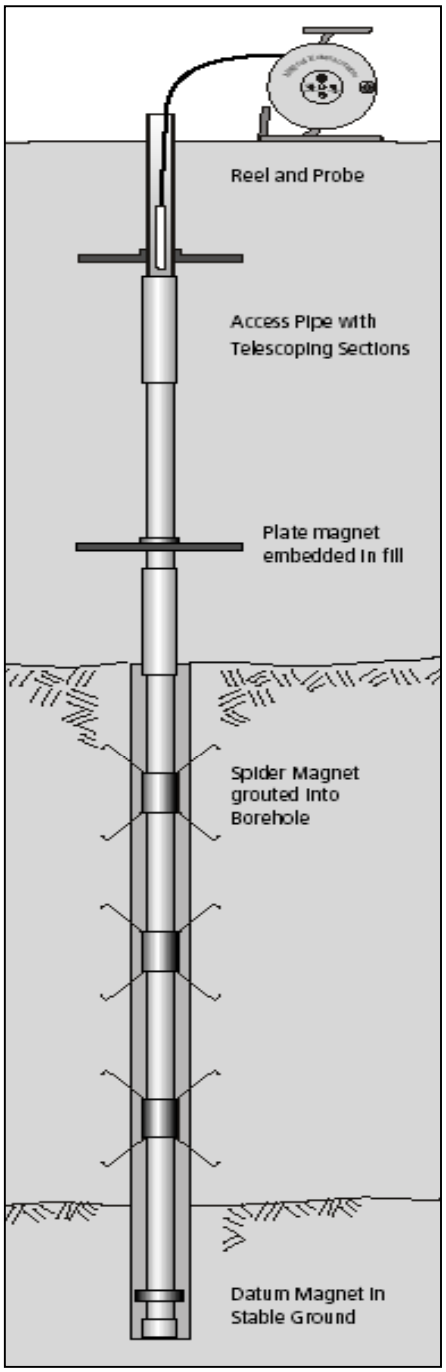


**Figure 3-2 Installation of Magnet Extensometer.**

An electronic sensor or read-out box is required to measure the depth of each magnet. The electronic sensor consists of a torpedo-like probe that is attached to a steel measuring-tape and a tape reel that contains a sensor light and buzzer. The sensor light and buzzer alarm each time the probe passes a magnet as it is lowered into the borehole by the operator. A baseline reading of each magnet's depth is made after the magnets have been positioned and coupled to the surrounding soil. Also, the elevation of the top

of the PVC casing is surveyed. Any subsequent settlement is measured by an increase in depth to each magnet as referenced to the baseline readings.

Readings of the magnet extensometer are made by lowering the probe, which is attached to a measuring tape and reel, through the PVC access pipe to find the depth of each magnet. When the probe enters a magnetic field, a reed switch closes, activating the light and buzzer on the tape reel. The operator then reads the depth on the tape, which has graduations of 3 mm (0.01 ft), and records the depth of each magnet. When the bottom of the access pipe is founded on uncompressible soil or rock, the depth of each magnet is referenced to a datum magnet that is fixed to the bottom of the access pipe. If the bottom of the access pipe is not in stable ground, the depth of each magnet is referenced to the top of the pipe, which is optically surveyed before readings are taken.

Installation and reading of the magnetic extensometers and other instruments used on the I-15 Reconstruction Project were done according to specifications that were developed especially for the project. These specifications include installation details, quality control, data reading, reduction and reporting requirements (UDOT, 1998).

Magnetic extensometer data were taken at about a dozen locations along the I-15 Reconstruction Project alignment. A complete set of magnetic extensometer data is located in the ArcView GIS database. These data and the fill height versus elapsed time measurements at these sites were used to estimate the settlement of various soil layers within the subsurface profile and to interpret the loading conditions that produced the measured settlement. The magnetic extensometer data were also used to help estimate the preconsolidation stress at different depths within the soil profile, as described later.

### 3.1.2 Standard Penetration Test

The Standard Penetration Test (SPT) is used to determine the SPT N value (ASTM D 1586), which is commonly called the "SPT blow count." The SPT N value is an indicator of the soil's density for cohesionless soils and the soil's stiffness for cohesive soils. It also can be empirically correlated to other engineering properties. The test is conducted inside a borehole with a split-spoon sampler attached to the bottom of the drilling rod that is resting on the bottom of the borehole. The split-spoon sampler is then driven into the ground by a drop hammer weighing 68 kg (140 lbs) falling through a height of 760 mm (30 in) and the number of hammer blows is counted. The number of blows required to drive the sampler three successive 150 mm (6 in) increments is recorded. The first increment [0 to 150 mm (0 to 6 in)] is not included in the N value as it is assumed that this interval has been partially disturbed by the drilling process. The SPT N is the number of blows required to achieve penetration in the 150 to 450 mm (6 to 18 in) interval. After the test, the recovered sample is preserved in an airtight container for inspection, classification and soil index property testing.

The SPT N values and soil logs of the split-spoon samples were used in this research to confirm the soil type and other soil index properties. The soil logs and supporting data are found in Dames and Moore (1996a, b, c) and Kleinfelder (1996a, b, c, d).

### 3.1.3 Cone Penetrometer (CPT)

This study focused on CPT soundings that are located between North Temple and 3300 South Street. For some locales, the CPT locations were provided on photocopied plan sheets, but the project coordinates of the CPT locations were not provided electronically. Thus, a digitizing tablet was used to estimate the project coordinates (i.e., project northings and eastings). These layout maps were also used to estimate the elevation of the boreholes and CPT soundings.

The electronic CPT files were plotted and analyzed for those soundings near the magnetic extensometer locations. Figure 3.1 is an example of how the CPT data were plotted to begin the subsurface interpretation at a particular magnetic extensometer location. The CPT plots were used to help identify major soil layers and their depths.

The layering scheme that was adopted consisted of (from top to bottom): Recent Alluvium, Upper Bonneville Clays, Interbeds, Lower Bonneville Clay, older Pleistocene Alluvium, Cutler Dam Lake Deposits (Figure 3.1). These types of plots were also essential for defining the different soil layers that contributed to the settlement. These major soil divisions (Figure 3.1) are generally identifiable in all CPT soundings found along the I-15 alignment from 600 North Street to about 3500 South Street. The CPT data were also used to develop the CPT correlations that will be discussed later in this report.

It is important to note that some of the pore water pressure measurements that were made by the piezocone, as it was pushed through some of the layers, are suspect for some of the CPT soundings. Often, the pore pressure measurement is not typical for a saturated clayey soil until the piezocone has been pushed some distance into the clay layer (Figure 3.3). For example, in this figure, the Bonneville Clay is first encountered at a depth just slightly greater than 5 m (16 ft). However, the pore pressure trace on this log does not show full pore pressure development until about 6.5 m (21 ft). Similarly, there is a lagging pore pressure response starting at a depth of about 10.5 m (34 ft) and continuing to a depth of 12 meters (39 ft).

The lagging response in the pore pressure measurements seems to be associated with partial desaturation of the porous element as it was pushed into dense sands that overlie and are found within the Lake Bonneville deposits. These issues were discussed with the CPT vendor during the I-15 design (Bartlett, personal communication) and it was admitted that the pore pressure data is suspect in some of the soundings. Some investigators have recommended a correction of the pore pressure data as shown in Figure 3.4. However, such a correction linearly-increasing with depth may not always be justified, because there are thin silt layers within the clay that are partially responsible for the “jagged” pore pressure trace seen in the bottom part of Figure 3.4.

In summary, the pore pressure data from the CPTU appears to be the least reliable data in the I-15 Reconstruction CPT data set. The large variations and issues with the pore pressure measurements are probably associated with partial desaturation of the porous element as it was pushed into dense sand and silty sand layers that overlie and are found within the Lake Bonneville deposits. Due to the poorer quality of the pore pressure data, the final CPT correlations herein are based on cone tip resistance and sleeve friction only.

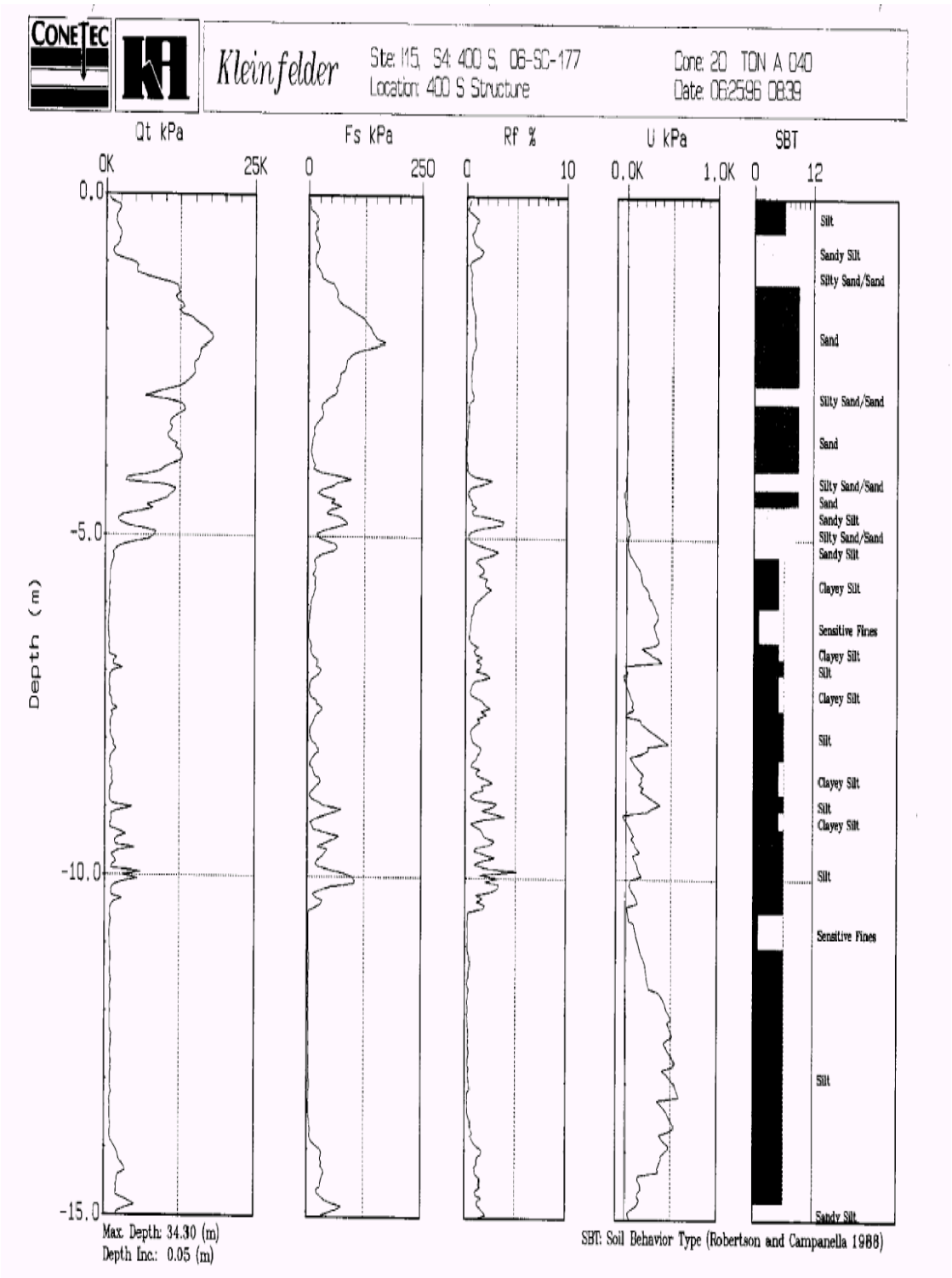


**Figure 3-3 CPT Log with Piezocone Measurements Showing Delayed Pore Pressure Response.**

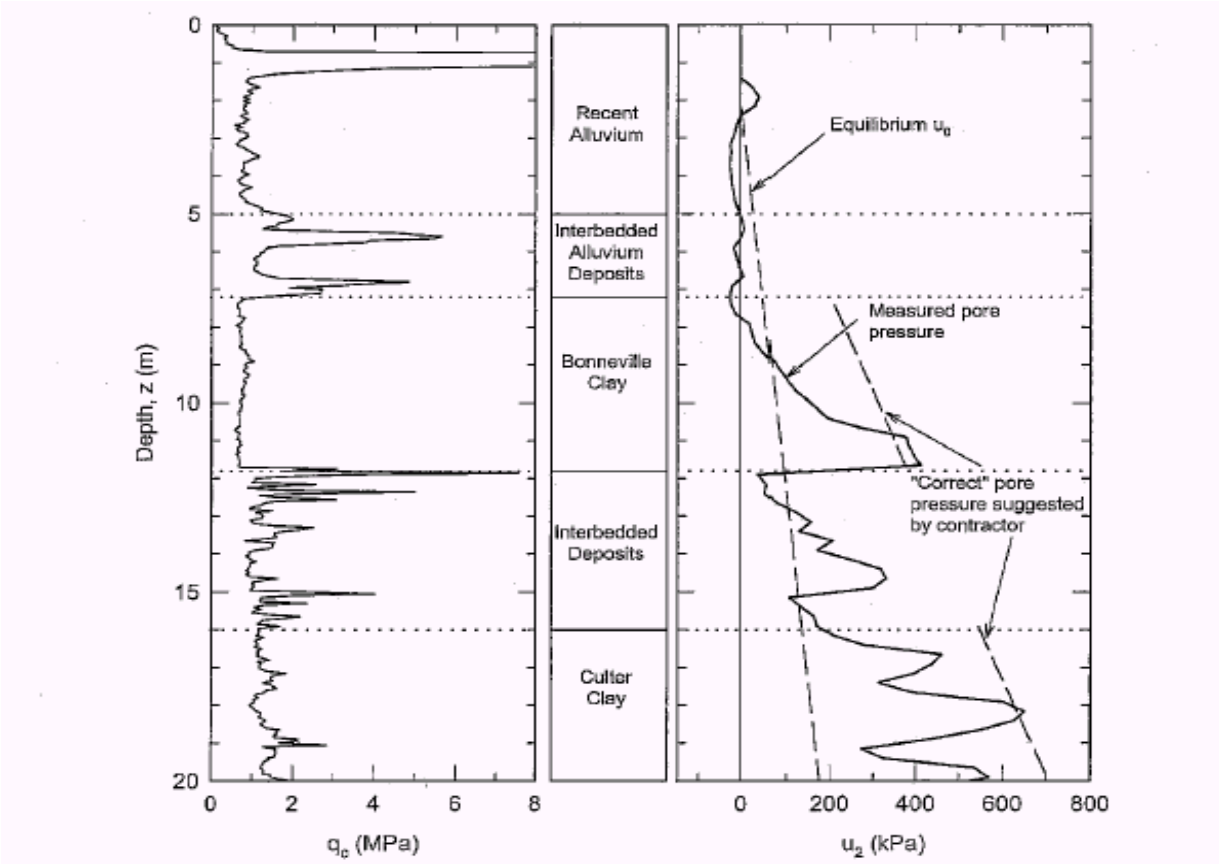


**Figure 3-4 Erroneously Low Pore Pressure Measurements in CPT Sounding from the I-15 Reconstruction Project (after Ladd and DeGroot, 2003).**

### 3.1.4 Sampling

The undisturbed samples for laboratory testing were retrieved from borings advanced with either hollow-stem auger or rotary wash methods. Undisturbed sampling primarily consisted of Shelby tube sampling (76 mm (3.0 in) outside diameter) with a few boreholes sampled by fixed piston methods.

Extensive laboratory testing was performed by various geotechnical firms prior to the start of the I-15 Reconstruction Project. The laboratory data consisted primarily of classification, index, moisture-density, unconfined shear strength and oedometer testing. Kleinfelder (1996a, b, c, d) and Dames and Moore (1996a, b, c) performed the oedometer tests for the geographical areas included in this evaluation. A full set of the consolidation laboratory data used for this analysis is included in the ArcView GIS database.

### 3.1.5 Laboratory Testing

The laboratory shear strength testing performed for the I-15 Reconstruction Project is not part of this scope of this report, so only the consolidation testing will be discussed.

The one-dimensional compression and recompression or rebound characteristics of a soil may be estimated in the laboratory using an incremental load oedometer test (ASTM D2435). A cylindrical specimen of soil enclosed in a metal ring is subjected to a series of increasing static loads, while changes in the void ratio (or thickness) are recorded for each loading increment. From these changes at the end of each loading increment, the compressibility of the soil may be calculated. From a plot of compressibility versus the log of the applied stress, other consolidation parameters may be estimated (e.g., compression index, $C_c$, recompression index, $C_r$, and the compression ratio, CR). Also, if changes in void ratio are plotted versus elapsed time during an individual load increment, the rate of consolidation may be plotted. From these data it is possible to estimate the coefficient of consolidation ($C_v$), which governs the time rate of consolidation. The latter parameter is used to estimate the time required to reach a certain degree of consolidation.

## 3.2 Screening and Interpretation of Laboratory Data

### 3.2.1 Selection of Laboratory Data

This section explains how the laboratory data were screened and interpreted to improve the data quality for subsequent statistical analyses. Screening and consistent interpretation of data is important to improve the reliability of the results. Great measures were taken to eliminate incomplete data and to screen out tests that suffered from excessive sample disturbance. Data were not used if they failed to meet the quality criteria discussed below.

Data were not used for these analyses if portions were missing, incomplete and/or possibly inaccurate from data transcribing. The latter problem was evident from spreadsheet data obtained from some of the geotechnical consultants. Some of these data had missing rows or borehole identifications that did not match the tabulated data. A possible explanation for these errors and omissions is that data files had been transferred from one consultant to the next with very little quality control and checking for accuracy.

Sample disturbance and its effects on sample quality, especially the results of the oedometer testing, are major issues for the analyses contained herein. Drilling and sampling methods and the handling, transportation, storage and test preparation procedures have a strong influence on the degree of sample disturbance. As a prelude to the sample disturbance issue, C. C. Ladd (personal communication) suggested that many of the Shelby tube samples from the I-15 Reconstruction Project had evidence of moderate to significant sample disturbance. (C. C. Ladd is a professor at MIT and was also a senior consultant to Woodward-Clyde Consultants and aided in the review and design of the I-15 project.) Also, Holtz and Kovacs (1981) discuss the effects and evidence of sample disturbance. In short, sample disturbance increases the slope of the recompression curve (i.e., $C_r$ increases), decreases the slope of the virgin compression curve (i.e., $C_c$ decreases) and adds uncertainty in selecting the preconsolidation stress due to the roundness of the consolidation curve.

It is important to this research that reliable estimates of consolidation properties are obtained from representative samples. Otherwise, the use of poor or overly disturbed

samples will introduce bias into the regression analyses and design process. However, past experience has shown that it is difficult to obtain soil samples of the Lake Bonneville deposits for laboratory testing without causing some level of sample disturbance. Because of this, C. C. Ladd (personal communication) recommended that the geotechnical state of practice be changed in the Salt Lake Valley to include: (1) mud rotary drilling for better borehole stabilization, (2) piston sampling, (3) sample quality assessment using X-ray radiography to view sample quality and (4) special handling and extrusion procedures as described by Ng (1998). These recommendations are currently being researched by the University of Utah and Utah State University. However, these recommendations were made after the I-15 Reconstruction Project data were gathered, and they were not implemented for the dataset used in this report.

The initial review of the data showed that many of the consolidation curves from the I-15 oedometer testing had evidence of sample disturbance. This conclusion was reached by observing the roundness (i.e., lack of a sharp break) between the recompression line and virgin compression line in the oedometer data. Thus, the data needed to be screened to remove poorer quality tests. To this end, the sample quality criteria given by Anderson and Kolstad (1979) were used in this report. The Anderson and Kolstad (1979) criteria are a quantitative assessment of the level of disturbance. The I-15 design team also used these same criteria to screen the oedometer data that was to be used in the design process (Saye and Ladd, 1999).

Anderson and Kolstad (1979) suggest that the vertical strain required to consolidate the sample back to its in situ vertical effective stress ($\sigma'_{vo}$) is a relative indicator of sample quality. Ideally, very little strain should be measured upon recompression of the sample back to $\sigma'_{vo}$. One the other hand, if large strain occurs in recompression, then the sample may suffer from disturbance. The table below shows the "sample quality designations" used by Anderson and Kolstad (1979).

**Table 3-1 Sample Quality Designations**

| Vertical Strain | Sample Quality Level. |
|---|---|
| < 1% | A |
| 1-2% | B |
| 2-4% | C |
| 4-8% | D |
| > 8% | E |

Sample quality level A is very good to excellent, quality level B is good, quality level C is fair, quality level D is poor and quality level E is very poor. Data with a "sample quality level" of D or E were screened out of the data set and are not used in this report due to the potential of introducing large bias into the subsequent analyses.

To use the Anderson and Kolstad (1979) criteria, one must calculate the vertical strain level at the in-situ vertical effective stress. The vertical strain level was calculated from the following equation:

$$\varepsilon(\%) = [(H_{so} - H_s) / (H_{so})] \times 100 \qquad 3\text{-}1$$

where:

$H_{so}$ = Initial Sample Height

$H_s$ = Sample Height at $\sigma'_{vo}$

Also, the in-situ vertical stress was calculated for the corresponding depth of the sample found on the soil log or laboratory data sheet. The saturated soil unit weights given in Section 3.3.1 were used for the effective stress calculations. These estimates were made by Woodward-Clyde (1997) and are average values for the various soil layers for the I-15 Reconstruction Project geotechnical data.

### 3.2.2 Interpretation of Laboratory Consolidation Curves

The oedometer data for the I-15 Reconstruction Project was provided in two different formats: (1) void ratio versus log of vertical effective stress and (2) vertical strain versus vertical effective stress. Kleinfelder (1996a, b, c, d) provided consolidation curves with vertical strain plotted on the y-axis and vertical effective stress on the x-axis. Dames and Moore (1996a, b, c) provided void ratio (y-axis) versus vertical effective stress plots. These different data formats required that the data be converted to a common format before they could be analyzed. Thus, the Kleinfelder data was converted to void ratio versus vertical effective stress using the equations given below. To make the conversion, the initial void ratio was first calculated from the information given on the laboratory data sheets. The formulas and derivations to do this are as follows:

$$e_o = V_v / V_s \qquad 3\text{-}2$$

$$V_v = 1 - V_s \qquad 3\text{-}3$$

$$V_s = \frac{M_S}{\rho_S} = \frac{W_S}{\gamma_S} = \frac{\gamma_d}{G_S * 9.81 \frac{kN}{m^3}} \qquad 3\text{-}4$$

where:

Vv = Volume of voids

Vs = Volume of solids

$M_s$ = Mass of the solids

$W_s$ = Weight of the solids

$\gamma_d$ = Dry unit weight of soil

$\gamma_s$ = Unit weight of the solids

$\rho_s$ = Density of the solids

$G_S$ = Specific gravity of the soil

The change in void ratio ($\Delta e$) was then calculated using the following steps:

$$\Delta e = e_o - e_f \qquad 3\text{-}5$$

Vertical strain and void ratio are then related by:

$$\varepsilon = \Delta e / (1 + e_o) \qquad 3\text{-}6$$

Once the oedometer data were converted to a common format, it was then possible to begin the data interpretation. The consolidation properties of most interest to this study are the preconsolidation stress, $\sigma'_p$, and the compression ratio, CR.

### 3.2.3 Calculation of Preconsolidation Stress from Laboratory Data

There are different methods of determining $\sigma'_p$ from laboratory oedometer data. Casagrande (1936) developed the most commonly used method and this method which was used in this report. Figure 3.5 shows the Casagrande (1936) as described in Holtz and Kovacs (1981). The following steps describe this construction.

1. Choose by eye the point of minimum radius (or maximum curvature) on the consolidation curve (point A in Fig. 3.5)
2. Draw a horizontal line from point A.
3. Draw a line tangent to the curve at point A.
4. Bisect the angle made by steps 2 and 3.
5. Extend the straight-line portion of the virgin compression curve up to where it meets the bisector line obtained in step 4. The point of intersection of these two lines is the preconsolidation stress (point B of Fig. 3.5).

### 3.2.4 Calculation of Field Consolidation Curve from Laboratory Data

In addition to the preconsolidation stress, it is possible to estimate the compression index, $C_c$, and compression ratio, CR for these data. However, an additional correction to the virgin compression curve is required to minimize the effects of sample disturbance as developed by Schmertmann (1955). The Schmertmann correction allows for disturbance of the clay due to sampling, transportation, and storage of the sample plus subsequent trimming and reloading during the consolidation test. This correction allows for a more direct comparison between compressibility measured in the laboratory oedometer test with that measured in the field by the magnetic extensometers.

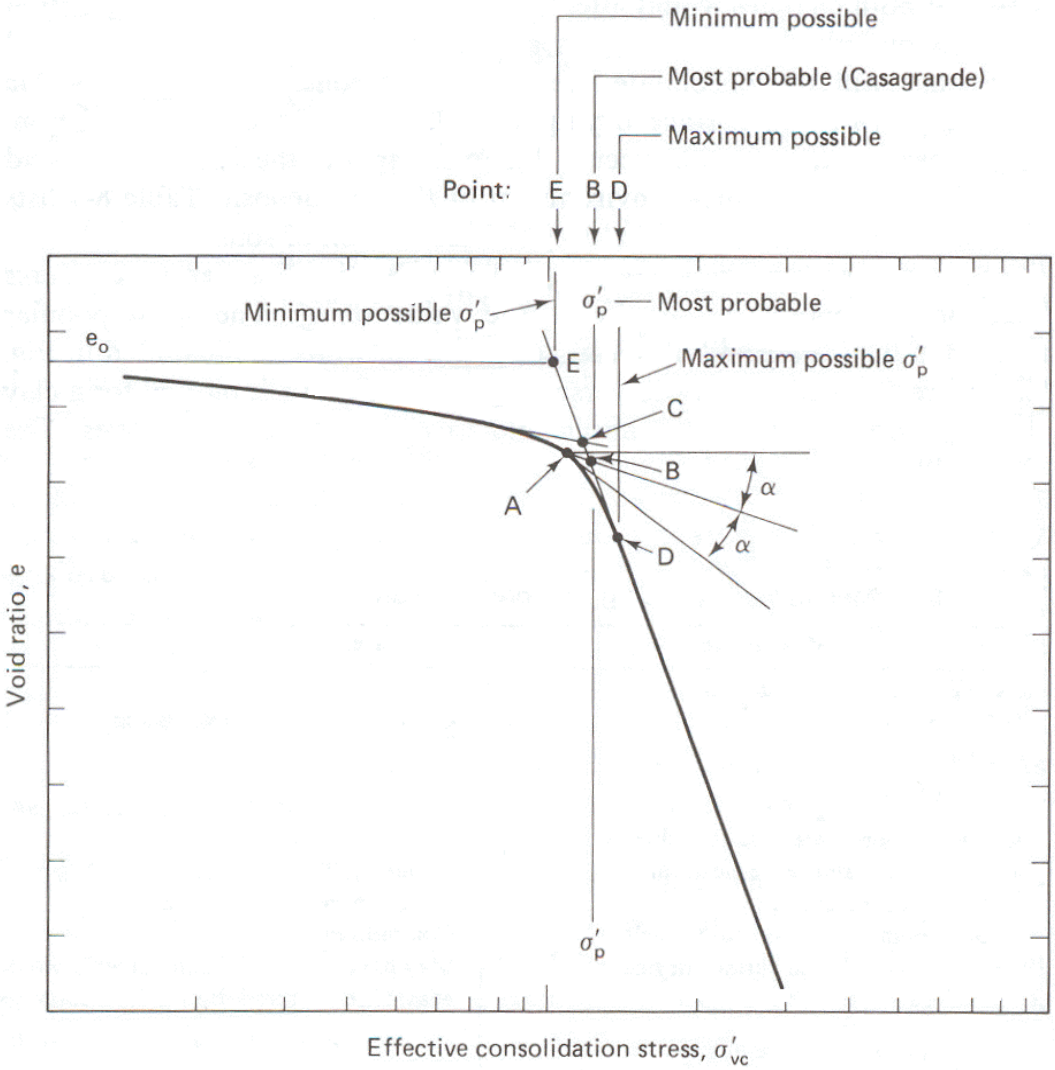


**Figure 3-5 Casagrande's Method for Determining Preconsolidation Stress (Holtz and Kovacs, 1981).**

The laboratory consolidation curves were corrected to a "field consolidation curve" as shown in Figure 3.6. The Schmertmann (1955) correction procedure for overconsolidated soil, as given in Holtz and Kovacs (1981), is described below. (The overconsolidation construction was selected because experience has shown that the clays along the I-15 alignment are overconsolidated.)

1. Perform the Casagrande (1936) construction and evaluate the preconsolidation pressure $\sigma'_p$
2. Calculate the initial void ratio $e_o$. Draw a horizontal line from $e_o$, parallel to the log effective stress axis, to the existing vertical overburden pressure $\sigma'_{vo}$. This establishes control point 1, illustrated by triangle 1 in Fig. 3.6.

3. From control point 1, draw a line parallel to the rebound-reload curve to the preconsolidation pressure $\sigma'_p$. This will establish control point 2, as shown by triangle 2 in Fig. 3.6.

4. From a point on the void ratio axis equal to 0.42 $e_o$, draw a horizontal line, and where the line meets the extension of the laboratory virgin compression curve L, establish a third control point, as shown by triangle 3. The coefficient of $e_o$ is not a "magic number," but is a result of many observations on different clays.

5. Connect control points 1 and 2, and 2 and 3 by straight lines. The slope of the line F joining control points 2 and 3 defines the compression index $C_c$ for the field virgin compression curve. The slope of the line joining control points 1 and 2 of course represents the recompression index $C_r$.

Schmertmann (1955) describes the assumption made in using a 0.42 $e_o$ value for the anchor point (i.e., virgin-slope intersection point) of the field curve (Figure 3.6). Because the intersection of the field initial virgin slope with the initial virgin slopes of laboratory consolidation tests ranges from about 40 to 46 percent of the sample's initial void ratio, $e_0$, Schmertmann (1955) recommended that an initial virgin-slope intersection point at 42 percent of $e_o$ be used as a reasonable estimate for most clays.

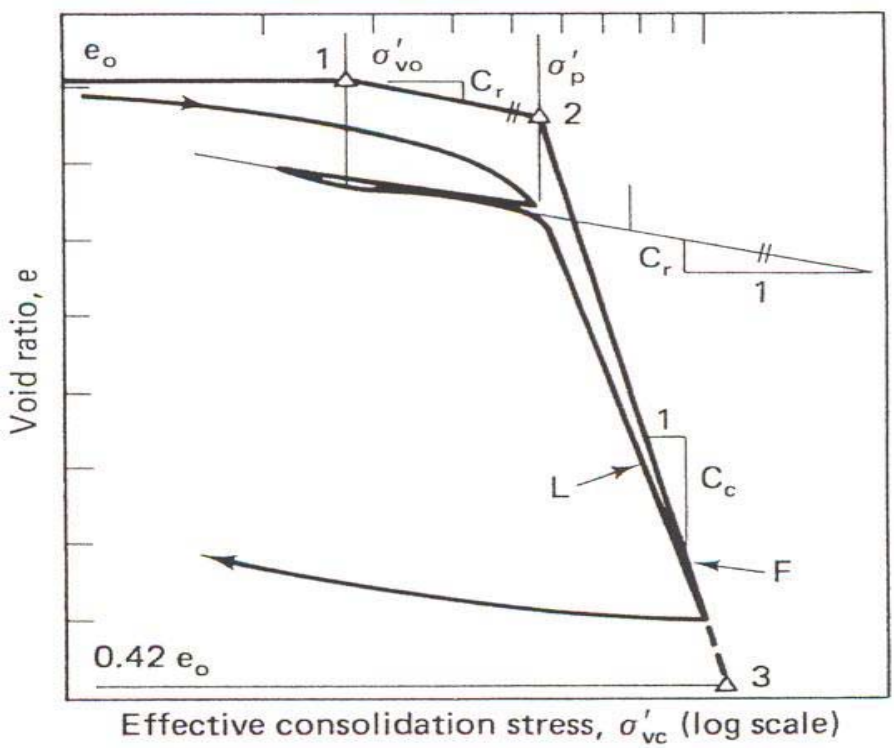


**Figure 3-6 Illustration of Schmertmann Procedures to Obtain the Field Virgin Compression Curve for OC Soil (Holtz and Kovacs, 1981).**

Because the Kleinfelder (1996a, b, c, d) consolidation curves were reported in terms of vertical strain, ε, and not void ratio, e, the following relations were used in applying the Schmertmann (1955) technique to Kleinfelder's data:

$$e_f = 0.42\ e_o \qquad 3\text{-}7$$

$$\Delta e = e_o - 0.42 e_o \qquad 3\text{-}8$$

$$\Delta e = 0.58 e_o \qquad 3\text{-}9$$

$$\varepsilon = \Delta e / (1 + e_o) \qquad 3\text{-}10$$

$$\varepsilon = 0.58\ e_o / (1 + e_o) \qquad 3\text{-}11$$

Using the equivalent of Δe written in terms of strain (Eq. 3-10) made it possible to correct the Kleinfelder consolidation curves using the Schmertmann (1955) technique. Also for these data, the slope of the field corrected virgin compression curve produces the compression ratio, CR, instead of the compression index, $C_c$. However, the two definitions of slopes can be related by the following:

$$C_c = CR * (1+e_0) \qquad 3\text{-}12$$

Figure 3.7 is an example of the correction method outlined above, as applied to a compression curve obtained from the Kleinfelder (1996a, b, c, d) consolidation curves.

When a vertical stress versus void ratio consolidation curve is used (e.g., Dames and Moore consolidation curves), then $C_c$ can be corrected to a field $C_c$ value without applying Equations 3-7 through 3-11. The field corrected $C_c$ value can then be converted to a field corrected CR value by using Equation 3-12. (Another symbol used for CR is $C_{c\varepsilon}$ (Holtz and Kovacs, 1981). However, the remainder of this text uses the symbol CR, which is meant to be a field corrected virgin compression ratio.)

## 3.3 Interpretation of Consolidation Properties from Magnet Extensometer Data

The primary goal of interpreting the magnetic extensometer data was to see if these data could be used to estimate the preconsolidation stress and the compression ratio for the various geologic units in the soft soil profile that is found the central part of the Salt Lake Valley. This section discusses how the fill height associated with beginning of primary consolidation was calculated from the data available at each magnet extensometer installation. This section also discusses how the strains associated with recompression and virgin compression were calculated by using differences in the magnet elevations at beginning and end of primary consolidation. It also explains how the settlement data were extrapolated to estimate the end of primary consolidation for magnet extensometer installations where the surcharged fill was removed before the end of primary consolidation had been reached. Section 3.4 discusses the numerical modeling that was required to estimate the vertical effective stress associated with the beginning and end of primary consolidation.

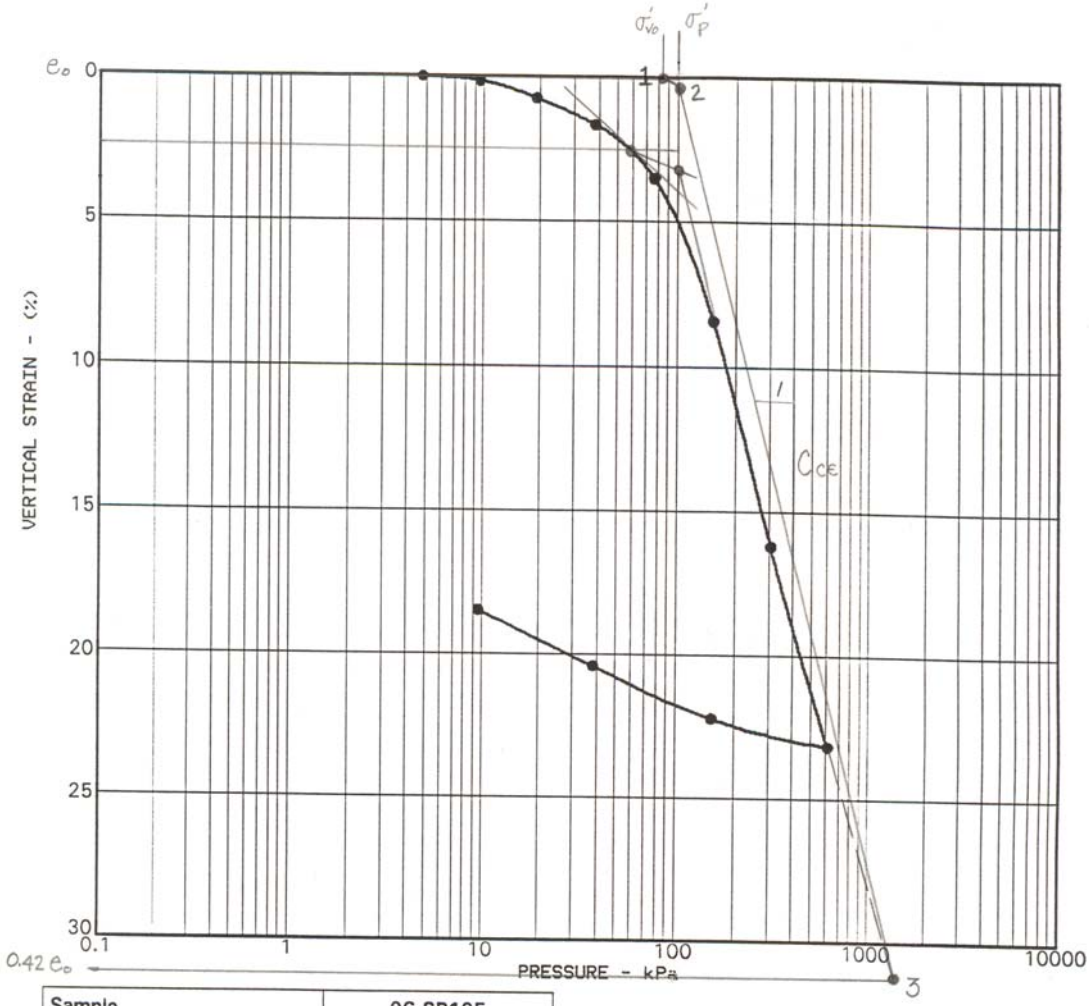


| | |
|---|---|
| Sample | 06 SB105 |
| Depth | 7.6 m |
| Description | Elastic SILT |
| USCS Classification | MH |
| Overburden Pressure | 84 kPa |
| Preconsolidation Pressure | 100 kPa |
| Compression Index | 0.224 |
| Recompression Index | 0.030 |
| Overconsolidation Ratio | 1.2 |

| | Initial | Final |
|---|---|---|
| Dry density, kN/m^3 | 10.0 | 12.3 |
| Water content, % | 60.6 | 45.5 |
| Sample height, mm | 25.40 | 20.71 |

Water added at initial load

KLEINFELDER

PROJECT NO. 30-8146-02

I-15 Corridor Reconstruction
Section 4: 600 South Interchange

CONSOLIDATION TEST

PLATE

E-201

**Figure 3-7 Illustrations of Schmertmann (1955) and Casagrande (1936) Techniques to Find the Preconsolidation Stress and the Field Consolidation Curve.**

### 3.3.1 Development of Subsurface Profile

Before the magnet extensometer data could be interpreted, it was important to assign the magnet positions to their respective geologic units. This aided in the interpretation of the magnet extensometer data and also allowed for a comparison of the preconsolidation stress and compression ratio within each geologic unit.

As discussed previously, the soil samples for the I-15 Reconstruction Project were taken from six different geologic units: Recent Alluvium, Upper Lake Bonneville, Interbedded Lake Bonneville, Lower Lake Bonneville, Pleistocene Alluvium, and Cutler Dam Lake Deposits. These six soil layers were defined by interpreting CPT data, field logs, and laboratory testing. The effective and total stress calculations used in the numeric modeling (Section 3.4) also required estimates of the soil's unit weight. The unit weights listed in Tables 3.2 and 3.3 were obtained from Woodward-Clyde (1997). The unit weights for the above geologic units were estimated from the average (i.e., mean) of all laboratory tests performed in their respective geographical area. Table 3.2 is for the 600 South design segment and Table 3.3 is for the 2400 South design segment. These mean values were used to estimate the total and effective vertical stresses of the various layers.

**Table 3-2 Average Unit Weights for Soil Layers in the 600 South Design Area**

| Depth (Meters) | Soil Type | Unit Weight ($kN/m^3$) |
|---|---|---|
| 0 – 5 | Alluvium | 19.2 |
| 5 – 12 | Upper Bonneville | 18.2 |
| 12 – 16 | Interbeds | 18.8 |
| 16 – 22 | Lower Bonneville | 18.2 |
| 22 – 25 | Pleistocene | 19.5 |
| 25 – 30 | Cutler Dam | 18.4 |

**Table 3-3 Average Unit Weights for Soil Layers in the 2400 South Design Area**

| Depth (Meters) | Soil Type | Unit Weight ($kN/m^3$) |
|---|---|---|
| 0 – 5 | Alluvium | 19.2 |
| 5 – 11 | Upper Bonneville | 18.2 |
| 11 – 14 | Interbeds | 18.8 |
| 14 – 22 | Lower Bonneville | 18.2 |
| 22 – 26 | Pleistocene | 19.5 |
| 26 – 30 | Cutler Dam | 18.4 |

### 3.3.2 Available Magnetic Extensometer Data

Magnetic extensometer data was evaluated for eight locations that ranged from 500 North Street to 2400 South Street. The data were obtained from the I-15 design team (Terracon) in spreadsheet format and, for the most part, have not been published. A complete set of data is located in the ArcView GIS database.

The magnetic extensometer data were provided by the I-15 Reconstruction Project design-build team in terms of date, elevation and settlement. Optical surveying was done to the top of the magnet extensometer PVC casing to establish the initial elevation of each magnet. Survey and reading of the depth to each magnet was also repeated during the project, so that changes in elevation could be tracked as settlement progressed.

The settlement plots developed herein included elapsed time (x-axis) and settlement (y-axis) for each magnet in the borehole. Figure 3.8 is an example of one of the magnet plots and the corresponding fill height versus time that caused the settlement at the magnet array.

### 3.3.3 Calculation of Beginning of Primary Consolidation Settlement

The magnetic extensometer measures settlement that occurs in recompression and virgin compression. If the strain associated with recompression is not separated from the virgin compression strain, then estimates of the compression ratio (CR) will be incorrect. Thus, it was necessary to eliminate the recompression settlement from the CR calculation. To do this, it was necessary to accurately identify the fill height that corresponds to the beginning and the end of primary consolidation (BOP and EOP), respectively. This was done using the magnet extensometer data and the corresponding fill height versus time data.

For example, plots like Figures 3.8 and 3.9 were used to separate recompression from virgin compression. In constructing the plots, fill-height versus settlement curves were made for each of the extensometer locations. Then, the settlement associated with individual layers was calculated by subtracting the settlement associated with the deeper layers. (Note that each magnet records an aggregate settlement of all layers found below the magnet of interest.) Next, from the settlement plot for each layer and the corresponding fill height versus time plot, it was possible to tell when virgin compression was triggered in each layer. This step was relatively easy because of the abrupt change in slope of the layer settlement curve. This abrupt change was seen as a marked increase in the rate of settlement (Figure 3.9). The fill height and corresponding date that produced the sharp increase in settlement for each layer was used as the beginning of primary settlement (BOP) (i.e., virgin compression settlement).

The recompression part of the settlement curve was estimated as the settlement that occurred prior to the BOP, or in other words prior to the occurrence of a sharp increase in the rate of settlement.

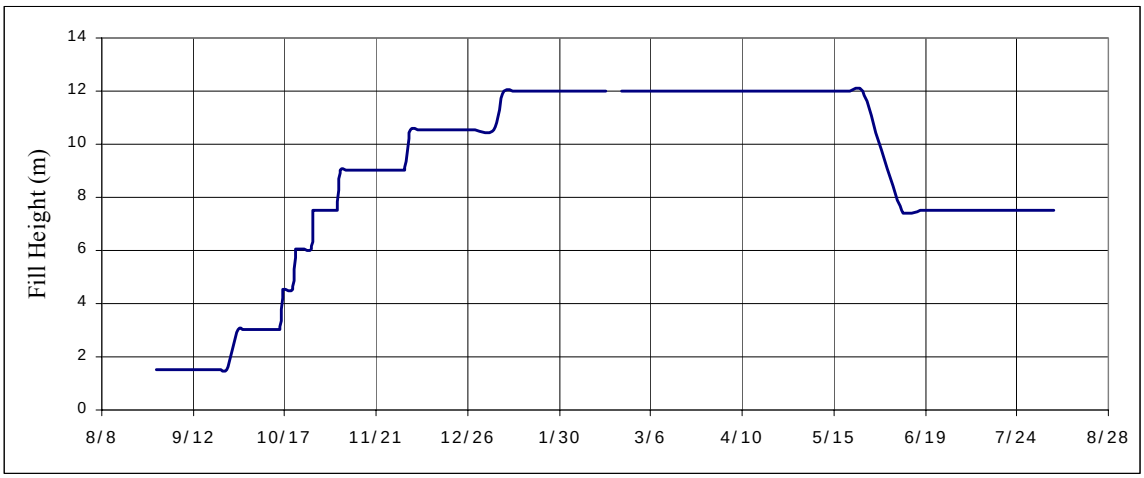


**Figure 3-8 Example of Fill Height Versus Elapsed Time Data from the I-15 Reconstruction Project, Salt Lake City, Utah.**

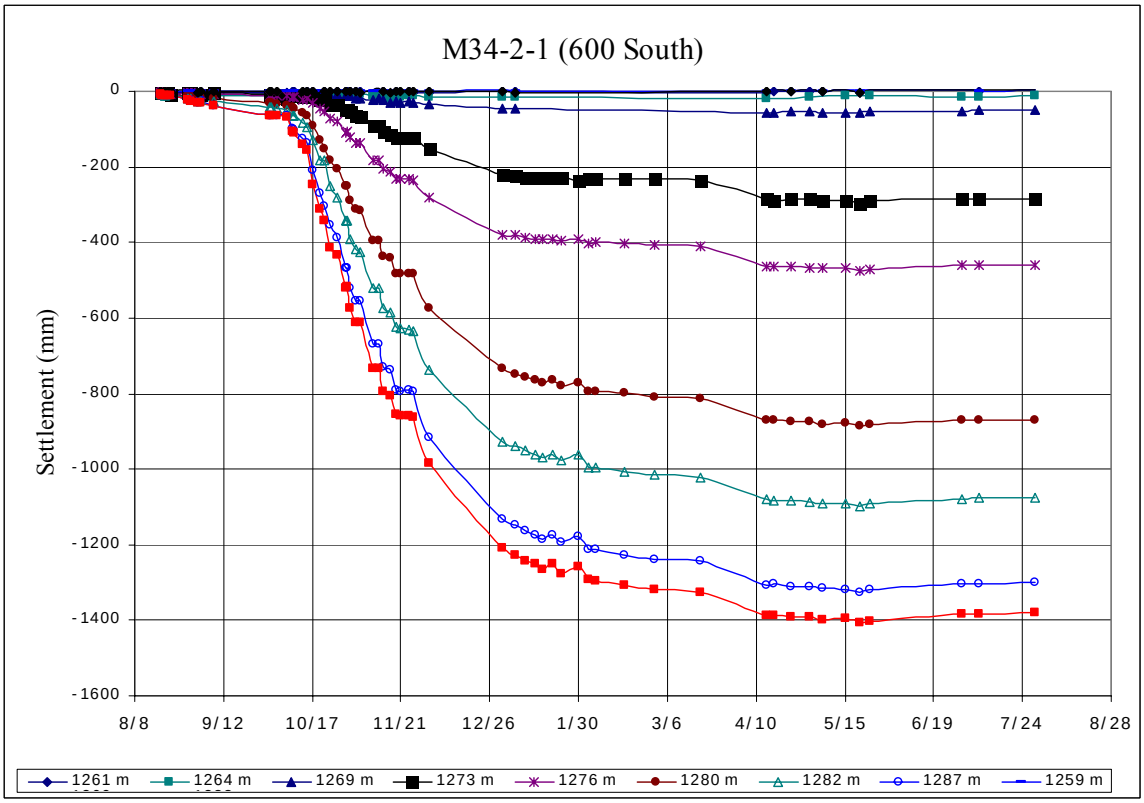


**Figure 3-9 Example of Settlement Versus Elapsed Time from Magnetic Extensometer for the I-15 Reconstruction Project, Salt Lake City, Utah.**

### 3.3.4 Calculation of End of Primary Consolidation Settlement

At many locations the surcharge fill was removed prior to reaching the EOP settlement. Thus, the amount of EOP settlement had to be estimated using the Asaoka (1978) method. This was necessary for each individual magnet settlement record because the EOP generally had not been reached when the data gathering had stopped. The Asaoka (1978) method consists of extrapolating the settlement record to calculate the settlement at EOP using settlement data that have been taken at equal time increments. Also, this method should only be applied to field data where the applied load remains constant over the part of the settlement record that is to be extrapolated.

Jamiolkowski et al. (1985) summarizes the important steps of the of the Asaoka (1978) projections. An example of the Asaoka method is located in Figure 3.10.

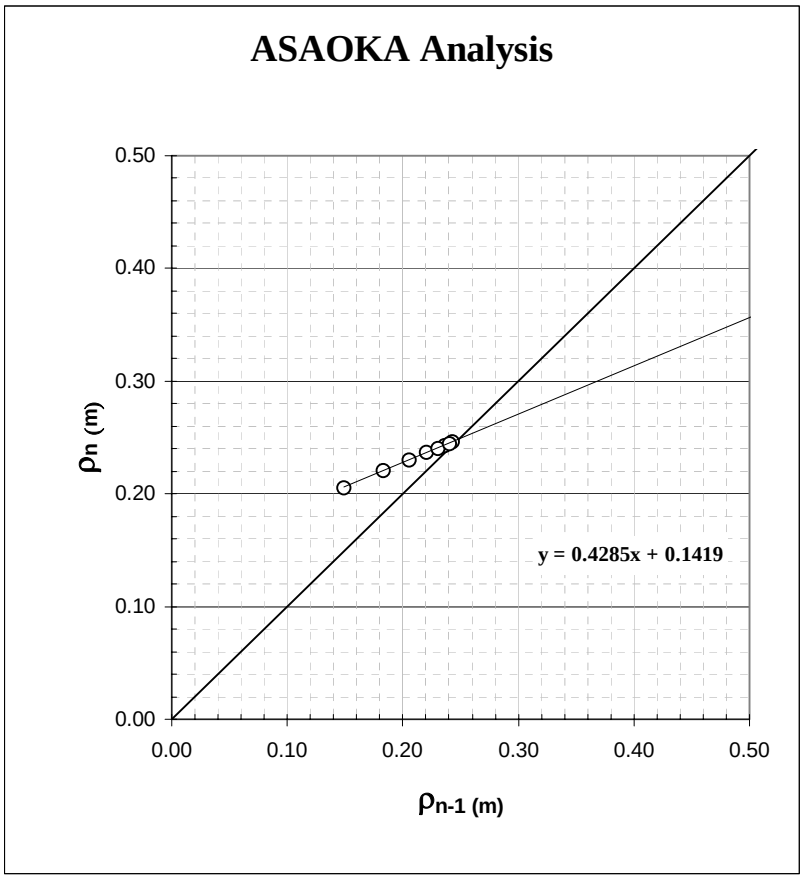


**Figure 3-10 Illustration of Asaoka Procedure to Calculate the EOP Consolidation.**

The steps of the Asaoka (1978) procedure are (Jamiolkowski et al., 1985):

1. From the time-settlement curve select a series of settlement values $\rho_1, \rho_2 \ldots, \rho_n$, such that $\rho_n$ is the settlement at time $t_n$ and the time interval $\Delta t = (t_n - t_{n-1})$ is constant.

2. From this series, plot the settlement values $\rho_{n-1}$ versus $\rho_n$.

3. All points lie on a straight line, such that:

$$\rho_n = \rho_0 + \beta\rho_{n-1} \qquad 3\text{-}13$$

   where $\rho_0$ and $\beta$ are two constants, which depend on the selected time interval $\Delta t$.

4. The estimated EOP is the point where the above line intersects the 45-degree line. (In other words, EOP is reached when $\rho_{n-1}$ and $\rho_n$ are equal.)

Figure 3.10 shows that the total settlement at the EOP is represented by the intersection of the two lines. According to the plot, the total settlement is approximately 0.25 meters (10 in) for the layer analyzed.

An Asaoka (1978) projection will generally produce a straight line in step 3 if the behavior of the soil follows the assumptions of Terzaghi's 1-D consolidation theory. However, if secondary compression starts, then the plot may deviate from a straight line and have an upward curvature (Jamiolkowski et al., 1985). Also, experience from the I-15 Reconstruction Project shows that upward curvature is also produced in a multi-layered system where individual layers are consolidating at different rates.

### 3.3.5 Calculation of Vertical Strain from Magnet Extensometer Data

Once estimates of BOP and EOP settlement had been obtained for each magnet, the strain associated with each layer was calculated. This section describes how the vertical strain associated with recompression and primary (i.e., virgin) compression was calculated for each layer.

The magnet data received from the design-build team were tabulated in terms of elevation of each magnet versus time. However, if strain is desired between two magnets, then the differential settlement must be calculated between the respective magnets. This differential settlement is then divided by the initial distance between the same magnets (i.e., initial thickness of the layer between the magnets) to calculate the strain at time, t. This process must be done for recompression and virgin compression strains so these components can be separated into their respective parts. These strains can then be used to calculate the recompression and compression ratios. The method and equations used to calculate vertical strain are as follows:

Calculate the strain associated with recompression, $\varepsilon_{cr}$ (%), by applying the following equation to each magnet interval (i.e., the layer found between two respective magnets):

$$\varepsilon_{cr} = \left[\left(\frac{(H_{1i} - H_{2i}) - (H_{1BOP} - H_{2BOP})}{H_{1i} - H_{2i}}\right) * 100\right] \qquad 3\text{-}14$$

where:

$H_{1i}$ = initial height (elevation) of top magnet

$H_{2i}$ = initial height (elevation) of bottom magnet

$H_{1BOP}$ = height (elevation) of top magnet at beginning of primary consolidation

$H_{2BOP}$ = height (elevation) of bottom magnet at beginning of primary consolidation

In a similar manner, calculate the strain associated with primary consolidation (i.e., virgin compression), $\varepsilon_{cc}$ (%), by applying the following equation:

$$\varepsilon_{cc} = \left[\left(\frac{(H_{1BOP} - H_{2BOP}) - (H_{1EOP} - H_{2EOP})}{H_{1BOP} - H_{2BOP}}\right) * 100\right] \qquad 3\text{-}15$$

where:

$H_{1EOP}$ = height (elevation) of top magnet at end of primary consolidation

$H_{2EOP}$ = height (elevation) of bottom magnet at end of primary consolidation

Once the vertical strains were determined for all layers found between to successive magnets, the total consolidation strain, $\varepsilon_{ct}$, was calculated for each interval between successive magnets. The $\varepsilon_{ct}$ was calculated from:

$$\varepsilon_{ct} = \varepsilon_{cr} + \varepsilon_{cc} \qquad 3\text{-}16$$

Table 3.4 shows examples of $\varepsilon_{ct}$, $\varepsilon_{cr}$, and $\varepsilon_{cc}$ for a typical magnet extensometer array.

**Table 3-4 Example Calculations from Magnetic Extensometer M34-2-1**.

| $H_{1i}$ – $H_{2i}$ | $H_{1BOP}$ - $H_{2BOP}$ | $H_{1EOP}$ - $H_{2EOP}$ | $\varepsilon_{cr}$ | $\varepsilon_{cc}$ | $\varepsilon_{ct}$ | CR @ 3 m Fill Height | CR @ 1.75 m Fill Height |
|---|---|---|---|---|---|---|---|
| (m) | (m) | (m) | (%) | (%) | (%) | | |
| 1.88 | 1.86 | 1.79 | 1.064 | 3.763 | 4.827 | 0.093 | 0.054 |
| 4.34 | 4.33 | 4.13 | 0.230 | 4.619 | 4.849 | 0.132 | 0.083 |
| 2.39 | 2.37 | 2.18 | 0.837 | 8.017 | 8.854 | 0.300 | 0.201 |
| 3.65 | 3.64 | 3.25 | 0.274 | 10.714 | 10.988 | 0.437 | 0.296 |
| 3.37 | 3.36 | 3.19 | 0.297 | 5.060 | 5.356 | 0.246 | 0.170 |
| 4.16 | 4.15 | 3.92 | 0.240 | 5.542 | 5.783 | 0.285 | 0.199 |

### 3.3.6 Calculation of Compression Ratio for Primary Consolidation

The strain associated with primary consolidation, $\varepsilon_{cc}$ (%), can be converted to the compression ratio, CR, if the vertical effective stress associated with the beginning and end of primary consolidation are known. This was done using the following equation:

$$CR = \left[\left(\frac{\frac{\varepsilon_{cc}}{100}}{\log\left(\frac{\sigma_{vf}}{\sigma_{pf}}\right)}\right)\right] \qquad 3\text{-}17$$

where:

$\varepsilon_{cc}$ = primary consolidation strain (%)

$\sigma_{vf}$ = final effective vertical stress**

$\sigma_{pf}$ = preconsolidation stress**

** These stresses are defined in the next section.

Table 3.4 also gives an example of the calculated compression ratios for magnet extensometer M34-2-1. Notice that this table give compression ratios calculated for 1.75 and 3 m (5.7 and 9.8 ft) fill heights. This was done to cover the uncertainty associated with the fill height and corresponding effective vertical stress that triggered primary consolidation. This and other issues are discussed in the next section.

## 3.4 Calculation of Preconsolidation Stress Using Numerical Modeling

The advantage of using field performance data, such as magnet extensometers, is that vertical strain can be measured in situ under actual conditions. However, an important disadvantage of this method is that the increase in stress that produced the vertical strain cannot be measured directly, but must be estimated. To this end, a finite element program was used using elastic theory. This allowed the calculation of the increase in vertical stresses at the various magnet extensometer locations in the soil profile using the embankment heights and geometries that existed at the various magnet extensometer arrays.

The finite element program selected was SIGMA/W™. SIGMA/W is a finite element program developed by Geo-slope International that can be used for stress and deformation analyses of earthen structures and foundation soils. SIGMA/W is formulated to solve 2-dimensional plane strain or 2-D axisymmetric problems using a small displacement, small strain, or incremental load formulation. For soil models with nonlinear material properties, SIGMA/W solves the equations iteratively using the Newton-Raphson technique. Soil properties are updated every iteration until a converged solution is achieved.

The interpretation of the magnetic extensometer data required the calculation of the increase in the vertical stress caused by the embankment loading. No deformation analyses were attempted. Thus, a linear elastic formulation was used that divided the subsurface profile into a multi-layered system with elastic soil properties assigned to each layer. The soil properties that SIGMA/W requires for elastic analyses are: soil density, Young's modulus of elasticity, Poisson's ratio and the weight of any body loads being applied. The embankment is treated as a body load using its geometry and appropriate unit weight.

These elastic properties were estimated by dividing the soil profile into six layers as described in Section 3.2 and calculating Young's modulus, E, for each layer. Estimates of E were made from the shear wave velocity measurements, $V_s$, and using elastic theory to relate $V_s$ and E. $V_s$ measurements versus depth were obtained from the seismic cone penetrometer tests performed by ConeTec for the I-15 Reconstruction Project. The $V_s$ measurements were averaged with respect to the corresponding soil layers as given in Table 3.5.

**Table 3-5 Properties Used for SIGMA/W Analysis**

| **600 SOUTH** | | | | **Shear Wave** | | **Young's** |
|---|---|---|---|---|---|---|
| **Depth** | **Soil Type** | **G** | $v_s$ | **Velocity** | $G_{max}$ | **Modulus** |
| **(m)** | | **(kN/m$^3$)** | | **(m/s)** | **(kPa)** | **(kPa)** |
| 0-5 | Alluvium | 19.2 | 0.35 | 146 | 41700 | 113000 |
| 5-12 | Upper Bonneville | 18.2 | 0.49 | 170 | 53600 | 161000 |
| 12-16 | Interbeds | 18.8 | 0.49 | 235 | 106000 | 318000 |
| 16-22 | Lower Bonneville | 18.2 | 0.49 | 201 | 75000 | 225000 |
| 22-25 | Pleistocene | 19.5 | 0.49 | 237 | 112000 | 335000 |
| 25-30 | Cutler Dam | 18.4 | 0.49 | 247 | 114000 | 343000 |
| Fill | Fill | 21.2 | 0.35 | 130 | 36600 | 98700 |

| **2400 SOUTH** | | | | **Shear Wave** | | **Young's** |
|---|---|---|---|---|---|---|
| **Depth** | **Soil Type** | **G** | $v_s$ | **Velocity** | $G_{max}$ | **Modulus** |
| **(m)** | | **(kN/m$^3$)** | | **(m/s)** | **(kPa)** | **(kPa)** |
| 0-5 | Alluvium | 19.2 | 0.35 | 156 | 47600 | 129000 |
| 5-11 | Upper Bonneville | 18.2 | 0.49 | 168 | 52400 | 157000 |
| 11-14 | Interbeds | 18.8 | 0.49 | 230 | 101000 | 304000 |
| 14-22 | Lower Bonneville | 18.2 | 0.49 | 200 | 74200 | 223000 |
| 22-26 | Pleistocene | 19.5 | 0.49 | 246 | 120000 | 361000 |
| 26-28 | Cutler Dam | 18.4 | 0.49 | 268 | 135000 | 404000 |
| Fill | Fill | 21.2 | 0.35 | 130 | 36600 | 98700 |

Values of E can be calculated from $V_s$, soil density and Poisson's ratio. Using elastic theory, the maximum shear modulus, $G_{max}$, can be calculated from $V_s$ using the following equation (Kramer, 1996):

$$G_{max} = \rho_{soil} * V_s^{\,2} \qquad 3\text{-}18$$

We should note that values of $G_{max}$ correspond to very low levels of shear strain. Values of $G_{max}$ obtained from this equation are appropriate for a strain range of about $1 \times 10^{-4}$, or less. This modulus is appropriate for estimating stress distribution in the various layers, but cannot be used to calculate strain or deformation. From $G_{max}$ values, estimates of Young's modulus, E, were calculated using the following equation:

$$E_t = G_{max} * 2(1 + \nu) \qquad 3\text{-}19$$

where:

$E_t$ = Young's tangent modulus

$\nu$ = Poisson's Ratio

Because values of $E_t$ were calculated from $G_{max}$, they are initial tangent moduli. The values of $E_t$ calculated from Equation 3-19 are not appropriate for large strain problems, such as foundation settlement calculations and consolidation. However, they are appropriate for calculating the stress distribution that develops in a multi-layered elastic system. Table 3.5 is a table of the elastic properties that were used in SIGMA/W.

Values of Poisson's ratio were estimated for the appropriate soil type from typical values published in the EPRI (1994) manual. The values of 0.35 in Table 3.5 are typical published values for granular soils. The values of 0.49 are typical published values for clays, which represent "undrained" Poisson's ratio values. (SIGMA/W will not allow 0.5 to be used, because it generates a numerical error, so 0.49 was used.) Note also that in elastic theory, a Poisson's ratio of 0.5 means that the elastic medium does not undergo any volumetric strain (i.e., any vertical strain in the z direction is compensated for by horizontal strain in the x and y directions so that the net volumetric strain is zero).

"Undrained" values of Poisson's ratio are most appropriate for saturated clayey soils where no significant void ratio or pore pressure change has occurred from the applied load. However, the Bonneville and Cutler Dam Clays are primarily silty clays and clayey silts, where void ratio change and excess pore pressure dissipation may occur relatively quickly after a change in vertical stress, especially at stress levels below the preconsolidation stress. Thus, when consolidation with time is considered, an initial undrained loading condition will progress to a partially drained condition and finally reach a drained condition as EOP settlement is achieved.

Unfortunately, "drained" values of Poisson's ratio are not commonly published in the geotechnical literature and many typical values do not distinguish between "undrained" and "drained" values. The SIGMA/W models developed herein used 0.49 for all clay layers, which truly represents "undrained" values. However, because the EOP condition is a "drained" condition, and to explore the sensitivity of the SIGMA/W analysis to the

assumed Poisson's ratio, supplemental runs were performed using Poisson's ratio of 0.4 instead of 0.49 for all clay layers. The resulting stress distribution from these extra runs differed by no more than 4 percent, thus showing that the stress distribution predictions are not particularly sensitive to the assumed Poisson's ratio values used for the clay layers.

Figures 3.11 and 3.12 are examples of an embankment layout and the results that can be obtained from SIGMA/W. Figure 3.11 shows the layering system used in the model, the original I-15 embankment (broad, low-lying embankment) and the newly constructed embankment (steep, trapezoidal embankment). Figure 3.12 shows the increase in total vertical stress caused by the placement of the new embankment atop the old embankment. These types of models were constructed for all magnet extensometer locations.

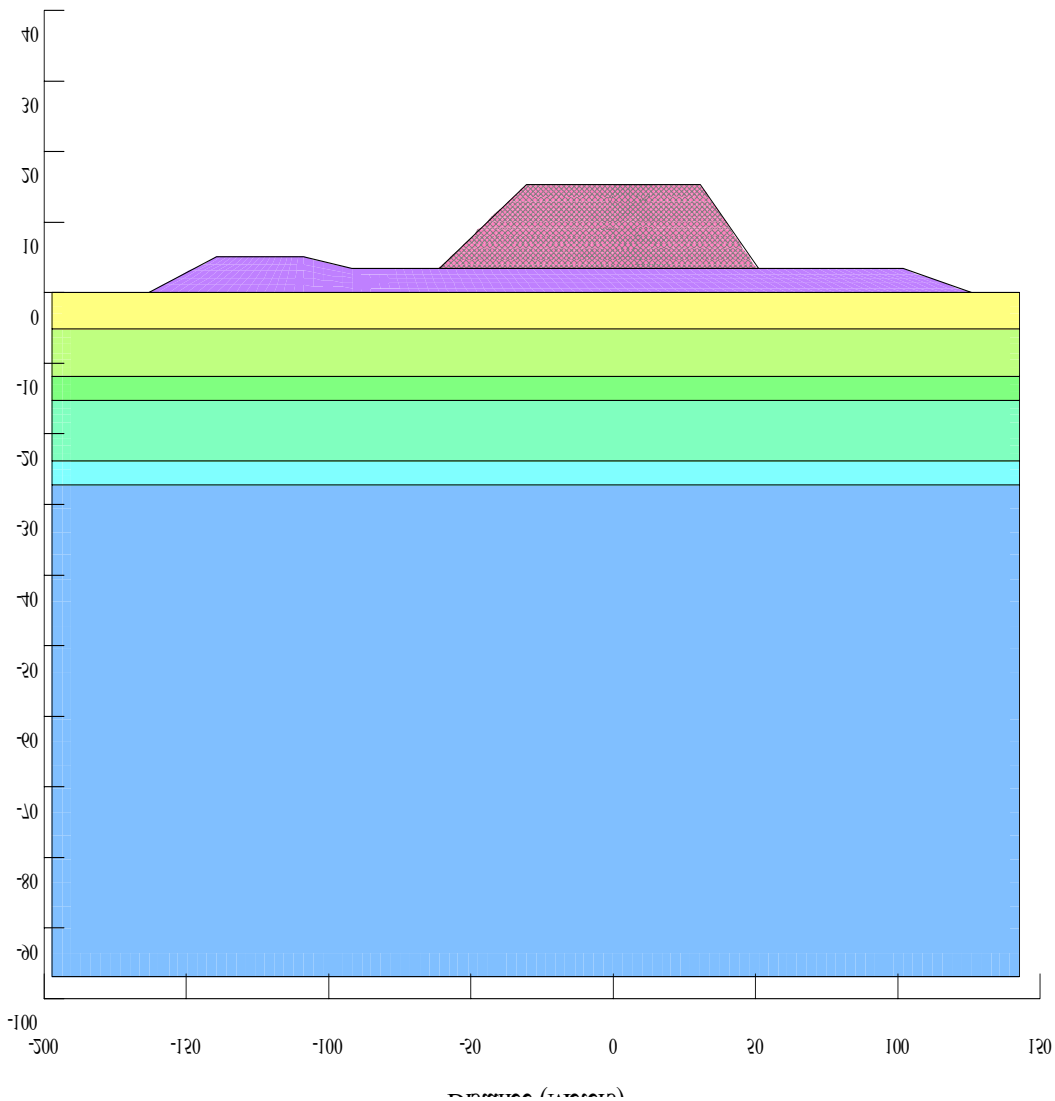


**Figure 3-11 Example Layout of Soil Profile and Embankment with Surcharge Using SIGMA/W.**

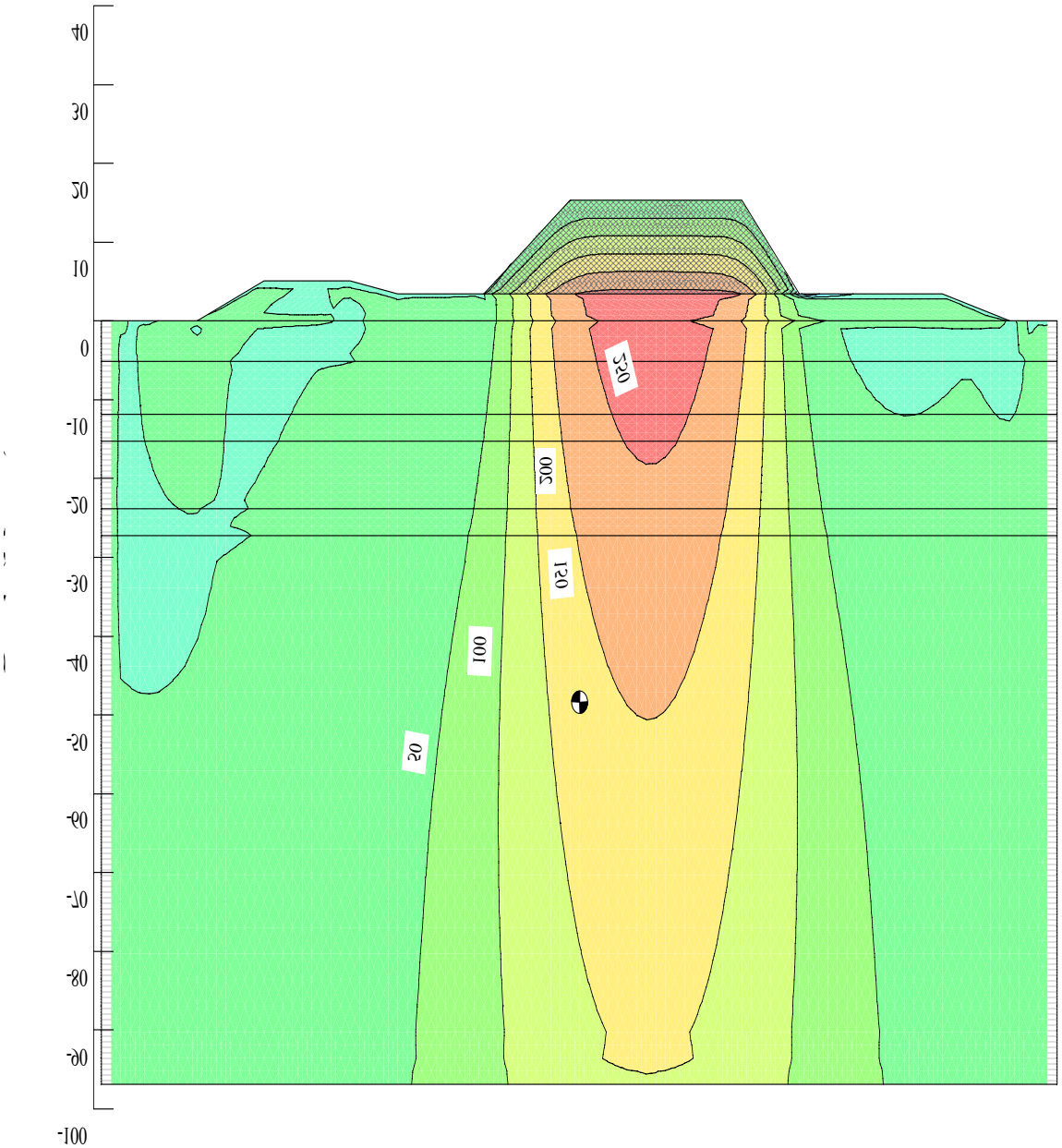


**Figure 3-12 Example Stress Distribution Output from SIGMA/W.**

The SIGMA/W results can be very sensitive to the type and size of element used in the soil profile. Infinite elements were used on the outside edges of the soil profile to remove the influence of the model's boundary on the solution. Infinite elements have the effect of keeping the stresses from being confined at boundary edges. The profiles had boundary conditions that constrained the element in the "x" direction on the sides of the profile. The depth of the profile was increased until the stresses were unaffected. This depth was used as the bottom of the profile and remaining models were modeled at that depth.

Figure 3.12 indicates that the increase in vertical stress from the embankment loading is greatest directly underneath the centerline of the embankment and varies with depth and

horizontal position. (This type of output can also be produced in a table format showing the increase in vertical stresses at specific depths within the soil profile.) Once this information is obtained, it is possible to determine the effective vertical stress versus depth at the magnet locations, as described in the following paragraphs.

The SIGMA/W modeling provided estimates of the increase in vertical stress for the various embankment geometries and horizontal location of the magnet extensometer borehole. However the calculations associated with the BOP and EOP stresses are based on effective stress calculations, not total stress calculations. Thus, it was necessary to estimate the BOP and EOP effective vertical stresses for various stages of embankment construction. This was done in four steps:

1. Calculation of the in-situ 1-D effective vertical stress profile resulting for level ground conditions (i.e., before any embankment was placed over the foundation soil) using hydrostatic conditions, the appropriate soil unit weights for each layer and an EXCEL™ spreadsheet.

2. 2-D SIGMA/W modeling of the increase in vertical stress caused by the presence of the pre-existing I-15 embankment (i.e., old embankment that was placed before the reconstruction).

3. 2-D SIGMA/W modeling of the increase in vertical stress caused by the construction of the new embankment that was placed atop and adjacent to the old embankment

4. 2-D SIGMA/W modeling of the final new embankment geometry (i.e., full embankment height plus surcharge) to estimate the effective vertical stress associated with end of primary consolidation (EOP). Effective vertical stresses for steps 2, 3 and 4 were calculated by adding the increases in stress calculated by SIGMA/W to the initial vertical effective stress profile estimated in step 1.

Table 3-6 is an example of the above steps for a magnet location in the 600 South area. The values tabulated for steps 2 and 3 represent the increased vertical stress from the old and new embankment, respectively, at their full height.

**Table 3-6 Example Calculations from SIGMA/W Modeling in Tabular Form**

| | | Step 1 | Step 2 | Step 3 | Step 4 |
|---|---|---|---|---|---|
| **Location Magnet** | **Depth (m)** | **$\sigma'_{vo}$ (kPa)** | **$\Delta\sigma_{old}$ (kPa)** | **$\Delta\sigma_{new}$ (kPa)** | **$\sigma'_{vf}$ (kPa)** |
| 600 South M33-9-1 | 0 | 0.00 | 115.88 | 184.35 | 300.23 |
| | 4 | 57.18 | 119.10 | 200.65 | 376.93 |
| | 8 | 90.74 | 118.23 | 204.18 | 413.15 |
| | 12 | 124.30 | 115.17 | 194.74 | 434.21 |
| | 15 | 150.67 | 117.11 | 204.74 | 472.52 |
| | 20 | 193.82 | 112.62 | 182.43 | 488.87 |

The approach outlined above assumes that no excess pore pressure above hydrostatic conditions existed in the subsurface soil profile for steps 2, 3 and 4. This is a reasonable assumption for step 2, because the fill had been in place for approximately 35 years, thus no residual excess pore pressures from the first loading event should exist. For step 3, it was assumed that any increase in excess pore water pressure due to the new embankment load was relatively small and dissipated quickly for loading conditions that are occurring in recompression (i.e., for states of stress below the preconsolidation stress). In other words, this calculation assumes that excess pore pressure dissipation and void ratio change are occurring rapidly enough to keep pace with the rate of embankment construction. This assumption is supported by field pore pressure measurements which suggest that excess pore pressures can dissipate relatively quickly in the silty clay layers that comprise the Lake Bonneville and Culter Dam deposits for fill heights that are not high enough to have triggered primary consolidation in the foundation soils.

For step 3, the height of the new embankment was modeled incrementally so that the increase in stress that triggered the BOP consolidation could be estimated. The fill height corresponding to BOP consolidation was estimated by examining the plots of the individual magnets and determining the height of embankment that produced a sharp increase in the settlement curve of each layer (see Section 3.3.3). Once the embankment height associated with BOP was identified, that fill height was modeled in SIGMA/W to estimate the effective vertical stress at that embankment height. For some cases it was unclear which fill height or lift had triggered BOP consolidation. For example, Table 3.4 shows that BOP consolidation was triggered at a fill height somewhere between 1.75 m and 3.0 m (5.7 and 9.8 ft). For such cases, the newly placed embankment was modeled in SIGMA/W for two heights, one immediately before the placement of the new lift (i.e., 1.75 m (5.7 ft) in Table 3.4) and one corresponding to the fill height after the placement of the new lift (i.e., 3.0 m (9.8 ft) in Table 3.4). The effective vertical stresses for these two possible conditions were then averaged to produce an estimate of the preconsolidation stress used in the statistical analysis discussed in Section 4.

Another important point that needs discussion is the fact that BOP consolidation was triggered in successively deeper layers as the fill height increased. To account for this the new embankment, construction was modeled in successive 0.5 to 1 m (1.6 to 3.3 ft) increments, so this effect could be taken into account in the estimation of the preconsolidation stress. For example, Figure 3.8 and 3.9 show how BOP consolidation was triggered in successively deeper layers by successively later lifts. This example illustrates the following points:

1. For the highest magnet [elev. 1288 m (4226 ft)] the beginning of primary consolidation began when the fill height reached about 3 m (10 ft).

2. For the next deepest magnet [elev. 1280 m (4199 ft)] primary consolidation began at a fill height between 3 to 5 m (10 to 16 ft).

3. For the deepest magnet [elev. 1276 m (4186 ft)] primary consolidation began when the fill height had about 4.5 to 6 m (15 to 20 ft).

These uncertainties were also accounted for in the SIGMA/W modeling, and the range of preconsolidation stresses are presented in the figures given within the next section, where development of the regression model is discussed.

# 4 Development of Regression Model

## 4.1 Introduction to Multiple Linear Regression

Multiple linear regression (MLR) is a statistical method used to estimate the linear relationship between a dependent variable and one or more independent variables. The dependent variable is the variable that is to be estimated and the independent variables are the predictor variables that are correlated with the dependent variable. MLR is based on a least squares fit: the model is fit such that the sum-of-squares of differences of observed and predicted values is minimized. In applying MLR analysis, it is assumed that changes in the independent variable, X(s), are accompanied by a corresponding change in the response of the dependent variable, Y. The true response, $\cap$, is expressed in terms of unknown parameters, B(s) that accompany the X(s).

$$\cap = \phi(X_1, X_2, \ldots, X_p; B_1, B_2, \ldots, B_p) \qquad 4\text{-}1$$

For example, in this study it is postulated that the preconsolidation stress and compression ratio are related to several independent variables measured by the CPT.

$$\cap = \phi(\sigma'_p, q_t, f_s, \sigma'_{vo}, \sigma_{vo}; B_{\sigma'p}, B_{qt}, B_{fs}, B_{\sigma'vo}, B_{\sigma vo}) \qquad 4\text{-}2$$

where:

$\sigma'_p$ = Preconsolidation stress

$q_t$ = Corrected tip stress

$f_s$ = Sleeve resistance

$\sigma'_{vo}$ = Effective vertical stress

$\sigma_{vo}$ = Total vertical stress

$B_{\sigma'p}$, $B_{qt}$, $B_{fs}$, $B_{\sigma'vo}$, and $B_{\sigma vo}$ = to unknown parameters corresponding to $\sigma'_p$, $q_t$, $f_s$, $\sigma'_{vo}$, and $\sigma_{vo}$

Ideally, the value of $\cap$ for a given set of X(s) is the same each time an experiment is performed. But, in reality, $\cap$ is seldom exactly observed due to the presence of other uncontrolled and unmeasured factors that affect $\cap$. The deviation of the observed response, Y, from $\cap$ is called experimental error, $\varepsilon$.

$$\cap - Y = \varepsilon \qquad 4\text{-}3$$

In MLR analysis, $\phi$ is approximated by an additive, linear model. The values of Y and the X(s) can be often transformed (e.g., 1/X, log X, $e^x$, etc.) in order to produce a linear form.

$$Y = b_0 + b_1x_1 + b_2x_2 + \ldots + b_px_p + e \qquad 4\text{-}4$$

The fitted regression coefficients, $b_0, \ldots, b_p$, are best-fit estimates of the B(s), and e is a best-fit estimate of ε. MLR analysis uses the method of ordinary least squares to estimate the B(s) by minimizing the error sum of squares:

$$S_e = \Sigma(e)^2 \qquad 4\text{-}5$$

where:

e = difference between the measured response, Y, and the response predicted by the regression equation, $\hat{Y}$, i.e.,

$$e = Y - \hat{Y} \qquad 4\text{-}6$$

To provide best-fit estimates of the B(s), it is assumed: (1) the ε(s) are random variables with an expected value of zero (i.e., E(ε) = 0), (2) the variance of the ε(s) is constant for all values of the X(s) (i.e., V(ε) is constant), (3) the ε(s) are not correlated and (4) the values can be measured without error. Also, if the ε(s) appear to be normally distributed, then partial and sequential t and F tests can be performed on each of the b(s) to verify that these coefficients are statistically significant (i.e., $b_0, \ldots, b_p$ are not equal to zero) (Draper and Smith, 1981). Standardized residual plots are commonly used to evaluate the validity of these assumptions (Figure 4.1). Also, these plots give the investigator valuable information about the general performance of the MLR model. The standardized residual, $e_s$, for each observation is calculated from:

$$e_s = e/(\text{standard deviation of } e) \qquad 4\text{-}7$$

where:

$$e = Y - \hat{Y} \qquad 4\text{-}8$$

Typically, the $e_s$(s) from the model are plotted against the corresponding X(s) and $\hat{Y}$(s) to confirm that the $e_s$(s) are independent and have a constant variance with a mean of zero. An acceptable standard residual plot gives the impression of a horizontal band of data centered on zero. Approximately 95 percent of the $e_s$(s) should fall within ± 2 standard deviations of zero, and almost all $e_s$(s) should fall within ± 3 standard deviations of the zero line (Figure 4.1).

Data with a nonconstant variance are usually corrected by transforming Y or by using weighted, least-squares regression analysis (Draper and Smith, 1981). The linear trend shown in Figure 4.1c suggests that the $e_s$(s) are not independent or that some other X is needed in the model. A residual plot displaying curvature (Figure 4.1d) indicates that a higher order term, a cross-product, or a transformation of Y, or of the X(s), is needed to produce a more linear form.

The performance of MLR models is judged by the coefficient of determination, $R^2$:

$$R^2 = [\Sigma(Y^2) - S_e - (\Sigma Y)^2/n]/[\,\Sigma(Y^2) - (\Sigma Y)^2/n)] \qquad 4\text{-}9$$

where n is the sample size. The value of $R^2$ ranges from 0 to 1 and measures the proportion of the variability of Y being explained by the X(s). For example, an $R^2$ of 0.50 means that 50 percent of the variability in Y is being explained by the X(s). An $R^2$ value of 1.0 means that all Y values are being perfectly predicted by the X(s).

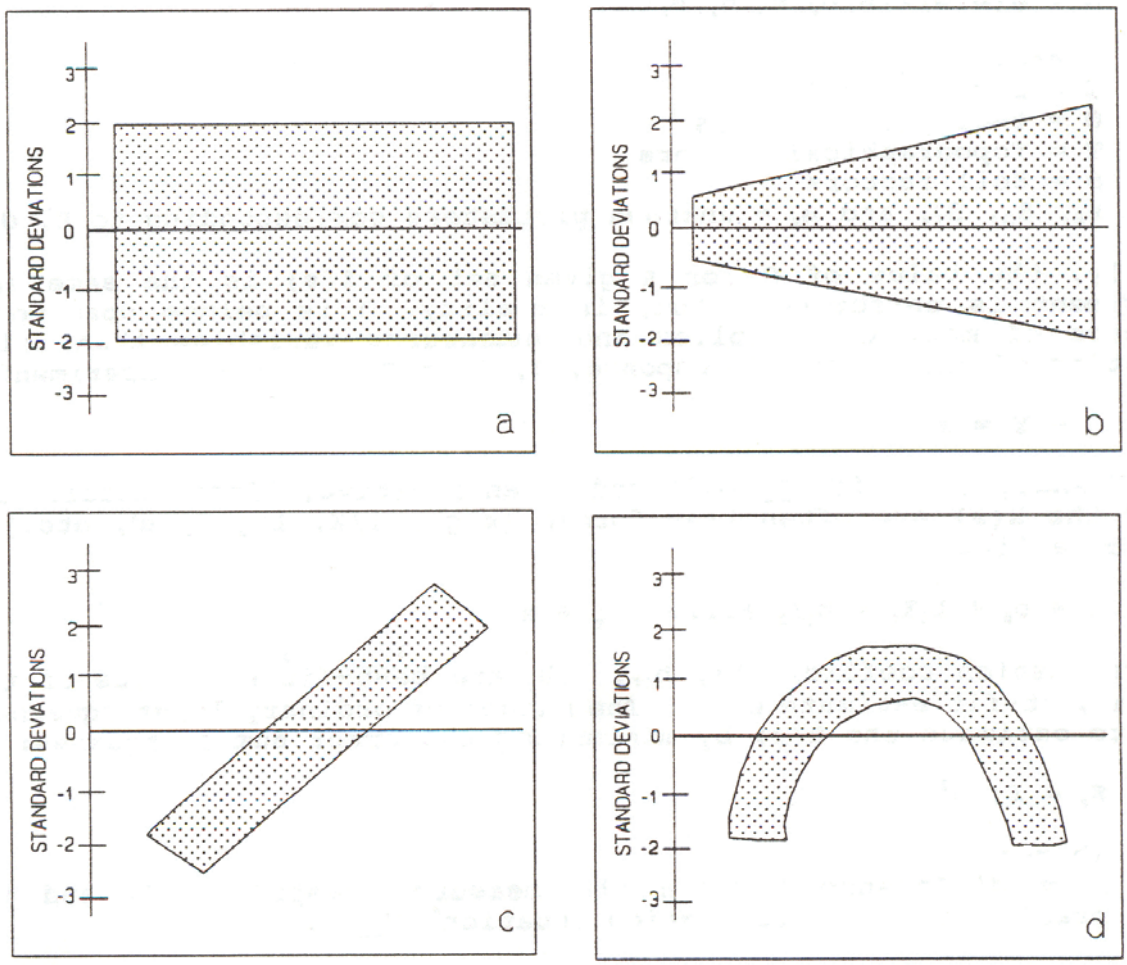


**Figure 4-1 Examples of Standard Residual Plots. (a) Satisfactory residual plot gives overall impression of horizontal box centered on zero line. (b) A plot showing nonconstant variance. (c) A plot showing a linear trend suggesting that the residuals are not independent and that another variable is needed in the model. (d) A plot illustrating the need for a transformation or a higher order term to alleviate curvature in the residuals.**

For these analyses, a stepwise regression procedure has been used. This procedure begins by searching the set of possible X(s) or transformations of X(s) for that with the highest correlation with Y, and this X enters the model first. In the next step, the remaining X(s) are re-examined to find the X that yields the next highest improvement in $R^2$ and this X is added to the model. The process of examining and adding X(s) to the model continues until no additional X(s) can be found that significantly improve $R^2$.

Also, variables that become nonsignificant during later steps are removed from the model prior to beginning the next step. This can sometimes happen when variables are correlated and a later combination of variables gives better predictive performance than earlier combinations.

## 4.2 Pairing of CPT Data with Estimates of Consolidation Properties

Decisions had to be made regarding the use and pairing of the field and laboratory data with the CPT data for the final regression analysis. In order to compare the field-calculated values of consolidation properties with those determined from the laboratory results, the data set was divided into two general areas: (1) 600 South and (2) 2400 South. This division of the data was for plotting and comparison purposes only, so that the individual points could be better scrutinized (Figures 4.2 to 4.5). Also, the field and laboratory data were broken into geologic units so that possible trends within a given unit could be evaluated. Further, there was some uncertainty in selecting the fill height that triggered virgin compression behavior for some of the magnetic extensometer data, so these data were plotted with a lower bound, average and upper bound estimate at various depths. The lower bound estimate is shown with a minus symbol, the average estimate is shown with an open symbol and the upper bound estimate is shown with a plus symbol (Figures 4.2 and 4.3).

A visual comparison of field-calculated versus laboratory-determined preconsolidation stresses for the 600 South Street area shows that field-calculated values are slightly higher for much of the profile, except for the Cutler Dam clay (Figure 4.2). This is especially noticeable for the upper Lake Bonneville clay unit in Figure 4.2.

There are a few explanations for this slight bias between the two types of data in Figure 4.2. First, although the laboratory-determined values have been screened for disturbance effects, they still may be suffering from some disturbance effects, which can produce a lower estimate of the preconsolidation stress. Second, the two types of data come from differing stress conditions. The preconsolidation stress for the laboratory determined values are for 1-D compression in an oedometer; whereas the field-calculated values are really from field conditions where 2-D or 3-D strains occurred. Certainly differences in the stress conditions (1-D versus 2-D or 3-D) can account for some of the differences in preconsolidation stress seen in Figure 4.2. However, the data shown in Figure 4.3 for the 2400 South Street area do not show any significant bias between the two data types.

Figure 4.2 also shows that preconsolidation stress for the Cutler Dam Lake deposits is highly variable, based on the laboratory data. This unit has high variability in engineering properties because it is often interbedded with silt and sand units that are difficult to correlate from one location to the next. The magnet extensometer data is more consistent with the lower range of the laboratory data for this unit and are believed to be more representative of the clay found in this unit. Also, it is possible that some cementation is playing a role in the wide variation of preconsolidation stress found in this interval.

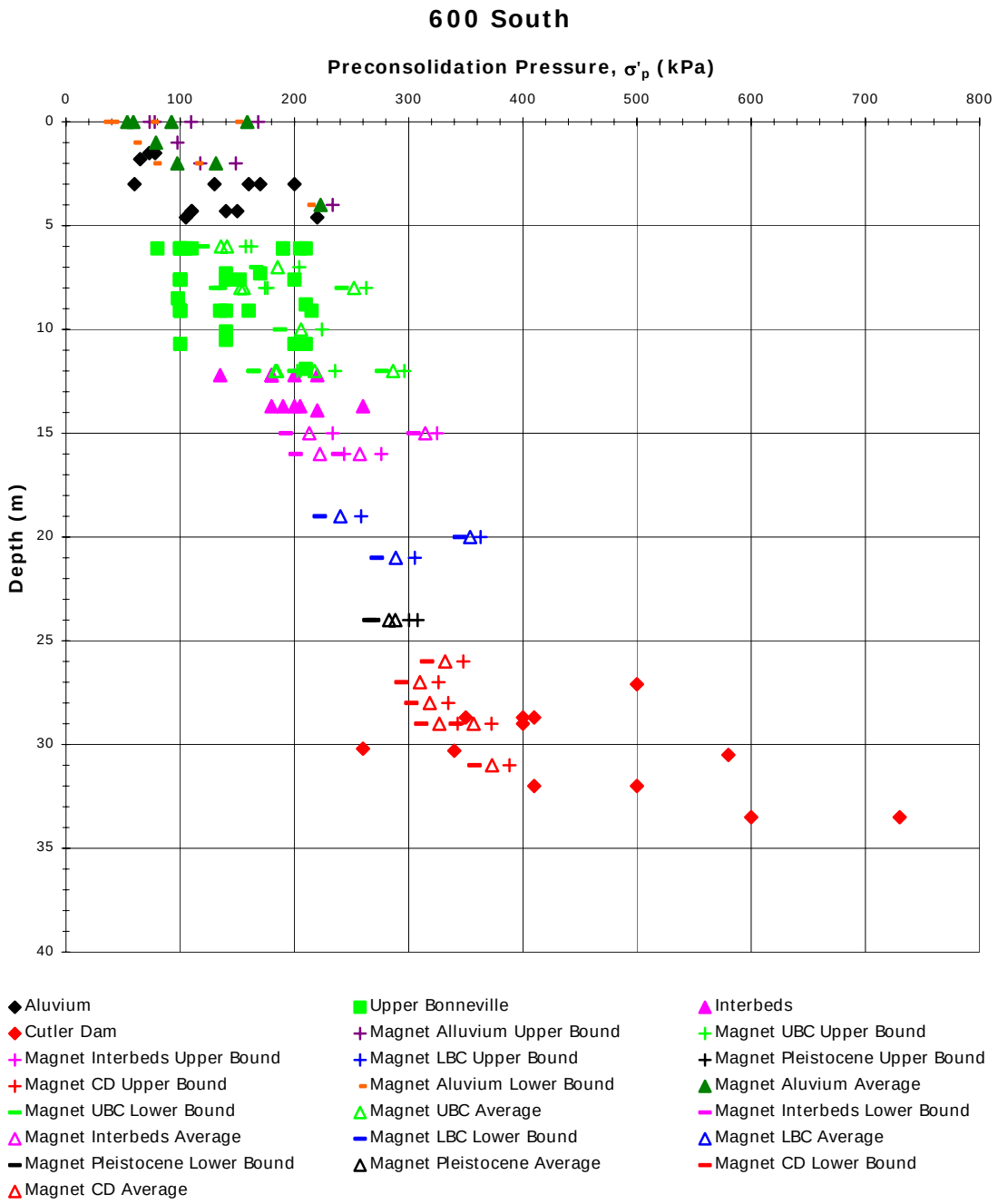


**Figure 4-2 Preconsolidation Pressures in the 600 South Area that Consists of Laboratory Data, Magnet Extensometer High, Average, and Low Range of Data.**

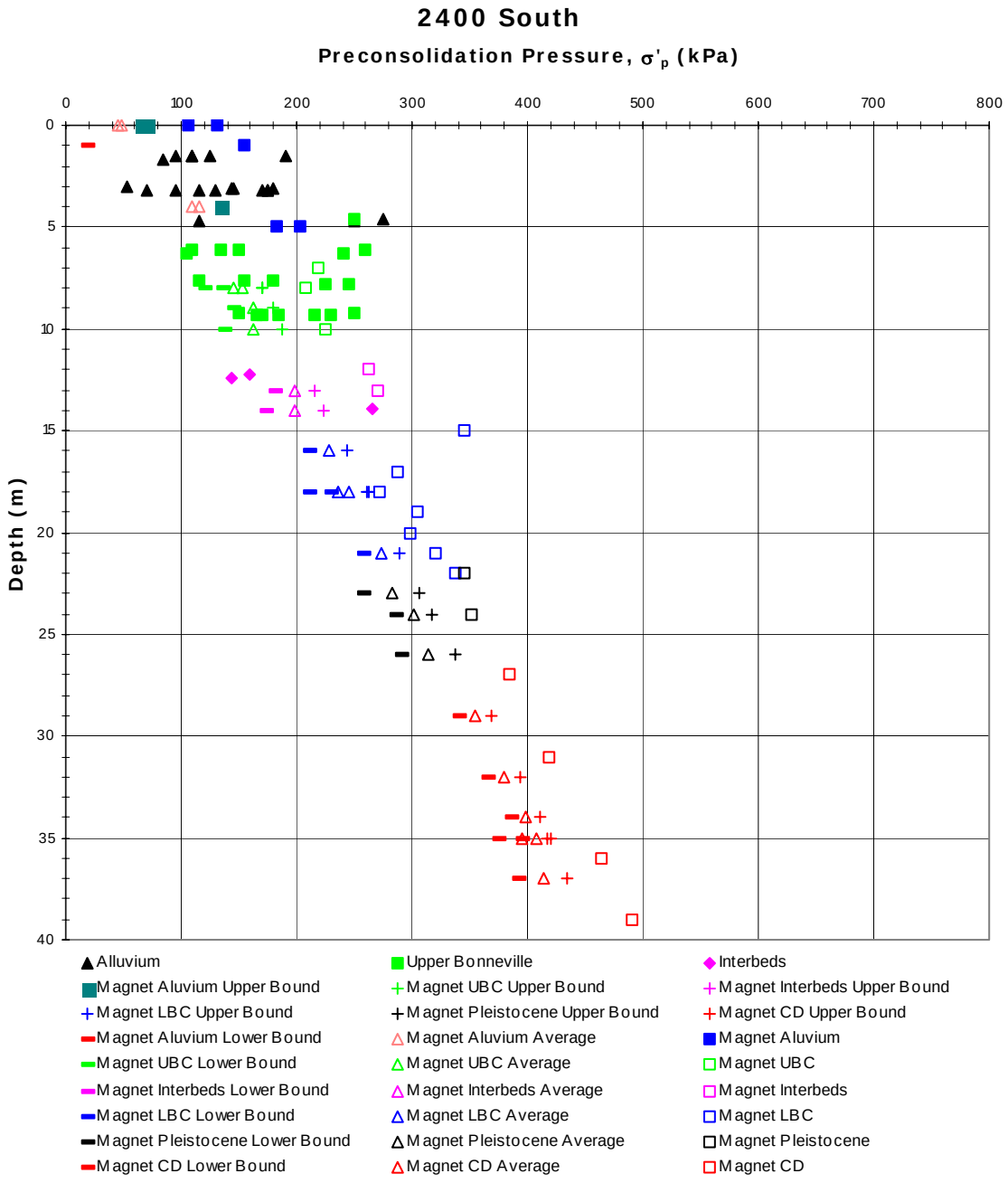


**Figure 4-3 Preconsolidation Pressures in the 2400 South Area that Consist of Laboratory Data, Magnet Extensometer High, Average, and Low Range of Data.**

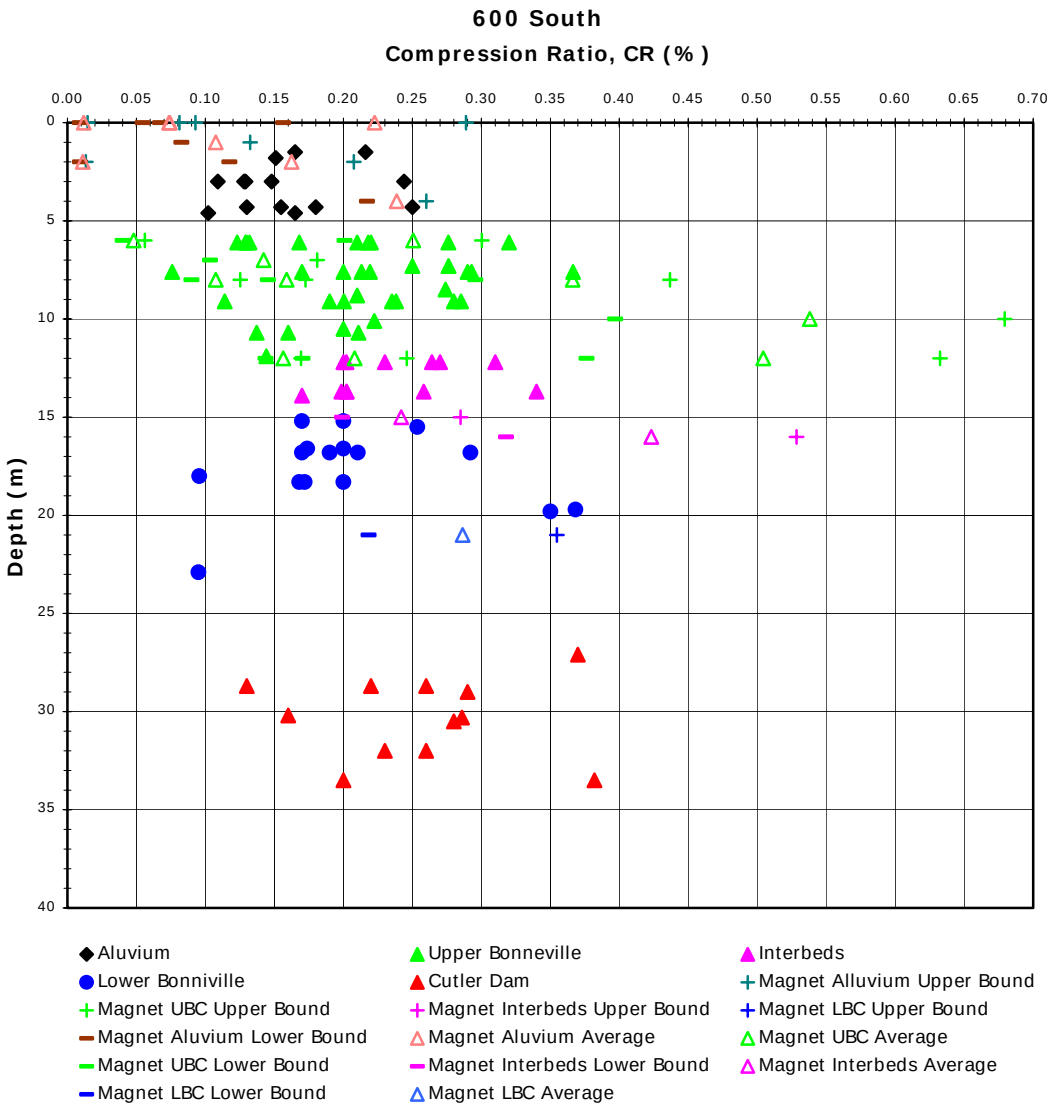


**Figure 4-4 Compression Ratios in the 600 South Area that Consists of Laboratory Data, Magnet Extensometer High, Average, and Low Range of Data.**

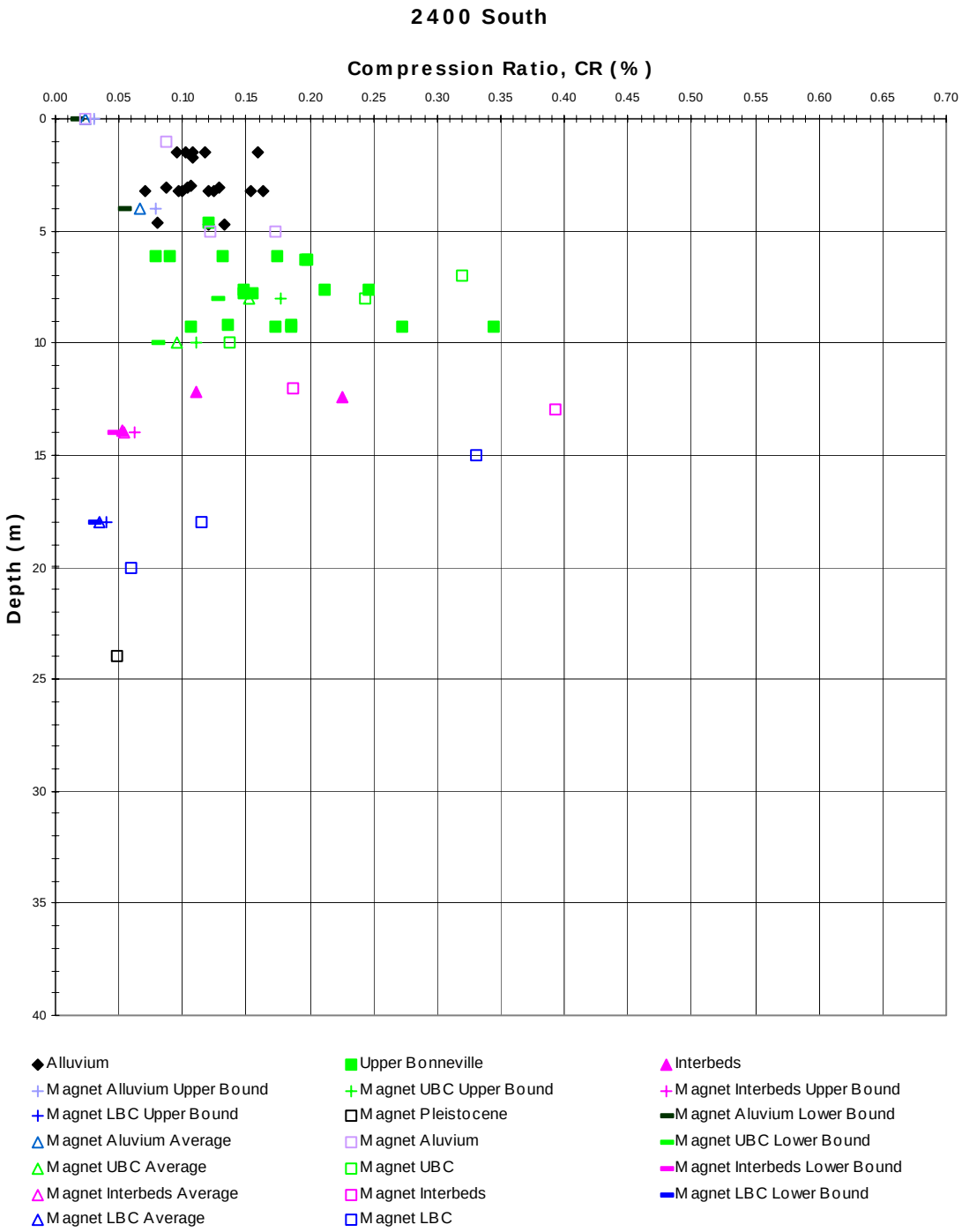


**Figure 4-5 Compression Ratios in the 2400 South Street Area that Consists of Laboratory Data, Magnet Extensometer High, Average, and Low Range of Data**

Figure 4.3 also shows that there are not many laboratory data for the 2400 South Street area for units below the upper Lake Bonneville clay. Ultimately, it was decided to use only the field-calculated values of preconsolidation stress and compression ratio for the final regressions with the CPT data. This decision was based on the following considerations:

The potential of sample disturbance that still may be present in the laboratory data for the 600 South area.

1. The lack of laboratory data for the 2400 South Street area below the upper Lake Bonneville sediments.

2. The field-calculated values are believed to be more representative of the soil layers and have less variability than the laboratory data, which are essentially point estimates.

3. Spatial uncertainty in pairing the laboratory data with CPT soundings due to lack of surveyed CPT locations.

The last two reasons warrant further discussion. Laboratory data is essentially a point estimate because of the small thickness, 25 mm (1.0 in), of the laboratory sample. In contrast, consolidation properties back calculated from the magnetic extensometer data represent average properties appropriate for the soil interval that is found between the magnet positions in the borehole. Typically, this interval is on the order of a few meters, depending on the particular borehole location and depth interval. Hence, properties determined from the magnetic extensometer data will show less variability, because these estimates are essentially averages for a layer. In addition, it was difficult to pair the laboratory data with a given CPT sounding because of uncertainty in the elevations of the CPT data. Dames and Moore (1996a, b, c, d) did not provide surface elevations for the CPT data in their report, thus the surface elevation had to be estimated from borehole maps that were contoured to 1 m vertical elevations. Because of this spatial uncertainty, it was difficult to pair the CPT data with the corresponding laboratory data.

Table 4.1 shows seven magnetic extensometer locations where readings were taken between North Temple Street and 2400 South Street. Though there were nine locations available, two of the magnetic extensometer locations, M28-1-1 and M34-1-1B, were not be used in the analysis. Extensometer M28-1-1 only had approximately one month of data that made it impossible to project the end of primary consolidation settlement. The fill data was not accurate for the extensometer M34-1-1B, so it was also not included.

Table 4.1 also lists the CPT sounding that was paired with each magnetic extensometer. These CPT soundings were selected because they were the closest to the magnetic extensometer location.

**Table 4-1 Magnetic Extensometers and CPT Soundings Used in Regression Analysis.**

| Magnetic Extensometer | CPT Sounding |
|---|---|
| M28-0-1B | SV-CB-22A |
| M27-6-1 | SV-CB-10A |
| M27-8-1 | SV-CB-19A |
| M33-9-1 | 06-RC-12 |
| M34-2-2B | 06-RC-15 |
| M34-2-1 | 06-RC-12 |
| M32-9-1 | 06-WC-84 |

To better correlate the CPT and magnetic extensometer data, the interbedded fine sand layers that are present in the Bonneville sediments must be filtered out of the CPT data before averaging. This filtering allowed for a more representative average of the CPT sounding for the compressible, fine-grained soil, especially for the interbeds that are found between the upper and lower Lake Bonneville clay. The filtering was accomplished by using the soil behavior type index $I_c$ (NCEER 1997). $I_c$ is calculated as follows:

$$I_c = \left[(3.47 - \log Q)^2 + (1.22 + \log F)^2\right]^{0.5} \qquad 4\text{-}10$$

where:

$$Q = [(q_c - \sigma_{vo})/P_a][(P_a/\sigma'_{vo})^n] \qquad 4\text{-}11$$

$$F\ (\%) = [f_s/(q_c - \sigma_{vo})] \times 100 \qquad 4\text{-}12$$

$P_a$ = 1 atm of pressure in the same units used for $\sigma'_{vo}$.

For equation 4.2-1, the value of the exponent n varies from 0.5 to 1, depending on the grain characteristics of the soil (Olsen, 1997). For the soil type involved in this research, a value of 1 was used for the exponent n, which is an appropriate value for clayey soil types. Data values from the CPT sounding were entered in the above equations. Data that produced an $I_c \leq 2.6$ was considered to be granular soil and was eliminated for the interval averages described in the following paragraphs. The granular layers are generally thin (less than about 100 mm (4 in)) and do not constitute a major soil type in the Lake Bonneville interval found in the study area.

After filtering out the granular layers (thin beds of fine sand and non-plastic silt) from the CPT data, the magnet positions within each borehole were assigned elevations. From these elevations, the CPT data from the soundings was paired with each magnet position. For the preconsolidation stress analyses, the pairing of data was accomplished by a 1-m (3.3 ft) average of the CPT measurements by starting 0.5 meters (1.6 ft) above each magnet elevation and averaging the CPT data for a 1-m (3.3 ft) interval. This 1-m (3.3 ft) average was considered to account for any vertical spatial variation in soil type at a particular magnet position.

In pairing the data for the compression ratio analyses, the CPT measurements were averaged between magnet positions within a single borehole in the same elevation interval. The compression ratio was determined from the compression that occurred in this same interval, as described in the previous chapter.

The averaged CPT measurements used in the regression analyses included corrected tip stress, sleeve stress, preconsolidation stress, and compression ratio. Also, averages of total and vertical effective stress were required for the regression analyses.

Now that the process for averaging the CPT measurements has been described, a brief discussion of the effects of filtering on these averages is appropriate. The filtering out of granular soils from the CPT interval ensures that the average CPT value is not unduly biased by the presence of thin, fine sand layers. These sand layers are typically medium dense sand that, if used in the average, would unduly increase the CPT tip stress and other measurements. This potential bias, if not eliminated, can produce a non-representative average for the fine-grained compressible material found in that same interval.

Table 4.2 includes the different magnets, their locations, and the calculated preconsolidation stresses and compression ratios for the corresponding intervals. This table is the data set that was used in the MLR analyses.

**Table 4-2 Magnets, Their Locations, and the Calculated Preconsolidation Stresses and Compression Ratios.**

| Location | Magnet | Depth (m) | Average Total Preconsolidation Stress (kPa) | Average Compression Ratio |
|---|---|---|---|---|
| **600 South** | **M32-9-1** | 0 | 53.63 | 0.0118 |
| | | 2 | 97.54 | 0.0112 |
| | | 6 | 135.66 | 0.0481 |
| | | 8 | 152.70 | 0.1075 |
| | | 12 | 184.77 | |
| | | 16 | 222.28 | |
| | | 24 | 288.37 | |
| **600 South** | **M33-9-1** | 0 | 158.69 | 0.0742 |
| | | 4 | 222.87 | 0.2386 |
| | | 8 | 252.10 | 0.1589 |
| | | 12 | 286.38 | 0.1564 |
| | | 15 | 314.55 | |
| | | 20 | 353.85 | |

| Location | Magnet | Depth (m) | Average Total Preconsolidation Stress (kPa) | Average Compression Ratio |
|---|---|---|---|---|
| **600 South** | **M34-2-1** | 0 | 59.01 | 0.0736 |
| | | 1 | 78.84 | 0.1075 |
| | | 6 | 140.88 | 0.2506 |
| | | 8 | 155.53 | 0.3662 |
| | | 12 | 183.24 | 0.2081 |
| | | 15 | 212.96 | 0.2419 |
| | | 19 | 240.25 | |
| | | 24 | 282.94 | |
| | | 27 | 309.89 | |
| | | 28 | 318.44 | |
| | | 29 | 326.93 | |
| **600 South** | **M34-2-2B** | 0 | 92.36 | 0.2226 |
| | | 2 | 131.31 | 0.1625 |
| | | 7 | 185.33 | 0.1422 |
| | | 10 | 205.72 | 0.5382 |
| | | 12 | 217.74 | 0.5044 |
| | | 16 | 257.17 | 0.4232 |
| | | 21 | 288.76 | 0.2864 |
| | | 26 | 331.94 | |
| | | 29 | 356.85 | |
| | | 31 | 372.95 | |
| **2400 South** | **M27-8-1** | 0 | 131.97 | 0.0334 |
| | | 1 | 154.91 | 0.0869 |
| | | 5 | 203.20 | 0.1736 |
| | | 7 | 218.96 | 0.3198 |
| | | 12 | 262.08 | 0.1863 |
| | | 13 | 270.23 | 0.3924 |
| | | 15 | 287.18 | |
| | | 17 | 304.30 | |
| | | 19 | 320.92 | |
| | | 21 | 337.51 | |
| | | 22 | 345.79 | |
| **2400 South** | **M28-0-1B** | 0 | 105.99 | 0.0242 |
| | | 5 | 182.31 | 0.1211 |
| | | 8 | 208.21 | 0.2430 |
| | | 10 | 225.62 | 0.1376 |
| | | 15 | 272.01 | 0.3312 |
| | | 18 | 297.81 | 0.1151 |
| | | 20 | 315.69 | 0.0598 |
| | | 24 | 352.17 | 0.0479 |
| | | 27 | 384.69 | |
| | | 31 | 418.66 | |
| | | 36 | 463.52 | |
| | | 39 | 490.44 | |

| Location | Magnet | Depth (m) | Average Total Preconsolidation Stress (kPa) | Average Compression Ratio |
|---|---|---|---|---|
| **2400 South** | **M27-6-1** | 0 | 45.18 | |
| | | 4 | 108.90 | |
| | | 8 | 145.04 | |
| | | 10 | 162.69 | |
| | | 14 | 198.58 | |
| | | 18 | 235.90 | |
| | | 23 | 282.40 | |
| | | 26 | 313.58 | |
| | | 35 | 395.77 | |
| | | 37 | 413.95 | |

## 4.3 Development of Regression Models for Preconsolidation Stress

After the CPT data was paired and averaged from all the magnets, MLR analyses can be started. The equation below was developed by Woodward-Clyde for use on the I-15 Reconstruction project, but did not use magnetic extensometer data Gummow (1999):

$$\sigma'_p = [0.0991\ (f_s/\sigma'_{vo})^{-0.39}]\ [q_t - \sigma_{vo}] \qquad 4\text{-}13$$

$\sigma'_p$ = Preconsolidation stress

$q_t$ = Corrected tip stress

$f_s$ = Sleeve resistance

$\sigma'_{vo}$ = Effective vertical stress

$\sigma_{vo}$ = Total vertical stress

The functional form of this equation was tried using the data from this report (Figure 4.6). One of the fitted trend lines is a power fit and produced an $R^2$ value of 0.5893. The next fitted trend line is an exponential fit and has an $R^2$ value of 0.4276.

One problem encountered with the power fit is the sensitivity of this equation to small changes in the independent variable term, especially in the range between 0.0 and 0.50. This sensitivity to Y as a function of X is undesirable from a predictive standpoint, and it is not clear whether or not the abrupt curvature demonstrated by the power model is justified. The exponential fit, although it has a lower $R^2$ value, does not exhibit extreme curvature and is less sensitive to changes in the X variable between 0.0 and 0.5.

Mayne and Chen (1994) propose a functional form that includes the difference between the corrected tip stress and the total vertical stress:

$$\sigma'_p = B_0(q_t - \sigma_{vo})^{B1} \qquad 4\text{-}14$$

This functional form was also tested with the following results:

$$\sigma'_p = 0.286(q_t - \sigma_{vo})^{1.104} \qquad 4\text{-}15$$

This equation and the data are shown in Figure 4.7. Although this form produced a lower $R^2$ value, it has some very pleasing statistical qualities. For instance, the sensitivity of Y to X has been removed and that the data are approximately equally dispersed about the regression line.

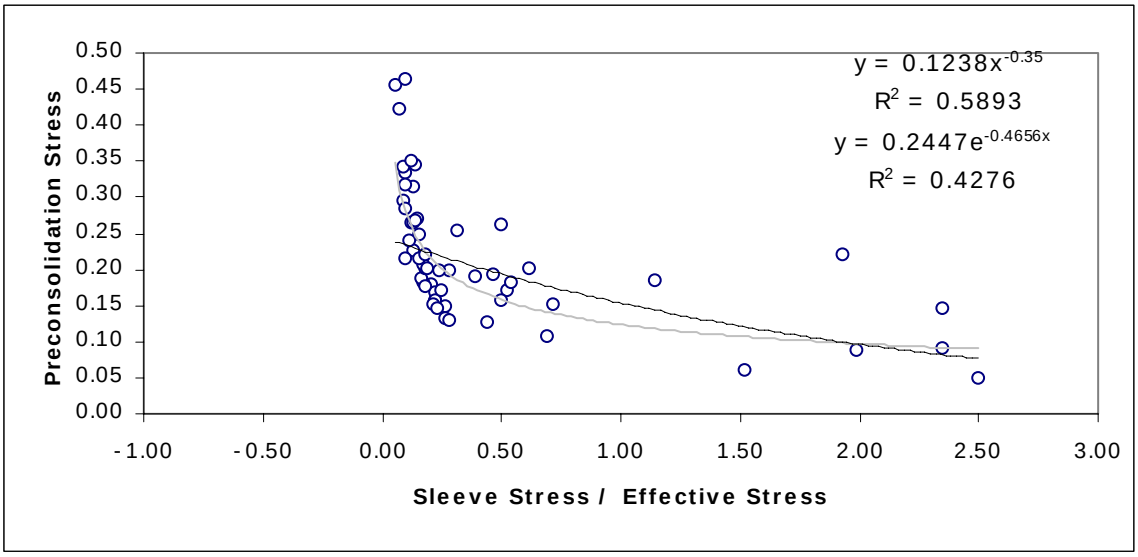


**Figure 4-6 Plot of Woodward Clyde Correlation Equation with Data from this Report.**

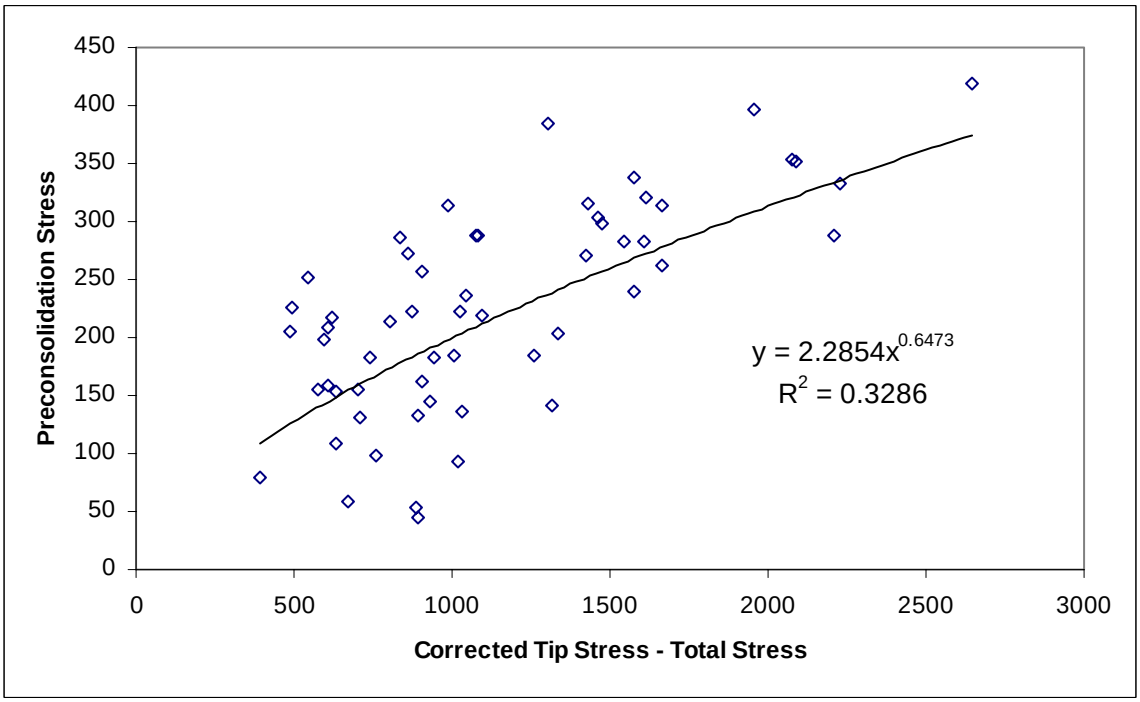


**Figure 4-7 Plot of Mayne and Chen Correlation with Salt Lake Valley.**

To improve the relatively low $R^2$ value of 0.3286, additional analyses were completed to find other variables that may improve the predictive performance. Models that were attempted included the following functional form for X:

$$\sigma'_p = B_0 (q_t - \sigma_{vo}')^{B1} \qquad 4\text{-}16$$

$$\sigma'_p = B_0 (q_t / \sigma'_{vo})^{B1} \qquad 4\text{-}17$$

$$\sigma'_p = B_0 (q_t / \sigma_{vo})^{B1} \qquad 4\text{-}18$$

The trend line for equation 4-16 did not fit the data well. The second model produced a lot of variability and was judged to be unacceptable. The last model produced a very pleasing plot with moderate curvature and a $R^2$ value of 0.5994 (Figure 4.8). Also, the data are approximately equally scattered about the regression line, which is another desirable characteristic.

It was originally thought that a model similar to the functional form of Mayne and Chen (1994) would produce the best results, but this proved not to be true for this particular data set. The reason for this is not clear, but the data fit shown in Figure 4.8 was certainly superior to all other models that were attempted.

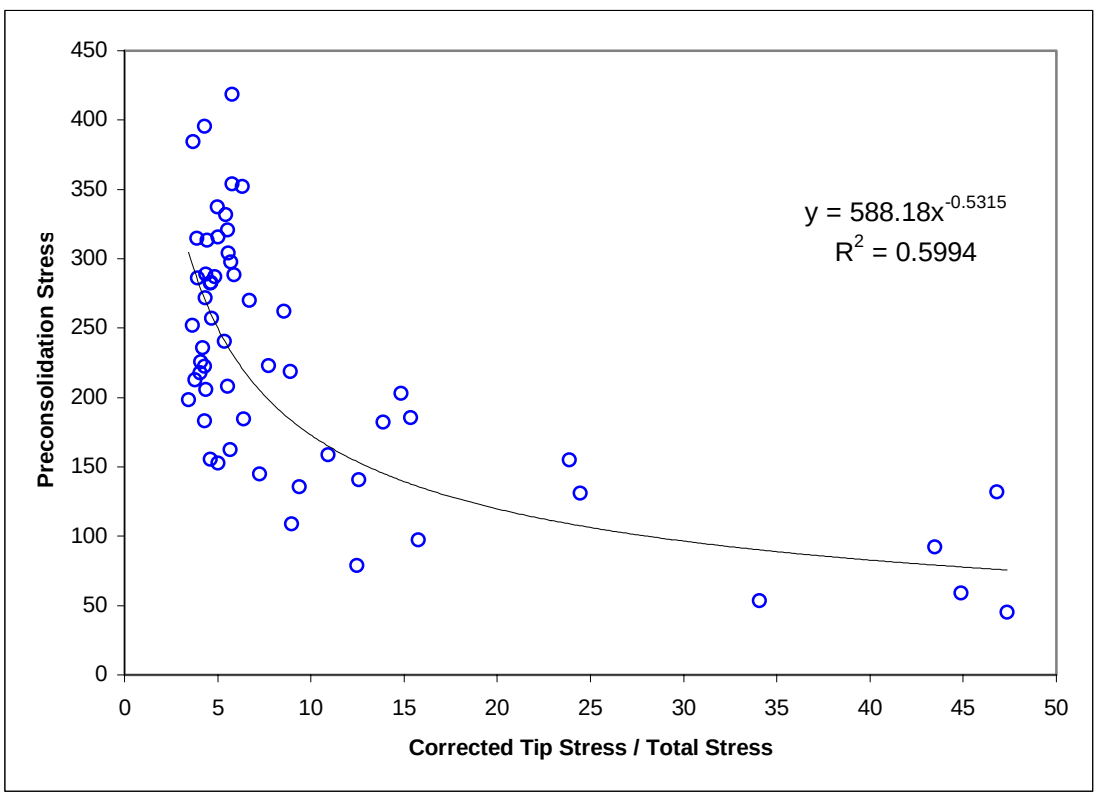


**Figure 4-8 Plot of Corrected Tip Stress Divided by Total Stress and Preconsolidation Stress**

Next, the regression of corrected tip stress divided by total stress was performed using Microsoft EXCEL for the MLR analysis. First, the sleeve stress was reviewed to see if a possible correlation between preconsolidation stresses could be seen. It was expected that this sleeve fiction could improve the predictive power of the regression from work that was done by Woodward Clyde (1999) on the I-15 Reconstruction Project. The following model was developed:

$$\sigma'_p = \beta_0 (q_t / \sigma_{vo})^{\beta 1} (f_s)^{\beta 2} \qquad 4\text{-}19$$

This model has the general form:

$$Y = \beta_0 X_1^{\beta 1} X_2^{\beta 2} \qquad 4\text{-}20$$

This can be converted to a linear form for multiple regression using:

$$\text{Log } Y = \text{Log } \beta_0 + \beta_1 \text{Log} X_1 + \beta_2 \text{Log} X_2 \qquad 4\text{-}21$$

Table 4.3 gives the regression summary statistics for equation 4-21, which includes the logarithmic transformations of $\sigma'_p$, $(q_t / \sigma_{vo})$, and $f_s$ to define Y, $X_1$ and $X_2$, respectively. By including the $X_2$ variable (i.e., log $f_s$), the correlation was improved by about 15 percent (Table 4.3) over the model that did not include the sleeve stress (Figure 4.8).

**Table 4-3 Linear regression output using log of corrected tip stress as X1 and average sleeve stress as X2; Y = log of preconsolidation stress.**

| *Regression Statistics* | |
|---|---|
| Multiple R | 0.867319904 |
| **R Square** | **0.752243817** |
| Adjusted R Square | 0.743067662 |
| Standard Error | 0.109579276 |
| Observations | 57 |

| | *df* | *SS* | *MS* | *F* | *Significance F* |
|---|---|---|---|---|---|
| Regression | 2 | 1.968723555 | 0.984361778 | 81.97811 | 4.35173E-17 |
| Residual | 54 | 0.648411357 | 0.012007618 | | |
| Total | 56 | 2.617134912 | | | |

| | **Coefficients** | Standard Error | *t Stat* | *P-value* | *Lower 95%* |
|---|---|---|---|---|---|
| **Intercept** | 2.36342188 | 0.08242365 | 28.6740714 | 2.35E-34 | 2.19817225 |
| X Variable 1 | -0.64968782 | 0.05080924 | -12.7868031 | 5.71E-18 | -0.75155431 |
| X Variable 2 | 0.35535494 | 0.06157733 | 5.77087275 | 3.96E-07 | 0.23189972 |

From the above model and equations and the coefficients in the regression output (Table 4.3), the MLR model can be back transformed to:

$$\sigma'_p = 230.90\ (q_t / \sigma_{vo})^{-0.6497}\ (f_s)^{0.3554} \qquad 4\text{-}22$$

where:

$\sigma'_p$ = Preconsolidation stress (kPa)

$q_t$ = Corrected tip stress (kPa)

$f_s$ = Sleeve resistance (kPa)

$\sigma_{vo}$ = Total vertical stress (kPa)

From a statistical standpoint, equation 4-22 is acceptable; but from an application standpoint it is desirable to have a regression model that is not dependent upon the stress units that have been used. This model can be formed as:

$$\sigma'_p / \sigma_{vo} = \beta_0\ (q_t / \sigma_{vo})^{\beta 1}\ (f_s / \sigma_{vo})^{\beta 2} \qquad 4\text{-}23$$

Note that in this model all variables (Y, $X_1$ and $X_2$) have been divided by $\sigma_{vo}$, which makes all variables dimensionless. Equation 4-23 can be linearized by:

$$\text{Log}\ (\sigma'_p / \sigma_{vo}) = \text{Log}\ \beta_0 + \beta_1 \text{Log}(q_t / \sigma_{vo}) + \beta_2 \text{Log}(f_s / \sigma_{vo}) \qquad 4\text{-}24$$

Because the above model is a slight change in the functional form that was in the previous regression, Figure 4.9 shows the relation between dependent and independent variables. This figure shows that both X's are correlated with Y and both X's are correlated with each other. (Note that Figure 4.9 shows an approximate linear relationship between the transformed Y variable and the transformed X variables.) Equation 4-24 produces an acceptable result and has the highest $R^2$ of any model tested. Table 4.4 gives the summary statistics for the model given in equation 4-24. The back-transformed equation becomes:

$$\sigma'_p / \sigma_{vo} = 0.138148(q_t / \sigma_{vo})^{0.9382314}\ (f_s / \sigma_{vo})^{-0.165878} \qquad 4\text{-}25$$

The $R^2$ for this equation is approximately 74 percent. Table 4.4 suggests that the second X variable ($f_s / \sigma_{vo}$) is only marginally contributing to improving the model. If left out of the model, the equation becomes:

$$\sigma'_p / \sigma_{vo} = 0.311955\ (q_t / \sigma_{vo})^{0.6818076} \qquad 4\text{-}26$$

The $R^2$ value for this equation is also about 74 percent, and all regression coefficients are highly significant (i.e., are significantly contributing to the performance of the model). This is the final model that is recommended for use in predicting preconsolidation stress from the CPT.

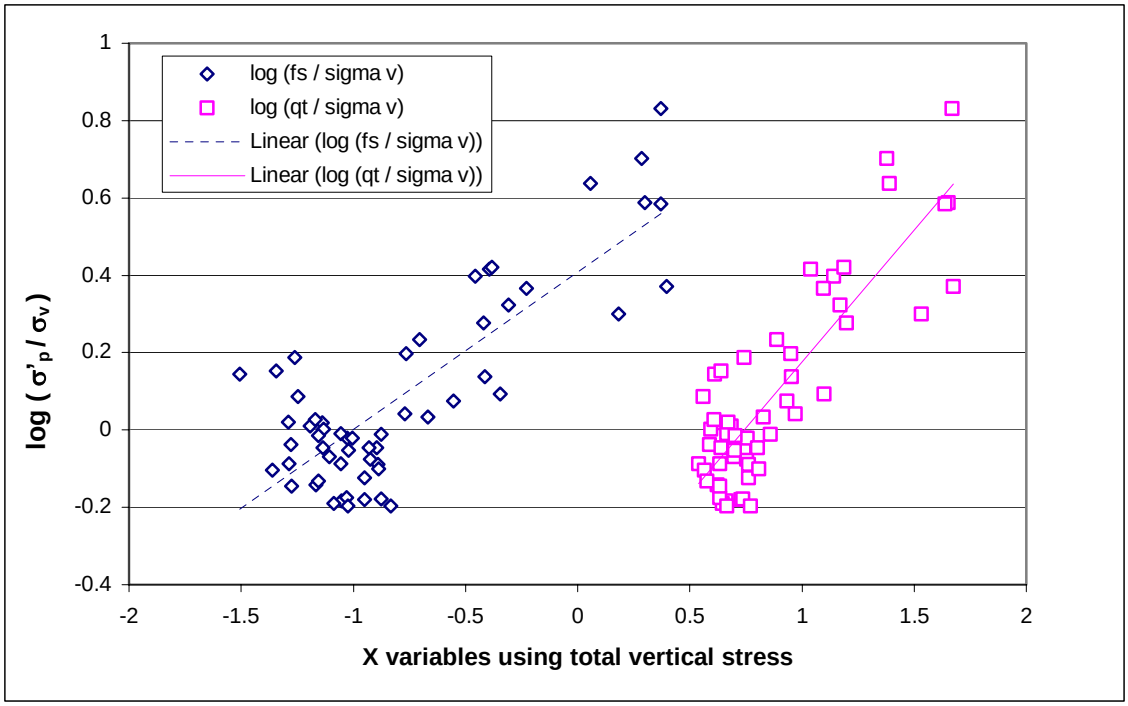


**Figure 4-9 Plot of Variables Used in Equation 4-24.**

**Table 4-4 Linear Regression Output for Equation 4-24.**

| *Regression Statistics* | |
|---|---|
| Multiple R | 0.8618544 |
| R Square | 0.7427931 |
| Adjusted R Square | 0.7332669 |
| Standard Error | 0.1292121 |
| Observations | 57 |

ANOVA

| | *df* | *SS* | *MS* | *F* |
|---|---|---|---|---|
| Regression | 2 | 2.6036647 | 1.3018324 | 77.973837 |
| Residual | 54 | 0.901571 | 0.0166958 | |
| Total | 56 | 3.5052357 | | |

| | *Coefficients* | *Standard Error* | *t Stat* | *P-value* |
|---|---|---|---|---|
| Intercept | -0.859654 | 0.3158404 | -2.721798 | 0.0087219 |
| log (qt / sigma v) | 0.9382314 | 0.2325445 | 4.0346313 | 0.0001734 |
| log (fs / sigma v) | -0.165878 | 0.1461907 | -1.134671 | 0.2615247 |

**Table 4-5 Linear Regression Output for Equation 4-26.**

| *Regression Statistics* | |
|---|---|
| Multiple R | 0.8582894 |
| R Square | 0.7366607 |
| Adjusted R Square | 0.7318727 |
| Standard Error | 0.1295493 |
| Observations | 57 |

ANOVA

| | *df* | *SS* | *MS* | *F* |
|---|---|---|---|---|
| Regression | 1 | 2.5821693 | 2.5821693 | 153.856 |
| Residual | 55 | 0.9230664 | 0.016783 | |
| Total | 56 | 3.5052357 | | |

| | *Coefficients* | *Standard Error* | *t Stat* | *P-value* |
|---|---|---|---|---|
| Intercept | -0.505908 | 0.0507327 | -9.972033 | 6.17E-14 |
| log (qt / sigma v) | 0.6818076 | 0.0549673 | 12.403871 | 1.44E-17 |

Regression models were also attempted that used the effective vertical stress instead of the total vertical stress in the denominator of equation 4-26. The attempted model has the form:

$$\text{Log}\ (\sigma'_p / \sigma'_{vo}) = \text{Log}\ \beta_0 + \beta_1 \text{Log}(q_t / \sigma'_{vo}) + \beta_2 \text{Log}(f_s / \sigma'_{vo}) \qquad 4\text{-}27$$

The regression results for equation 4-27 are given in Table 4.6. Because of its lower $R^2$ value (47 percent versus 74 percent), this model is not recommended and has much poorer predictive performance.

**Table 4-6 Linear Regression Output for Equation 4-27.**

| *Regression Statistics* | |
|---|---|
| Multiple R | 0.6999048 |
| R Square | 0.4898667 |
| Adjusted R Square | 0.4709729 |
| Standard Error | 0.1191394 |
| Observations | 57 |

ANOVA

| | *Df* | *SS* | *MS* | *F* |
|---|---|---|---|---|
| Regression | 2 | 0.7360352 | 0.3680176 | 25.927343 |
| Residual | 54 | 0.7664862 | 0.0141942 | |
| Total | 56 | 1.5025215 | | |

| | *Coefficients* | *Standard Error* | *t Stat* | *P-value* |
|---|---|---|---|---|
| Intercept | -0.300135 | 0.3327254 | -0.902049 | 0.3710367 |
| log (qt / sigma v') | 0.5399807 | 0.2401387 | 2.24862 | 0.0286392 |
| log (fs / sigma v') | -0.021105 | 0.1315833 | -0.160393 | 0.8731703 |

## 4.4 Development of Regression Models for Compression Ratio

The next part of the regression analysis involved finding a correlation between the CPT and compression ratio. Again, as has been discussed previously, the data was averaged in the same manner as the preconsolidation stress data was. The first correlation that was investigated came from Woodward Clyde investigations. The equation is as follows:

$$CR = 0.0806 * (f_s/\sigma'_{vo})^{-0.3692} \qquad 4\text{-}28$$

$f_s$ = Sleeve resistance

$\sigma'_{vo}$ = Effective Stress

When the data from this report is correlated using the sleeve stress alone, poor results occur. Figure 4.10 illustrates compression ratio versus sleeve stress divided by effective stress. The correlation has an $R^2 = 0.1352$. This proves a poor correlation between the data collected for this project and sleeve stress divided by effective stress.

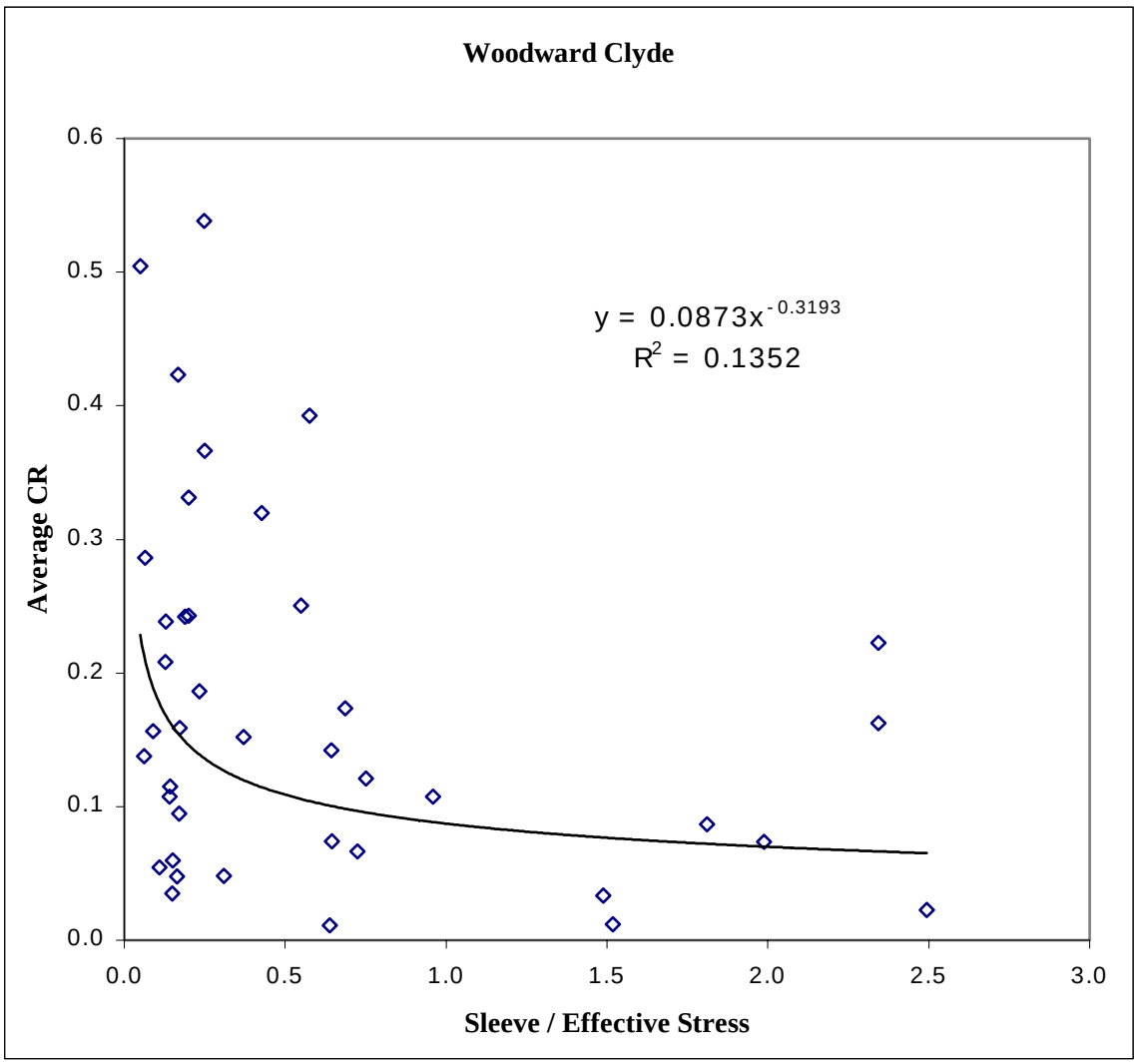


**Figure 4-10 Plot of Woodward Clyde Correlation Equation with this data.**

Next the corrected tip stress divided by the total stress was evaluated to see how well it would correlate to the compression ratio. The plot shown as Figure 4.11 illustrates this correlation. The plot has an $R^2 = 0.1778$ which again illustrates a poor correlation.

Next, multivariable linear regression was performed using EXCEL. The log of the average compression ratio was taken as the "Y" variable, log of tip stress divided by total stress as he "X1" variable, and log of the sleeve stress as the "X2" variable. Table 4.7 gives the statistical output and X1 and X2 variables.

As can be seen from the above plots and statistics, the correlation is poor. Many forms of the equation were evaluated in an attempt to obtain a good correlation for the compression ratio. Each form produced similar results. Thus, it is not recommended that the CPT be used to predict compression ratio for the Lake Bonneville deposits.

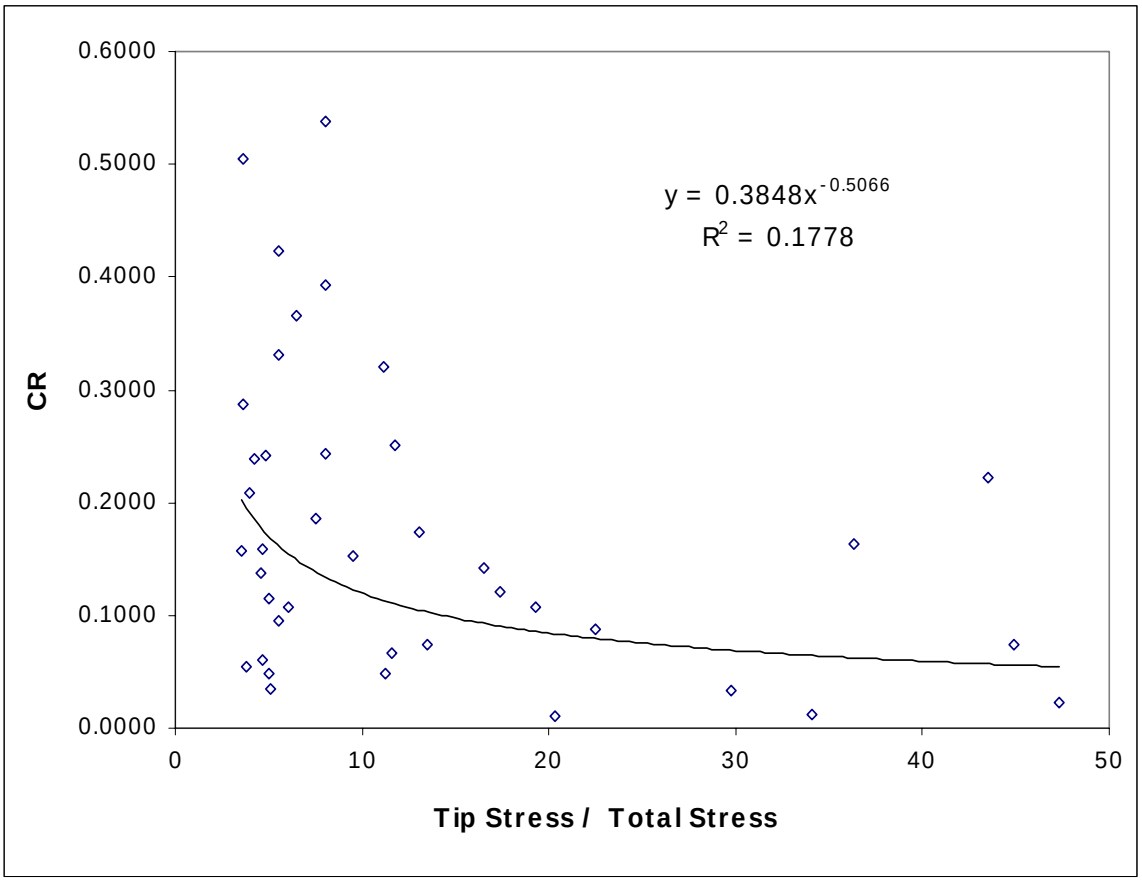


**Figure 4-11 Plot of tip stress divided by total stress and compression ratio.**

**Table 4-7 Linear Regression Output for Compression Ratio**

| *Regression Statistics* | |
|---|---|
| Multiple R | 0.4217 |
| **R Square** | **0.1779** |
| Adjusted R Square | 0.1334 |
| Standard Error | 0.3848 |
| Observations | 40.0000 |

| | *df* | *SS* | *MS* | *F* | *Significance F* |
|---|---|---|---|---|---|
| Regression | 2.0000 | 1.1853 | 0.5927 | 4.0021 | 0.0267 |
| Residual | 37.0000 | 5.4794 | 0.1481 | | |
| Total | 39.0000 | 6.6647 | | | |

| | *Coefficients* | *Standard Error* | *t Stat* | *P-value* | *Lower 95%* |
|---|---|---|---|---|---|
| Intercept | -0.4248 | 0.3595 | -1.1815 | 0.2449 | -1.1533 |
| X Variable 1 | -0.5121 | 0.2452 | -2.0881 | 0.0437 | -1.0090 |
| X Variable 2 | 0.0111 | 0.3404 | 0.0326 | 0.9742 | -0.6787 |

# 5 Conclusions and Summary

## 5.1 Significance of Research Findings

The primary consolidation settlement associated with the Lake Bonneville deposits pose significant concerns for building and roadway construction in the Salt Lake Valley. The amount of settlement associated with these deposits can be large, exceeding 1 m (3.3 ft) for typical highway embankment construction at bridge approaches. This amount of settlement, if not properly taken into account during geotechnical design and construction, can be damaging, or at least significantly impact the serviceability of buildings and bridges.

The Lake Bonneville deposits are also slightly to moderately overconsolidated. This means that upon initial application of a new load (such as an embankment fill), the amount of settlement will be modest. However, if the new load continues to increase past the preconsolidation stress, then the amount of settlement will significantly increase as primary consolidation is initiated. Thus, the estimation of the amount of new load required to trigger primary consolidation settlement is of great importance for geotechnical design. Loading conditions below the preconsolidation stress are generally small, occur relatively quickly, and thus can usually be managed. However, loading conditions above the preconsolidation stress are large, can be potentially damaging, and require months for the primary consolidation settlement to be completed.

In addition to estimating the preconsolidation stress, the compression ratio is another important soil parameter required for geotechnical design. This parameter is a measure of the compressibility (i.e., strain) of the soil for one log cycle increase in applied stress. The compression ratio is mainly a function of the initial void ratio of the soil and is also influenced by the stiffness of the soil fabric. Soils having a higher void ratio and a low stiffness are generally more compressible.

The goals of this research was to develop empirical methods for estimating the preconsolidation stress and compression ratio using cone penetrometer (CPT) data correlated with laboratory and magnet extensometer data. The extensive amount of data gathered from the I-15 Reconstruction Project provided the opportunity to develop empirical methods using multiple linear regression (MLR) techniques.

## 5.2 Recommended Empirical Model

An analysis of the data showed that reliable correlations exist between the preconsolidation stress and CPT measurements; however only weak correlations exist for the compression ratio. The final predictive model for preconsolidation stress (see Chapter 4) has the following functional form.

$$Y = \beta_0 X_1^{\beta 1} \qquad 5\text{-}1$$

This equation can be written in a linear form as follows:

$$\text{Log } Y = \text{Log } \beta_0 + \beta_1 \text{Log} X_1 \qquad 5\text{-}2$$

where:

$Y = \sigma'_p / \sigma_{vo}$

$X_1 = q_t / \sigma_{vo}$

$\sigma'_p$ = preconsolidation stress

$\sigma_{vo}$ = vertical total stress (overburden stress)

$q_t$ = corrected tip stress from the CPT

Regression analysis was performed to determine the best-fit values for the regression coefficients $\beta_0$ and $\beta_1$. These are: -0.505908049 and 0.6818076, respectively. The coefficient of determination, $R^2$, for this model is 74 percent and all regression coefficients are highly significant. Equation 5-2 can be back transformed to:

$$\sigma'_p / \sigma_{vo} = 0.3120 \, (q_t / \sigma_{vo})^{0.6818} \qquad 5\text{-}3$$

This equation is the final regression model. The unit of stress for $\sigma'_p$, $\sigma_{vo}$ and $q_t$ must be consistent, but any stress unit can be used.

MLR analysis was also performed to develop a correlation for the compression ratio using CPT data. However, the coefficients of determination for the attempted models were generally less than 20 percent, which indicates relatively poor predictive performance. Thus, no compression ratio versus CPT model is recommended for use at this time. Further, it appears that the CPT measurements are not a good indicator of compressibility of the soil fabric, thus it is doubtful that good correlations will ever be developed from this test.

## 5.3 Implementation of the Empirical Model

Use of equation 5-3 is recommended for geotechnical evaluations for locations underlain by the silty clay and clayey silt sediments of Lake Bonneville. These clayey deposits constitute the "deep water deposits" of Lake Bonneville that are found in the lower elevations of many northern Utah valleys located west of the Wasatch Fault. Although the recommended correlation was developed from Salt Lake Valley Lake Bonneville deposits, we expect that the model will have adequate performance for other northern Utah locales where Lake Bonneville clays are found. This expectation is based on the premise that because these clays have the same geologic origin, they will be reasonably similar in their geotechnical properties, regardless of the specific location. However, we have found that it is necessary to filter out the sand lenses within the clay layers before using the recommended model as discussed in Chapter 4.

We also anticipate that the scope of geotechnical laboratory testing can be reduced for many projects by performing CPT measurements and applying the developed model to predict the preconsolidation stress. It is recommended that CPT soundings be performed in the first phase of any subsurface investigation, followed by selective drilling, undisturbed sampling, and laboratory testing to confirm the reasonableness of the CPT

predictions. In some cases, further evaluations may be required, depending on the geotechnical issues at hand.

## 5.4 Future Research and Improvements

Although this research was unsuccessful at developing a compression ratio versus CPT correlation, subsequent research (Bartlett and Lee, 2004) has shown the compression ratio is strongly correlated with void ratio, moisture content, liquid limit and plastic index. Thus, these index properties can also be useful for estimating the consolidation properties of the Lake Bonneville clays and reducing the scope of geotechnical laboratory testing for many projects. These correlations are being published in a subsequent technical report to the Utah Department of Transportation (Bartlett and Lee, 2004). We also recommend that other types of in situ tests (e.g., dilatometer (DMT) and pressure meter (PMT)) be considered as possible alternatives for predicting soil compressibility.

Also, the accuracy of the developed correlation could be improved by additional data collection and subsurface instrumentation. For example, the inclusion of the pore pressure measurements from the piezocone should have contributed to the model, but these data for the I-15 Reconstruction Project suffered from partial desaturation problems, as discussed in Chapter 3. Also, as more data become available from other projects, we recommend that the data be compared with the current model and that the regression equation be updated, as necessary.

Page Left Blank Intentionally

# 6 References


ASTM D1586. "Method for Penetration Test and Split-Barrel Sampling of Soils," American Society for Testing and Materials. Vol. 04.08 Soil and Rock (I): D 420 – D4914, 1916 Race Street, Philadelphia, P.A, 1994. Version.

ASTM D2435. "Test Method for One-Dimensional Consolidation Properties of Soils," American Society for Testing and Materials. Vol. 04.08 Soil and Rock (I): D 420 – D4914, 1916 Race Street, Philadelphia, P.A, 1994. Version.

ASTM D3441. "Method for Deep, Quasi-Static, Cone and Friction-Cone Penetration Tests of Soil," American Society for Testing and Materials. Vol. 04.08 Soil and Rock (I): D 420 – D4914, 1916 Race Street, Philadelphia, P.A, 1994. Version.

Adan, S.M. and Rollins, K.M., (1993). "Damage Potential Index Mapping for Salt Lake Valley, Utah," Utah Geological Survey, 64 pp.

Anderson, A.A., and Kolstad, P., (1979). "The NGI 54 mm Samplers for Undisturbed Sampling of Clays and Representative Sampling of Coarser Material," Proceedings of the International Symposium on Soil Sampling, Singapore, pp. 1-21.

Asaoka, A., (1978). "Observational Procedure of Settlement Prediction," Soils an Foundations, Vol. 18, No. 4, pp. 87-101.

Bartlett, S. F., and Lee, H. S., (2004). "Estimation of Compression Properties of Clayey Soils, Salt Lake Valley, Utah," Utah Department of Transportation, Research Division, Report No. UT-04.28, Salt Lake City, Utah.

Bartlett, S. F., Monley, G., Soderborg, A., Palmer, A., (2001). "Instrumentation and Construction Performance Monitoring for the I-15 Reconstruction Project, Salt Lake City, Utah," Transportation Research Record No. 1772, Paper No. 01-3394, pp. 40-47.

Battaglio, M., Bruzzi, D., Jamiolkowski, M., and Lancellotta, R., (1986). "Interpretation of CPT's and CPTU's," Proceedings, Fourth International Geotechnical Seminar: Field Instrumentation and In-Situ Measurements, Singapore, pp. 129-143.

Casagrande, A. (1936). "The Determination of the Pre-Consolidation Load and Its Practical Signficance," Discussion D-34, Proceedings of the First International Conference on Soil Mechanics and Foundation Engineering, Cambridge, Vol. III, pp. 60 – 64.

Dames and Moore, (1996a). "Geotechnical Report for the Reconstruction of Structures and Embankments 600 South Section I-15 Corridor From 600 South to 960 South," UDOT Contract No. SP-15-7(129)310, Station 31+275 to 32+420, Salt Lake City, Utah, Sept. 1996.

Dames and Moore, (1996b). "Geotechnical Report for the Reconstruction of Structures and Embankments 1300 South Section I-15 Corridor," UDOT Contract No. SP-15-7(132)308, Station 29+300 to 31+275, Salt Lake City, Utah, Sept. 1996.

Dames and Moore, (1996c). "Geotechnical Report for the Reconstruction of Structures and Embankments 2400 South Section I-15 Corridor," UDOT Contract No. SP-15-7(1287308, Station 26+800 to 29+300, Salt Lake City, Utah, Sept. 1996.

Draper, N.R. and Smith, H., (1981). "Applied Regression Analysis," John Wiley & Sons, Inc., New York, 2nd Edition.

Electric Power Research Institute, (1990). "Manual on Estimating Soil Properties for Foundation Design," EPRI EL-6800 Project 1493-6 Final Report, August 1990.

Gummow, G., (1999). "Settlement Soil Profile Model Development for the I-15 Corridor Reconstruction Project, Salt Lake City, Utah," M.S. Project Brigham Young University, Provo, Utah, 1999.

Holtz, R.D. and Kovacs, W.D. (1981). "An Introduction to Geotechnical Engineering," Prentice-Hall, Inc., New Jersey, 733 pp.

Houlsby, G.T. and Teh, C.I., (1988). "Analysis of the Piezocone in Clay," Penetration Testing 1988 (ISOPT-1), Balkema, Rotterdam, Vol. 2, pp. 777-783.

Jamiolkowski, M., Ladd, C.C., Germaine, J.T., and Lancellotta, R., (1985). "New Developments in Field and Laboratory Testing of Soils," Proceedings of the Eleventh International Conference on Soil Mechanics and Foundation Engineering, Vol. 1, San Francisco, pp. 58-63.

Keaveny, and Mitchell, (1986). "Strength of fine-grained soils using the piezocone," Use of In-Situ Tests in Geotechnical Engineering, GSP 6, ASCE, Reston, Virginia, pp. 668-685.

Kleinfelder, Inc. (1996a). "Preliminary Geotechnical Exploration Report," I-15 Corridor Reconstruction Section 4, 600 South, Project No. SP-15-7(129)310, Station 32+080 to 35+044, Salt Lake City, Utah, Sept. 1996.

Kleinfelder, Inc. (1996b). "Geotechnical Exploration Report," I-15 Corridor Reconstruction Section 9, State Street, Project No. SP-80-3(41)125, Station 1+220 to 1+687, Salt Lake City, Utah, Sept. 1996.

Kleinfelder, Inc. (1996c). "Geotechnical Exploration Report," I-15 Corridor Reconstruction Section 8, 3300 South, Project No. SP-15-7(144)305, Station 28+600 to 24+500, Salt Lake City, Utah, Sept. 1996.

Kleinfelder, Inc. (1996d). "Geotechnical Exploration Report," I-15 Corridor Reconstruction Section 10, 900 W., Project No. SP-020(1)17, Station 1+000 to 10+640, Salt Lake City, Utah, Sept. 1996.

Konrad and Law (1987). Preconsolidation Pressure from Piezocone Tests in Marine Clays, Geotechnique, Vol. 37, No. 2, pp. 177-190.

Larsson, R. and Mulabdic, M., (1991). "Piezocone Tests in Clay," Swedish Geotechnical Institute Report No. 42, Linkoping, Sweden.

Lund, W. R., (1990). "Engineering Geology of the Salt Lake City Metropolitan Area, Utah," Utah Geological and Mineral Survey, The association of Engineering Geologists, Bulletin 126, Salt Lake City, Utah, pp. 1-66.

Mayne, P.W., (1986). "CPT indexing of In-situ OCR in Clays," Use of In Situ Tests in Geotechnical Engineering (GSP 6), ASCE, New York, pp. 780-793.

Mayne, P.W., (1991). "Determination of OCR in Clays by Piezocone Tests Using Cavity Expansion and Critical State Concepts," Soil and Foundations, Vol. 31, No. 2, pp. 65-76.

Mayne, P.W., and Bachus R.C., (1988). "Profiling OCR in Clays by Piezocone," Penetration Testing 1988 (ISOPT-1), Balkema, Rotterdam, Vol. 2, 857-864.

Mayne, P.W., and Chen, B.S., (1994). "Profiling the Overconsolidation Ratio of Clays by Piezocone Tests," Georgia Tech Research Corporation Project No. E20-648/X51, Atlanta, Georgia, Aug. 1994.

Mayne, P.W. and Holtz, R.D., (1988). "Profiling Stress History from Piezocone Soundings," Soils and Foundations, Vol. 28, No.1, pp. 16-28.

Meigh, A.C., (1987). "Cone Penetration Testing Methods and Interpretation," CIRIA Ground Engineering Report; In-Situ Testing, 1987.

NCEER (1997). "Proceedings of the NCEER Workshop on Evaluation of Liquefaction Resistance of Soils," Technical Report NCEER-97-0022, December 31, 1997.

Ng, N. S. Y., (1998). "Characterization of Consolidation and Creep Properties of Salt Lake City Clays," M.S. Thesis, Massachusetts Institute of Technology, February 17, 1998.

Personius, and Scott, (1992). Surficial geologic map of the Salt Lake City segment and parts of adjacent segments of the Wasatch fault zone, Davis, Salt Lake, and Utah Counties, Utah, U.S. Geological Survey Miscellaneous Investigations Map I-2106, scale 1:50,000.

Rowe, P.W., (1972). "The Relevance of Soil Fabric to Site Investigation Practice," 12th Rankine Lecture, Geotechnique, No. 2.

Sandven R., Senneset, K. and Janbu, N., (1988). "Interpretation of Piezocone Tests in Cohesive Soils," Penetration Testing 1988, Vol. 2, Balkema, Rotterdam, pp. 939-953.

Sanglerat, G., (1979). "The Penetrometer and Soil Exploration," Elsevier Publishing Co., Amsterdam, 2nd Edition, 1979.

Saye, S. R., and Ladd, C. C. (1999). "Design and Performance of the Foundation Stabilization Treatments for the Reconstruction of Interstate 15 in Salt Lake City, Utah," unpublished report given at a URS Corporation Seminar.

Schmertmann, J. H. (1955). "The Undisturbed Consolidation Behavior of Clay," Transactions, ASCE, Vol. 120, pp. 1201 – 1233.

Senneset, K., Sandven, R., and Janbu, N., (1989). "Evaluation of Soil Parameters from Piezocone Tests," Transportation Research Record 1235, Washington, D.C., pp. 24-37.

Tavenas, F. and Leroueil, S., (1979). "Clay Behavior and the Selection of Design Parameters," Proceedings, 7th European Conference on Soil Mechanics and Foundation Engineering, Vol. 1, Brighton, England, pp. 281-291.

Tavenas, F. and Leroueil, S., (1987). "State-of-the-Art on Laboratory and In-Situ Stress-Strain-Time Behavior of Soft Clays," Proceeding, International Symposium on Geotechnical Engineering of Soft Soils, Mexico City, pp. 1-146.

UDOT (1998). "Standard Specification 223 Instrumentation," Rev. 1, Mar. 16, 1998. I-15 Reconstruction Project," 28 p. and drawings.

Woodward-Clyde (1997). "Pre-Bid Analyses I-15 Improvements," W-C Project 96U115, Project Report, April 1997.

Wroth, C.P., (1984). "The Interpretation of In-Situ Soils Tests," Geotechnique, Vol. 34, No. 4, pp. 449-489.

Wroth, C.P., (1988). "Penetration Testing: A Rigorous Approach to Interpretation," Penetration Testing 1988 (ISOPT-1), Vol. 1, Balkema, Rotterdam, pp. 303-311.

Wroth, C.P. and Houlsby G., (1985). "Soil Mechanics – Property Characterization and Analysis Procedures," Proceedings, 11th International Conference on Soil Mechanics and Foundation Engineering, Vol. 1, San Francisco, pp. 1-54.